

1974

Inelastic analysis of reinforced concrete slabs, Final Version, May 1974.

W. S. Peterson

C. N. Kostem

J. M. Kulicki

Follow this and additional works at: <http://preserve.lehigh.edu/engr-civil-environmental-fritz-lab-reports>

Recommended Citation

Peterson, W. S.; Kostem, C. N.; and Kulicki, J. M., "Inelastic analysis of reinforced concrete slabs, Final Version, May 1974." (1974). *Fritz Laboratory Reports*. Paper 444.
<http://preserve.lehigh.edu/engr-civil-environmental-fritz-lab-reports/444>

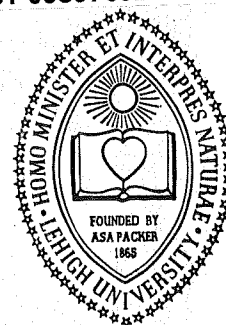
This Technical Report is brought to you for free and open access by the Civil and Environmental Engineering at Lehigh Preserve. It has been accepted for inclusion in Fritz Laboratory Reports by an authorized administrator of Lehigh Preserve. For more information, please contact preserve@lehigh.edu.

LEHIGH UNIVERSITY LIBRARIES



3 9151 00897692 6

LEHIGH UNIVERSITY



**OFFICE
OF
RESEARCH**

**THE INELASTIC ANALYSIS
OF REINFORCED
CONCRETE SLABS**

**FRITZ ENGINEERING
LABORATORY LIBRARY**

by

William S. Peterson

Celal N. Kostem

John M. Kulicki

DR. CELAL N. KOSTEM
Fritz Engineering Lab., 13
Lehigh University
Bethlehem, PA 18015 USA

Fritz Engineering Laboratory Report No. 378B.3

COMMONWEALTH OF PENNSYLVANIA

Department of Transportation

Bureau of Materials, Testing and Research

Leo D. Sandvig - Director

Wade L. Gramling - Research Engineer

Kenneth L. Heilman - Research Coordinator

Project 71-12: Overloading Behavior of Beam-Slab
Type Highway Bridges

THE INELASTIC ANALYSIS OF REINFORCED

CONCRETE SLABS

by

William S. Peterson

Celal N. Kostem

John M. Kulicki

This work was sponsored by the Pennsylvania Department of Transportation and the U. S. Department of Transportation, Federal Highway Administration.

The contents of this report reflect the view of the authors who are responsible for the facts and the accuracy of the data presented herein. The contents do not necessarily reflect the official views or policies of the Pennsylvania Department of Transportation or the Federal Highway Administration. This report does not constitute a standard, specification, or regulation.

LEHIGH UNIVERSITY

Office of Research

Bathlehem, Pennsylvania

May, 1974

Fritz Engineering Laboratory Report No. 378B.3

TABLE OF CONTENTS

	<u>Page</u>
ABSTRACT	
1. INTRODUCTION	1
1.1 Problem Statement	1
1.2 The Scope of the Reported Investigation	2
1.3 Requirements Placed on Analytic Model	3
1.4 Previous Studies	5
1.5 Analytical Model	9
2. THEORETICAL ANALYSIS	10
2.1 Introduction	10
2.2 Assumptions	11
2.2.1 Geometry Restrictions	11
2.2.2 Assumptions Regarding Strain Distribution	11
2.2.3 Small Deformations	12
2.2.4 Small Strains	12
2.2.5 Layering	13
2.3 Review of the Finite Element Method	13
2.4 Element Stiffness Formulation	17
2.4.1 Plate Bending and Inplane Displacement Functions	17
2.5 Strain-Displacement Relations	21
2.6 Layering	25
2.7 Element Stiffness Matrix	27

	<u>Page</u>
2.8 Assembly of the Global Stiffness Matrix	30
2.9 Incremental Iterative Solution Technique	32
3. MATERIAL BEHAVIOR	36
3.1 Concrete Stress-Strain Relationships	37
3.1.1 Nonlinear Stress-Strain Equation for Concrete	38
3.1.2 Linear Stress-Strain Equation for Concrete	42
3.1.3 Biaxial Failure Envelope - Definition of σ_p	44
3.1.4 Peak Strain Envelope - Definition of ϵ_p	48
3.1.5 Peak Slope - Definition of E_p	51
3.1.6 Stress-Strain Curves for Concrete	53
3.1.7 Constitutive Relationships for Concrete	54
3.1.8 Concrete Failure Modes	59
3.1.9 Cracked or Crushed Concrete	61
3.1.10 Unloading of Cracked and Crushed Concrete Layers	62
3.2 Stress-Strain Relationship for Steel	64
3.3 Additional Considerations	65
3.4 Limitations	68
4. CORRELATION WITH TESTS	69
4.1 Reinforced Concrete Beam	72
4.2 Simple-Free Slab	73
4.3 Corner-Supported Slab	74
4.4 Simply Supported Slab with Orthogonal Reinforcement	74

	<u>Page</u>
4.5 Simply Supported Slab with Diagonal Reinforcement	77
4.6 Fixed-Free Rectangular Slab	79
4.7 Fixed-Fixed Square Slab	81
5. SUMMARY AND CONCLUSIONS	83
6. APPENDIX	86
7. ACKNOWLEDGMENTS	106
8. FIGURES	107
9. REFERENCES	159

ABSTRACT

This report describes an approach for the flexural analysis of reinforced concrete slabs using a piecewise linear tangent stiffness finite element incremental method applied to a layered plate element. Each layer of each element is assumed to be in plane state of stress. Each layer has its own biaxial stress-strain characteristics type stress-strain curve and may have inelastic, cracking, crushing and yielding nonlinearities. Comparisons with laboratory tests of six reinforced concrete slabs and one beam are presented. The agreement between analytic and laboratory load deflection curves is quite good. Comparisons with experimentally observed crack patterns, steel strains, and concrete strains are also presented if these data were available.

1. INTRODUCTION

1.1 Problem Statement

The research described in this report has been conducted as a part of the research project entitled "The Overloading Behavior of Beam-Slab Type Highway Bridges" (Pennsylvania Department of Transportation Project 71-12). The goal of this project is the development of an analysis technique to predict the response of a beam-slab type highway bridge superstructure subjected to the passage of an overload vehicle. An overload vehicle is defined as one which exceeds in some way the design vehicle for which the superstructure was proportioned. Beam-slab superstructures are restricted to those consisting of a reinforced concrete deck and prestressed concrete I-beams.

The parent project is divided into three phases:

1. The development of an inelastic analysis technique for prestressed concrete beams (Refs. 19, 20, 23 and 45)
2. The development of an inelastic analysis technique for reinforced concrete slabs
3. The combining of the beam and slab analysis techniques developed in parts 1 and 2 to model the beam-slab superstructure.

This report covers the work conducted in phase 2 above, i.e. the development of a methodology to analytically describe the inelastic response of reinforced concrete slabs.

The slabs under consideration are assumed:

1. To lie in one plane, i.e. be planar
2. Have arbitrary but rectanlinear boundaries
3. Have tension and compression reinforcement placed at arbitrary angles and depths within the slab
4. To be subjected to transverse concentrated and patch loads, i.e. perpendicular to the plane of the slab, and concentrated in-plane loads, i.e. that will produce axial forces in the slab and moments
5. To fail by flexure

1.2 The Scope of the Reported Investigation

The following items have been studied within the framework of the investigation and are presented in this report:

1. An analytical modeling of reinforced concrete slabs using the finite element method
2. A biaxial failure envelope together with appropriate stress-strain laws used to develop constitutive relations, i.e. stress-strain relations, for concrete
3. An analysis technique using a piecewise linear tangent stiffness, incremental iterative approach
4. A comparison for verification with the results of seven laboratory tests reported in the literature

1.3 Requirements Placed on Analytic Model

The model used in this analysis must adequately reflect the behavior of eccentrically stiffened plate systems (Refs. 44,45). This requires the inclusion of three types of structural behavior: out-of-plane behavior, in-plane behavior and coupling behavior. The out-of-plane response of either isolated reinforced concrete slabs or bridge deck slabs is its flexural behavior produced by loads perpendicular to the plate or by edge moments. The in-plane behavior is a membrane stress state. This may be produced by loads or displacements acting parallel to the plane of the plate, or in the case of bridge decks, by the action of the slab as the compression flange of composite beams. The coupling response is an interaction between the in-plane and out-of-plane responses, that is the change in flexural response due to the presence of membrane forces and vice versa.

Coupling will be demonstrated through an example based on the response of a beam. The beam will have three displacements: an axial extension, U , a bending displacement, W , and a bending rotation which is a derivative of W . The strain at any point in the beam can be computed from Eq. 1.1 (Ref. 19), if the cross-sectional axes are principal axes:

$$\epsilon = \frac{dU}{dX} - z \frac{d^2W}{dX^2} \quad (1.1)$$

The uniaxial stress associated with combined bending and axial load can be given by Eq. 1.2

$$\sigma = E\epsilon = E \left(\frac{dU}{dX} - z \frac{d^2W}{dX^2} \right) \quad (1.2)$$

The normal force and bending moment are found by appropriate integrations over the axes noting that cross-sectional axis, z , is not a function of the position along the length of the beam described by coordinate x .

$$N = \int \sigma \, dA = \int E \frac{dU}{dX} \, dA - \int E Z \frac{d^2W}{dX^2} \, dA \quad (1.3)$$

$$M = \int \sigma Z \, dA = \int E Z \frac{dU}{dX} \, dA - \int E Z^2 \frac{d^2W}{dX^2} \, dA \quad (1.4)$$

The only way that coupling terms which involve "EZ" can drop out is if the axis defined by $Z = 0$ is at the centroid of the cross-sectional stiffness. In the case of an elastic beam under bending about a principal axis it is always possible to find a point such that $\int EZdA = 0$. Likewise for a beam undergoing symmetric nonlinear flexural response about a principal axis this is also possible. But for a beam which has an unsymmetric distribution of area or material properties or has different properties in tension and compression, or is under the nonlinear action of a moment and axial force there is no such point. In general, the strain at any point will involve a combination of bending and axial contribution and is said to be coupled. Thus, a nonlinear reinforced concrete beam which exhibits nonlinear material behavior will always be coupled. The same phenomenon exists in the nonlinear response of certain plate systems, such as reinforced concrete plates and eccentrically stiffened plates, but is much more complicated. This will be discussed further in Chapter 3.

The analytic model must be capable of producing the full range response of an isolated slab and be applicable to a similar analysis of bridge superstructures. A full range response covers not only the initial elastic response and an estimated ultimate load but also the nonlinear response in between. A nonlinear type of analysis will allow an assessment of the damage to the slab corresponding to some load level as would

be required in an overload analysis (Refs. 23 and 44). An elastic analysis or an ultimate strength analysis will not allow for the assessment of damage for a load between the last elastic load and the ultimate load.

Nonlinear material properties will be required in order to obtain the full range response. In the case of slabs this will require a nonlinear stress-strain relation and failure criteria which are both based on multiaxial stress states. The analysis technique being reported will include the cracking and crushing of concrete and the yielding of reinforcing bars.

The analysis technique should be capable of handling a wide range of load configurations. This is especially important when considering application to the overload response of beam slab bridges. The size, shape and load distribution of overload vehicles are not standardized and can be expected to vary from case study to case study.

It is not expected that the reinforced concrete deck slabs on beam-slab bridges will buckle out of their plane. Therefore, the analysis technique being reported will not consider buckling phenomenon.

1.4 Previous Studies

Numerous investigations have been conducted on linear elastic analysis and ultimate strength analysis of plates. The methods utilized in these investigations can permit only the study of the load deflection history from the unloaded state up to the occurrence of the first inelastic response (linear elastic analysis), or definition of the load corresponding

to the peak of the load deflection curve (ultimate strength analysis). The primary interest of the reported study lies in the determination of full load-deflection history from the unloaded state up to the ultimate load level (Refs. 4,42,43,44). Therefore, the literature survey will be restricted to the techniques and investigations which can be or have been applied to the determination of the full load-deflection history.

The analytical modeling of slabs and the methods of analysis employed by previous investigators can be grouped under three distinct categories: (1) Finite Difference Technique, (2) Lumped Parameter Technique, and (3) Finite Element Method. The inclusion of the material nonlinearities into analysis schemes has proceeded along two main paths: (1) the use of an assumed moment-curvature relationship for the given cross-section, and (2) the use of an assumed stress-strain characteristic for the material and the adoption of a failure surface (Ref. 45).

The methods of modeling and analysis will be discussed with respect to the requirements of reinforced concrete slab analysis and more specifically their applicability to the bridge overload problem in Section 1.5. In general it can be stated that some of the above techniques have pronounced drawbacks in their applicability to the bridge overload problem, regardless of their simplicity in the analysis of certain simple configurations, e.g. moment-curvature approach as used for one way slabs made of mild steel.

The finite difference technique has been applied to the inelastic analysis of plates by relatively few researchers (Refs. 5 and 47). This

has been due to the complexities in establishing either the appropriate nonlinear differential equation, or the assignment of proper stiffness properties in a piecewise linear incremental solution. Furthermore, the manual algebraic operations required and the coding of these operations for computer based solutions have always been discouraging. This approach is further complicated in bridge overload problems by the necessity to solve coupled in-plane and out-of-plane differential equations which is discussed in Section 1.3. This aspect alone necessitates the adoption of a solution technique other than finite differences.

Some of the complexities involved in the finite difference technique have been eliminated through the use of the lumped parameter technique. Lopez and Ang (Ref. 29) applied this method to steel plates. However, its applicability to reinforced concrete slabs, and especially to bridge overload analysis, presents a major problem, whose accuracy, generality and ease of usage have not been demonstrated as yet.

The finite element method has been extensively used in the analysis of steel and reinforced concrete plates (e.g. Refs. 1, 9, 10, 41, 44 and 48). Most of the early investigations were confined to plates made of elastic-perfectly-plastic materials, i.e. mild steel (Ref. 44). A necessary feature of the application of the finite element method as in previously described methods, is to provide a way of introducing material nonlinearities into the generation of the stiffness matrix via moment curvature or stress-strain relationships. This aspect will be treated in detail in Chapter 2. The use of moment curvature relations for the reinforced concrete slabs and the bridge deck requires the use of

moment-thrust-curvature relations due to the presence of axial forces in the bridge superstructure (Ref. 45). Furthermore, the biaxial, i.e. longitudinal and transversal bending of the bridge slab requires the adoption of two dimensional moment-curvature relationships. Presently relationships capable of defining two dimensional moment-thrust-curvature relationships are not developed enough for general usage.

The basic stress-strain relationships for concrete of various strengths and for steel reinforcing bars have been well defined and will be discussed further in Chapter 3 (Refs. 7, 19, 21, 24 and 27). Therefore the formulations that make use of these fundamental relationships are more reliable and applicable to a wide variety of slab bending problems, as opposed to the use of moment-curvature relationships. The use of material stress-strain relationships requires the adoption of a modeling scheme which can account for the penetration of the nonlinearity through the depth of the slab. This has been accomplished by the use of layering of the slab (Fig. 2). Excellent agreement has been noted in the previous investigations that utilized this approach (Refs. 2, 11, 12, 19, 20, 21, 22, 23, 26, 43, 45 and 46).

An extensive survey of the literature has indicated that so far no analytical study has been undertaken to predict the full inelastic response of beam slab bridges (Refs. 45 and 47). Similarly most of the studies that have been undertaken to predict the inelastic response of slabs did not use a model which was general enough to permit the extension or modification of the analysis scheme to bridges, e.g. exclusion of the in-plane behavior of the slab. Furthermore, the nature of the problem

requires solution of a large system of simultaneous equations many times. This requires the use of large scale digital computers. Consequently most of the investigations have been undertaken within the last decade (Refs. 44, 45 and 47).

1.5 Analytical Model

The analysis technique reported herein has been designed such that it will permit the interfacing of this work with the completed study on the inelastic response of prestressed concrete beams (Fig. 1; Refs. 19 and 23). Thus, the combination of these studies will be able to predict the overload response of beam-slab highway bridges. It has been observed that even though the dominant slab nonlinearity is due to flexural response, the in-plane, i.e. membrane, forces and deformation of the slab must be considered because of their effect on the total response (Refs. 12 and 26). It has also been observed that the coupling phenomenon is extremely important for the correct prediction of the inelastic response of the slab (Refs. 11, 12, 26 and 46). Therefore the analytical derivations have been carried out including coupling.

The slab is subdivided into finite elements which are interconnected at node points. The finite elements are further subdivided into layers through their thickness. Each layer is assumed to be in the state of plane stress. It is also assumed that the inelastic response and the progressive collapse of the slab is due to the flexural behavior and its associated in-plane and coupling behavior. Punching shear of the slab due to an overload vehicle has not been considered (Ref. 18.)

2. THEORETICAL ANALYSIS

2.1 Introduction

The slab analysis procedure being reported is based on the finite element method. A complete treatment of the finite element method can be found in numerous books on the subject (Refs. 13, 41 and 48). Therefore only the major concepts and necessary steps related to this research will be presented in Section 2.3.

The characteristics of the analytic model, i.e., the mathematical representation of the real structure, must be chosen to adequately describe the physical model. In the current context it is desired to describe the response of prestressed and reinforced concrete I-beam highway bridge superstructures subjected to an overload. Therefore the analytic model should satisfy the following requirements:

1. The flexural response, assumed to be the primary load carrying action in the slab as well as that of the complete superstructure, must be obtained.
2. The model must permit consideration of multi-axial plate bending.
3. The slab model must be applicable to the analysis of a highway bridge superstructure modeled as an eccentrically stiffened plate.
4. Eccentrically stiffened slabs can develop inplane stresses of the same magnitude or even greater than the bending stresses. Therefore the inplane stiffness of the slab must be considered.

5. Membrane boundary conditions corresponding to these inplane forces (see Chapter 1) are important in reinforced concrete slab analysis and must be considered (Refs. 11, 12, 26 and 46).
6. The slab model must allow for the inclusion of both concrete and steel.
7. Material nonlinearities due to cracking and crushing of the concrete and yielding of the steel must be considered.
8. In-plane shear deformation and effects have been considered.

2.2 Assumptions

Several assumptions are employed in the development of the analytical model. These assumptions and associated consequences will be discussed in the following paragraphs.

2.2.1 Geometry Restrictions

The overall investigation is restricted to right angle bridge superstructures. Consequently this analysis technique for reinforced concrete slabs has been developed for rectangular slabs. The same principles could be extended to non-rectangular slabs. The finite element chosen as the basic modeling unit is the rectangular plate bending element shown in Fig. 3.

2.2.2 Assumptions Regarding Strain Distribution

Kirchoff's assumption that plane sections normal to the middle surface of the plate before deformation remain plane and normal after

deformation is employed. Application of Kirchoff's assumption is a usual practice in bending solutions for thin plates. A thin plate is defined as a plate whose length and width dimensions are considerably greater than its thickness. It is also assumed that the slab does not change thickness due to the applied forces. Thus the strains and stresses normal to the plane of the slab are neglected. Application of Kirchoff's assumption and the elimination of the normal strain offer the following simplifications:

1. The reduction of a three dimensional continuum problem requiring six stress components to define the state of stress at a point to a two dimensional plate bending problem involving only three stress components (Refs. 41,48).
2. The strains at any depth in the plate can be computed from the displacements of the middle plane of the plate.

2.2.3 Small Deformations

The in-plane and bending displacements are assumed to be small in comparison to the dimension of the slab. This implies that the rectangular finite elements are still rectangular after deformation. Furthermore the geometry of the element need not be updated as the analysis proceeds.

2.2.4 Small Strains

The reinforced concrete slabs and highway bridge superstructures are assumed to be subjected to small strains. Thus the usual linear strain-displacement relations can be used as opposed to the more involved nonlinear equations necessary for the large strain formulations (Refs. 41,48).

2.2.5 Layering

The inclusion of material nonlinearities will cause the stiffness of the finite element to vary with depth. These material nonlinearities including cracking and crushing of the concrete and yielding of the steel are inherent in the stress-strain relations. The existence of both steel and concrete in the same finite element also causes a variation of stiffness through the depth of the element. To facilitate the computation of the element stiffness, the finite element will be divided into a series of layers through the depth (Figs. 2 and 3). The stiffness of the element will then be obtained by a summation of the stiffness of these layers. The stresses within a particular layer will be assumed to be constant within the layer for the purpose of computing the stiffness of each layer (Fig. 4B). Thus the stress field through the depth of the slab will vary in a step-like manner. Increasing the number of layers will improve the representation of the stress field.

2.3 Review of the Finite Element Method

The finite element method requires that the continuum be divided into an assemblage of subunits called finite elements. The elements are considered to be interconnected at discrete points called node points. Forces, displacements and coordinates for a typical node is shown in Fig. 3. In this context the continuum is a reinforced concrete slab. The stiffness properties of the elements can be found using the principles of the finite element method. The result is a set of equilibrium equations relating node point forces to node point displacements:

$$\{F^e\} = [k^e] \{\delta^e\} \quad (2.1)$$

Where: $\{F^e\}$ = a vector of applied elemental nodal forces

$[k^e]$ = the element stiffness matrix

$\{\delta^e\}$ = a vector of nodal displacements

Assembly of the elements to form the entire structural system results in a set of nodal equilibrium equations usually referred to as the displacement method of analysis. These equations are shown in Eq. 2.2:

$$\{F\} = [K] \{\delta\} \quad (2.2)$$

Where: $\{F\}$ = a vector of the forces applied to the structure at the nodes

$[K]$ = the assembled structural stiffness matrix

$\{\delta\}$ = a vector of node point displacements

The unknown node point displacements, $\{\delta\}$, are obtained by solving this set of simultaneous equations.

It can be shown that the element stiffness matrix can be evaluated using Eqs. 2.3a or b, (Refs. 13, 41 and 48)

$$[k^e] = [C]^{-1T} \int_V [Q]^T [D] [Q] \text{dvol} [C]^{-1} \quad (2.3a)$$

$$[k^e] = \int_V [B]^T [D] [B] \text{dvol} \quad (2.3b)$$

This presentation will be restricted to an explanation of the matrices in Eq. 2.3 rather than their derivation.

The stress-strain relationships for a layer can be expressed by an elasticity matrix, [D], as shown in Eq. 2.4:

$$\{\sigma\} = [D] \{\epsilon\} \quad (2.4)$$

The displacements within an element are assumed to be adequately described by a polynomial function of position within the element and initially unknown constants. This combination of functions and constants will be called a displacement function. Thus it is possible to define the displacements at any point within the element as:

$$\{\Delta(x,y)\} = [P(x,y)] \{\alpha\} \quad (2.5)$$

in which: $\{\Delta(x,y)\}$ = displacements at any position within the element defined by the coordinates (x,y)

$[P(x,y)]$ = particular functions of x and y, or their derivatives, used to describe the displacement fields

$\{\alpha\}$ = constant coefficients of the displacement functions

The individual $\{\alpha\}$ are evaluated using the boundary conditions given by the displacements at the node points of the element:

$$\{\delta^e\} = [C] \{\alpha\} \quad (2.6)$$

[C] is populated by substituting the coordinates of each node point, (x_n, y_n) , into Eq. 2.5 where:

$$\{\delta^e\} = \{\Delta(x_n, y_n)\} \quad (2.7)$$

$$[C] = [P(x_n, y_n)]$$

Solving Eq. 2.6 for the constant coefficients lead to:

$$\{\alpha\} = [C]^{-1} \{\delta^e\} \quad (2.8)$$

The differential operators necessary to define the strains in Eq. 2.4 in terms of the displacement fields in Eq. 2.5 will be called $[\Gamma]$.

Thus:

$$\{\epsilon\} = [\Gamma] \{\Delta(x,y)\} \quad (2.9a)$$

Substitution of Eq. 2.5 results in:

$$\{\epsilon\} = [\Gamma] [P(x,y)] \{\alpha\} = [Q] \{\alpha\} \quad (2.9b)$$

$[Q]$ is a connection matrix relating $\{\epsilon\}$ to $\{\alpha\}$ within the element. Substitution of Eq. 2.8 yields:

$$\{\epsilon\} = [Q] [C]^{-1} \{\delta^e\} = [B] \{\delta^e\} \quad (2.9c)$$

Matrix $[B]$ relates the strains within the element to the nodal displacements.

A summary of the necessary steps in the finite element method to formulate the elemental stiffness matrix is as follows:

1. Choose displacement functions and formulate the displacement field (Eq. 2.5).
2. Express the node point displacements in terms of the constant coefficients by substituting the known nodal point locations into step 1 (Eq. 2.6).
3. Solve for $\{\alpha\}$ (Eq. 2.8).
4. Substitute $\{\alpha\}$ into step 1 (Eq. 2.5).

5. Identify the strain-displacement relations and perform the required differentiation of the displacement function (Eq. 2.9a, 2.9b or 2.9c).
6. Find the stress-strain relationship, $[D]$ (Eq. 2.4).
7. Substitute the necessary matrices into Eq. 2.3 and perform the indicated integration. The result will be the element stiffness matrix.

2.4 Element Stiffness Formulation

The necessary steps in the formulation of the finite element method were discussed, abstractly, in Section 2.3. These steps will be discussed in detail with respect to the nonlinear analysis of reinforced concrete slabs in the following sections.

2.4.1 Plate Bending and Inplane Displacement Functions

The purpose of this section is to present the displacement functions and describe the displacement field, $\{\Delta(x,y)\}$.

Displacement functions are chosen so that the deformation of the finite element can be adequately described. These displacement functions are polynomial expressions in terms of the (x,y) inplane coordinate locations and unknown constants. As presented in Chapter 1 both the inplane and bending displacements must be considered.

The bending deformation of a plate can be fully described by the vertical displacement W , of the middle plane of the plate via assumptions

presented in Sec. 2.2. The bending deformation will consist of the vertical displacement, W , the rotation about the x -axis, θ_x , and the rotation about the y -axis, θ_y . The rotations may be obtained by differentiating the vertical displacement. Thus the displacement field which describes the bending deformations can be expressed in vector form as:

$$\begin{Bmatrix} W \\ \theta_x \\ \theta_y \end{Bmatrix} = \begin{Bmatrix} W \\ \frac{\partial W}{\partial y} \\ -\frac{\partial W}{\partial x} \end{Bmatrix} \quad (2.10)$$

The ACM-Adini, Clough, Melosh (Ref. 1) plate bending finite element will be used in this study. A review of the finite element displacement functions and the resulting stiffness matrices for the analysis of plate bending has been given by Clough and Tocher (Ref. 9) and Wegmuller and Kostem (Refs. 43, 44 and 45). They concluded that the ACM rectangular finite element gives very satisfactory results. By increasing the number of ACM finite elements used to model a particular continuum an apparent convergence to classical solutions has been demonstrated for several example problems (Refs. 9 and 44). The ACM displacement function expresses the vertical displacement, W , as a twelve term polynomial (Refs. 1, 9, 45 and 48).

$$\begin{aligned} W(x,y) = & A_1 + A_2 x + A_3 y + A_4 x^2 + A_5 xy + A_6 y^2 + A_7 x^3 + A_8 x^2 y + A_9 xy^2 \\ & + A_{10} y^3 + A_{11} x^3 y + A_{12} xy^3 \end{aligned} \quad (2.11)$$

The inplane deformation is characterized by two displacement functions U and V. U is defined as the inplane displacement directed along the x-axis and V is defined as the inplane displacement directed along the y-axis. The inplane displacement polynomials shown below have been presented by Clough (Ref. 8):

$$\begin{aligned} U(x,y) &= B_1 + B_2 x + B_3 y + B_4 xy \\ V(x,y) &= B_5 + B_6 x + B_7 y + B_8 xy \end{aligned} \tag{2.12}$$

Previous studies using these polynomials have been successfully carried out (Refs. 44 and 45).

Nodal points are considered to be located at the four corners of the rectangular finite element positioned on the reference plane in the middle of the plate. Nodal points are designated by the letters, I, J, K, L as indicated in Fig. 3. Thus all nodal point displacements refer to reference plane deformations. The terms "reference plane" and "middle plane" are considered to be interchangeable in this report. The total displacement vector is described in terms of five displacements for each nodal point, i.e. two inplane displacements and three bending displacements. The total number of displacements per finite element is twenty, i.e. four nodes at the corners with five degrees of freedom per node.

The displacement functions $W(x,y)$, $V(x,y)$ and $U(x,y)$ can be substituted into the displacement vector thereby defining the displacement field $\{\Delta(x,y)\}$ for any location given by the coordinates (x,y) :

$$\{\Delta(x,y)\} = \begin{Bmatrix} U \\ V \\ W \\ \theta_x \\ \theta_y \end{Bmatrix} = \begin{Bmatrix} U \\ V \\ W \\ \frac{\partial W}{\partial y} \\ -\frac{\partial W}{\partial x} \end{Bmatrix} \quad (2.13)$$

Thus Eq. 2.5 can be established once the displacement functions have been chosen.

The displacement field $\{\Delta(x,y)\}$, can be partitioned by separating it into those involving only inplane displacements and those involving only bending displacements:

$$\{\Delta(x,y)\} = \begin{Bmatrix} \Delta_u(x,y) \\ \text{-----} \\ \Delta_\phi(x,y) \end{Bmatrix} = \begin{Bmatrix} U(x,y) \\ V(x,y) \\ \text{-----} \\ W(x,y) \\ \theta_x(x,y) \\ \theta_y(x,y) \end{Bmatrix} \quad (2.14)$$

This will simplify further discussion of the stiffness matrices in the following sections. The subscripts u and ϕ refer to the inplane displacements and the bending displacements respectively. Substituting the displacement functions (Eqs. 2.11 and 2.12) into the right-hand side of the above equation leads to Eq. 2.15:

$$\{\Delta(x,y)\} = \begin{Bmatrix} \Delta_u(x,y) \\ \Delta_\phi(x,y) \end{Bmatrix} = \begin{bmatrix} P_u(x,y) & 0 \\ 0 & P_\phi(x,y) \end{bmatrix} \begin{Bmatrix} B \\ A \end{Bmatrix} \quad (2.15)$$

where $[P_u(x,y)]$ and $[P_\phi(x,y)]$ correspond to inplane and bending polynomial expression respectively. The vector $\begin{Bmatrix} B \\ A \end{Bmatrix}$ is the partitioned $\{\alpha\}$ vector

while the matrix $\begin{bmatrix} P_u(x,y) & 0 \\ 0 & P_\phi(x,y) \end{bmatrix}$ is the partitioned $[P(x,y)]$ matrix.

2.5 Strain-Displacement Relations

The strain-displacement relations are derived using the thin-plate small-deflection theory as mentioned in Section 2.2. The strain-displacement relationships for a point at a distance z from the reference plane are:

$$(\epsilon_x)_z = \frac{\partial U_z}{\partial x} \quad (2.16a)$$

$$(\epsilon_y)_z = \frac{\partial V_z}{\partial y} \quad (2.16b)$$

$$(\gamma_{xy})_z = \frac{\partial U_z}{\partial y} + \frac{\partial V_z}{\partial x} \quad (2.16c)$$

Where: z = distance of point under consideration from the reference plane

U_z = displacement in the x-direction at any depth, z

V_z = displacement in the y-direction at any depth, z

$(\epsilon_x)_z$ = strain in the x-direction at depth z

$(\epsilon_y)_z$ = strain in the y-direction at depth z

$(\gamma_{xy})_z$ = shear strain at depth z

The prescribed displacement functions correspond to reference plane displacements. The displacements U_z and V_z must be expressed in terms of these middle plane displacements. Kirchoff's assumption of plane sections permits the displacement for a point located at any distance, z, away from the reference plane to be expressed in terms of the inplane displacements of the reference plane plus the product of the rotations about the reference plane and the distance z as shown in Eqs. 2.17:

$$U_z = U - z \frac{\partial W}{\partial x} \quad (2.17a)$$

$$V_z = V - z \frac{\partial W}{\partial y} \quad (2.17b)$$

$$W_z = W \quad (2.17c)$$

Substituting Eqs. 2.17a and b into Eqs. 2.16a, b and c leads to Eq. 2.18 in which $\{\epsilon\}_z$ represents the strain at depth z:

$$\{\epsilon\}_z = \begin{Bmatrix} \epsilon_x \\ \epsilon_y \\ \gamma_{xy} \end{Bmatrix}_z = \begin{Bmatrix} \frac{\partial U}{\partial x} \\ \frac{\partial V}{\partial y} \\ \frac{\partial U}{\partial y} + \frac{\partial V}{\partial x} \end{Bmatrix} + z \begin{Bmatrix} -\frac{\partial^2 W}{\partial x^2} \\ -\frac{\partial^2 W}{\partial y^2} \\ -2 \frac{\partial^2 W}{\partial x \partial y} \end{Bmatrix} \quad (2.18)$$

In the equation above, the strain vector $\{\epsilon\}_z$ is separated into inplane and bending contributions. Identifying the required differentials of Eq. 2.18 to be $[\Gamma_u]$ and $[\Gamma_\phi]$, corresponding to the inplane and bending functions respectively, leads to Eq. 2.19:

$$\{\epsilon\}_z = [\Gamma_u] [P_u(x,y)] \{B\} + z [\Gamma_\phi] [P_\phi(x,y)] \{A\} \quad (2.19)$$

Performing the differentiation results in the following equation:

$$\{\epsilon\}_z = [Q_u] \{B\} + z [Q_\phi] \{A\} \quad (2.20)$$

Where:

$$[Q_u] = [\Gamma_u] [P_u(x,y)]$$

$$[Q_\phi] = [\Gamma_\phi] [P_\phi(x,y)]$$

The strains are now expressed in terms of the matrices $[Q_u]$ and $[Q_\phi]$, which are obtained by differentiating the functions $[P_u(x,y)]$, $[P_\phi(x,y)]$, and multiplying by the associated constant terms $\{B\}$ and $\{A\}$.

As indicated by Eq. 2.8, the unknown polynomial coefficients in Eq. 2.20 can be related to the nodal point displacement vector $\{\delta^e\}$. The inplane and bending displacement fields have been previously defined as $\{\Delta_u(x,y)\}$ and $\{\Delta_\phi(x,y)\}$ respectively. Substitution of the nodal point coordinates (x_n, y_n) into the above displacement fields result in the following expressions:

$$\{\delta_u^e\} = \{\Delta_u(x_n, y_n)\} = [C_u] \{B\} \quad (2.21a)$$

$$\{\delta_\phi^e\} = \{\Delta_\phi(x_n, y_n)\} = [C_\phi] \{A\} \quad (2.21b)$$

Where: $[C_u] = [P_u(x_n, y_n)]$

$$[C_\phi] = [P_\phi(x_n, y_n)]$$

$\{\delta_u^e\}$ and $\{\delta_\phi^e\}$ are the inplane and bending nodal point displacements. Solving for the vectors $\{A\}$ and $\{B\}$ leads to:

$$\{A\} = [C_\phi]^{-1} \{\delta_\phi^e\} \quad (2.22a)$$

$$\{B\} = [C_u]^{-1} \{\delta_u^e\} \quad (2.22b)$$

Substituting Eqs. 2.22a and b into the strain-displacement relation of 2.20 yields Eq. 2.23:

$$\{\epsilon\}_z = [Q_u] [C_u]^{-1} \{\delta_u^e\} + z [Q_\phi] [C_\phi]^{-1} \{\delta_\phi^e\} \quad (2.23)$$

Equation 2.23 is analogous to Eq. 2.9c and represents the strain displacement equation relating the strains at a distance z from the middle plane to the basic set of unknowns, i.e. the nodal point displacements. For convenience, the $[B_u]$ and $[B_\phi]$ matrices, defined in Eqs. 2.24a and b respectively, are substituted into Eq. 2.23 resulting in a shorter expression for the strain which is given in Eq. 2.24c:

$$[B_u] = [Q_u] [C_u]^{-1} \quad (2.24a)$$

$$[B_\phi] = [Q_\phi] [C_\phi]^{-1} \quad (2.24b)$$

$$\{\epsilon\}_z = [B_u] \{\delta_u^e\} + z [B_\phi] \{\delta_\phi^e\} \quad (2.24c)$$

2.6 Layering

Multiaxial bending of the slab causes a continuously varying biaxial stress field within the concrete as shown in Fig. 4A. The elasticity matrix $[D]$, for a non-linear material depends on the stress level, and, therefore, will also vary throughout the finite element. In order to evaluate the volume integral of Eq. 2.3, $[D]$ must be defined over the volume of the element. Since the explicit definition of the elasticity matrix for reinforced concrete under biaxial stress is prohibitively complex for solution purposes, this stiffness matrix is evaluated by a combination of explicit integration and numerical integration. The numerical integration is performed using a summation process, as explained in the following paragraphs.

A finite element will be divided into a series of layers as shown in Fig. 3. This idealization facilitates inclusion of material nonlinearities through the depth, i.e. layer to layer, and through the plane of the slabs, i.e. element to element. Each layer can have its own elasticity relations, $[D_i]$, which is dependent upon the representative state of stress existing within that layer, $\{\bar{\sigma}_i\}$. This implies that there is a constant state of stress and stiffness within any particular layer and that there is a step-like variation of stress and stiffness properties through the depth of the finite element as shown in Fig. 4B. A state of plane stress is assumed to exist within each layer.

The representative state of stress in a layer is taken to be $\{\bar{\sigma}_i\}$, the integrated average stress for the mid-plane of that particular

layer. The location of the mid-plane of layer-1 is defined by the distance \bar{z}_1 from the reference plane of the slab. The integrated average stress can be expressed in terms of the integrated average strain, $\{\bar{\epsilon}\}_{\bar{z}_1}$ using Eq. 2.25:

$$\{\bar{\sigma}_1\} = [D_1] \{\bar{\epsilon}\}_{\bar{z}_1} \quad (2.25)$$

By employing Eq. 2.24c the integrated average strain may be defined as:

$$\{\bar{\epsilon}\}_{\bar{z}_1} = \frac{1}{\text{Area}} \iint \left[\begin{array}{c} [B_u] \\ \bar{z}_1 [B_\phi] \end{array} \right] dx dy \left\{ \begin{array}{c} \delta u^e \\ \delta \phi^e \end{array} \right\} \quad (2.26a)$$

Where: $\text{AREA} = \int_{-b}^b \int_{-a}^a dx dy = 4ab$ (2.26b)

Substitution of Eq. 2.26a into Eq. 2.25 results in an equation defining the integrated average stress:

$$\{\bar{\sigma}_1\} = \frac{1}{\text{Area}} [D_1] \iint \left[\begin{array}{c} [B_u] \\ \bar{z}_1 [B_\phi] \end{array} \right] dx dy \left\{ \begin{array}{c} \delta u^e \\ \delta \phi^e \end{array} \right\} \quad (2.27)$$

Once the representative state of stress, given by $\{\bar{\sigma}_1\}$, is known the elasticity matrix, $[D_1]$, can be determined for various regions or layers. Numerical integration can then be performed and the stiffness matrix can be evaluated. The elasticity matrix is a function of $\{\bar{\sigma}_1\}$ which is, in turn, dependent on the elasticity matrix. Thus the stiffness matrix is stress-dependent and a step-by-step solution scheme is required. This will be discussed in Section 2.9.

Reinforcing bars are treated just the same as any other layer in the summation process but of course a uniaxial elasticity relationship

is used. A separate steel layer is assumed for each set of reinforcing bars placed at a particular depth and at a particular angle to the x-axis (as illustrated in Fig. 5). Idealizing the reinforcing bars as a layer and not as individual entities requires the computation of an equivalent steel layer thickness. The equivalent thickness of a steel layer must be such that the total area of steel in a cross-section perpendicular to the bar direction remains the same. The equivalent thickness for a steel layer can be represented by Eq. 2.28:

$$T_s = \frac{A_s}{b_s} \quad (2.28)$$

where A_s indicates the area of a reinforcing bar and b_s is the bar spacing. This approach to modeling steel reinforcement allows consideration of reinforcing systems which have variable bar spacing and size from element to element and are placed in arbitrary directions and depths within the slab.

Progressive cracking and crushing of the concrete and yielding of the steel through the depth of the slab during loading can be monitored by obtaining the stress history for each layer. The direction of principal stress that causes crushing or cracking of a particular concrete layer is not predefined by previous cracking or crushing and may vary from layer to layer through the depth of the slab.

2.7 Element Stiffness Matrix

From Eq. 2.3b the element stiffness matrix is defined as:

$$[k^e] = \int_V [B]^T [D] [B] dvol \quad (2.3b)$$

in which matrix [B] relates the strains to the nodal point displacements. Comparison of Eqs. 2.9c and 2.24c shows that Eq. 2.3b can be rewritten, in this context, as Eq. 2.29a:

$$[k^e] = \int_{\text{vol}} \begin{bmatrix} [B_u]^T \\ z[B_\phi]^T \end{bmatrix} [D] \begin{bmatrix} [B_u] & z[B_\phi] \end{bmatrix} d\text{vol} \quad (2.29a)$$

Performing the indicated matrix multiplication results in Eq. 2.29b:

$$[k^e] = \int_{\text{vol}} \begin{bmatrix} [B_u]^T [D] [B_u] & [B_u]^T [D] z [B_\phi] \\ [B_\phi]^T [D] z [B_u] & [B_\phi]^T [D] z^2 [B_\phi] \end{bmatrix} d\text{vol} \quad (2.29b)$$

The submatrices of Eq. 2.29b will be defined as shown below for convenience:

$$[k_{uu}] = \int_{\text{vol}} [B_u]^T [D] [B_u] d\text{vol} \quad (2.30a)$$

$$[k_{u\phi}] = \int_{\text{vol}} [B_u]^T [D] z [B_\phi] d\text{vol} \quad (2.30b)$$

$$[k_{\phi\phi}] = \int_{\text{vol}} [B_\phi]^T [D] z^2 [B_\phi] d\text{vol} \quad (2.30c)$$

$[k_{uu}]$ is the inplane stiffness matrix relating the inplane forces to the inplane displacements. $[k_{\phi\phi}]$ is the bending stiffness matrix relating bending forces to bending displacements. The off diagonal submatrix, $[k_{u\phi}]$, is the coupling stiffness matrix which interrelates the bending and inplane actions. The importance of the coupling stiffness terms has been discussed in Chapter 1.

As was noted in the discussion of layering in Section 2.6, the state of stress, and hence the terms of the elasticity matrix are assumed to be constant throughout a particular layer. Therefore, $[D]$ is not dependent on x or y coordinates. Likewise, since the displacement functions were independent of the coordinate z , $[B_u]$ and $[B_\phi]$ are also independent of z . Thus the integrations indicated in Eqs. 2.30 may be separated as shown in Eq. 2.31:

$$[k_{uu}] = \iint_{yx} [B_u]^T \left(\int_z [D] dz \right) [B_u] dx dy \quad (2.31a)$$

$$[k_{u\phi}] = \iint_{yx} [B_u]^T \left(\int_z [D] z dz \right) [B_\phi] dx dy \quad (2.31b)$$

$$[k_{\phi\phi}] = \iint_{yx} [B_\phi]^T \left(\int_z [D] z^2 dz \right) [B_\phi] dx dy \quad (2.31c)$$

As also mentioned in Section 2.6 a summation process will be used to approximate the integration over z . This will be done by integrating over each layer and then summing the results and storing them in the appropriate $[D_{uu}]$, $[D_{u\phi}]$ or $[D_{\phi\phi}]$ matrix. Thus the terms $[D_{uu}]$, $[D_{u\phi}]$ and $[D_{\phi\phi}]$ may be defined as shown below:

$$[D_{uu}] = \int_z [D] dz = \sum_{i=1}^L [D_i] (Z_{i+1} - Z_i) \quad (2.32a)$$

$$[D_{u\phi}] = \int_z [D] z dz = \frac{1}{2} \sum_{i=1}^L [D_i] (Z_{i+1}^2 - Z_i^2) \quad (2.32b)$$

$$[D_{\phi\phi}] = \int_z [D] z^2 dz = \frac{1}{3} \sum_{i=1}^L [D_i] (Z_{i+1}^3 - Z_i^3) \quad (2.32c)$$

Z_{i+1} and Z_i delineate the boundaries of layer i . L is the total number of layers. $[D_{uu}]$, $[D_{u\phi}]$ and $[D_{\phi\phi}]$ are often called, respectively, the inplane rigidity, the coupling rigidity and the bending rigidity.

Substitution of Eqs. 2.32 into Eqs. 2.31 results in the following expressions which can be explicitly integrated over the area of the elements:

$$[k_{uu}] = \iint_{yx} [B_u]^T [D_{uu}] [B_u] dx dy \quad (2.33a)$$

$$[k_{u\phi}] = \iint_{yx} [B_u]^T [D_{u\phi}] [B_\phi] dx dy \quad (2.33b)$$

$$[k_{\phi\phi}] = \iint_{yx} [B_\phi]^T [D_{\phi\phi}] [B_\phi] dx dy \quad (2.33c)$$

This integration leads to the force-displacement relations for the finite element given by Eq. 2.34:

$$\begin{Bmatrix} F_u^e \\ F_\phi^e \end{Bmatrix} = \begin{bmatrix} [k_{uu}] & [k_{u\phi}] \\ [k_{u\phi}]^T & [k_{\phi\phi}] \end{bmatrix} \begin{Bmatrix} \delta_u^e \\ \delta_\phi^e \end{Bmatrix} \quad (2.34)$$

$\{F_u^e\}$ and $\{F_\phi^e\}$ are, respectively, the inplane and bending forces applied to the nodes of the element. $\{\delta_u^e\}$ and $\{\delta_\phi^e\}$ are, respectively, the resulting inplane and bending displacements at the nodes of the element.

2.8 Assembly of the Global Stiffness Matrix

The individual element stiffness matrices are assembled to form the global stiffness matrix of the entire structure. This global stiffness

matrix relates the forces at the node points of the structure to the displacements of those node points. The process of assembly entails addition of the element stiffness terms which contribute to the same force-displacement location in the global stiffness matrix. The total force at a particular node is determined by adding up the contributing forces from the individual elements for that particular node. Thus the force-displacement relationship for the entire structure can be expressed as:

$$\{F_i\} = [K_{ij}] \{\delta_j\} \quad (2.35)$$

where i and j correspond to the various degrees of freedom at the node points. The subscript i indicates row positions in the force vector and stiffness matrix and j indicates row positions in the displacement vector and column locations in the stiffness matrix. Assembly procedures require that:

$$\{F_i\} = \sum_e \{F_i^e\} \quad (2.36a)$$

$$[K_{ij}] = \sum_e [k_{ij}^e] \quad (2.36b)$$

where the summation is carried out over all individual elements. The stiffness term k_{ij}^e in the above equation relates the force at node i to the displacement at node j for element e . Summing up the contributing stiffness terms from all elements as indicated in Eq. 2.36b gives the term K_{ij} which populates the (i,j) location in the global stiffness matrix. A solution for a structural system should satisfy compatibility and equilibrium. The assembly procedure guarantees displacement compatibility at

the node points. Equilibrium of forces at each node point is insured in the development of Eq. 2.3a.

2.9 Incremental Iterative Solution Technique

The nodal point forces are related to the nodal point displacements of the slab by a nonlinear system of equations, symbolically written as:

$$\{F\} = [K] \{\delta\} \quad (2.37)$$

where the global stiffness matrix, $[K]$, is a nonlinear function of the nodal point displacements, $\{\delta\}$. Expressing Eq. 2.37 in incremental form gives:

$$\dot{\{F\}} = [\bar{K}] \dot{\{\delta\}} \quad (2.38)$$

where the dot indicates an increment and $[\bar{K}]$ is the stiffness matrix at some stress level called a tangent stiffness matrix. $[\bar{K}]$ is assumed to be constant over an increment of load and the load-deflection history is obtained by adding up the increments of forces and displacements:

$$\{F\} = \Sigma \dot{\{F\}} \quad (2.39a)$$

$$\{\delta\} = \Sigma \dot{\{\delta\}} \quad (2.39b)$$

Thus the nonlinear response of the slab can be obtained in a piecewise-linear fashion by solving the system of linear equations given by Eq. 2.38 for each load step.

The elasticity matrix $[D_i]$ for each layer and thus the tangent stiffness matrix, $[\bar{K}]$, depends upon the current stress level. Therefore

an iterative procedure can be employed during each load step to obtain convergence of the displacement increment.

A failure criterion is needed in order to identify the onset of cracking or crushing within a layer. A biaxial failure envelope is used here and will be discussed in detail in Chapter 3. This failure envelope is shown in Fig. 9. The concept required in the current discussion is that some criteria must be applied to determine if cracking or crushing has occurred. An upper and a lower tolerance to the biaxial failure envelope is utilized. A load increment that produces a stress state outside the upper bound of the failure envelope will automatically be reduced so that the stress states of the next iteration, using the reduced force increment, will lie within the specified upper and lower bounds. Failure of the layer is deemed to occur if the stress state falls outside the lower bound to the failure envelope. Thus only a stress state that approximately satisfies the failure criteria to within the specified tolerance need be obtained.

A solution for an initial load vector which produces a stress field well within the elastic range is obtained. This initial solution is then scaled up to a specified percentage of the first cracking or first crushing load, whichever governs. A solution for an applied dead load can also be obtained. The dead load solution may reflect nonlinearities such as cracking or crushing of the concrete and yielding of the steel. The dead load stresses are considered in the initial scaling procedure. If a layer has cracked, crushed or yielded during the dead load solution procedure, then the initial scaling will not take place. After this

initial solution is obtained either an "incremental" or an "incremental-iterative" solution scheme may be chosen by the analyst. If the incremental-iterative option is chosen the following solution scheme is used until failure occurs:

1. Formulate the element stiffness matrices based on the current total stress level.
2. Form the global stiffness matrix by assembling the element stiffness matrices.
3. Solve for the displacement increment using the global stiffness matrix and the force increment. Next compute the strain and the stress increments.
4. If the displacement increment has converged to a specified tolerance go to step 7, otherwise continue.
5. If the stress state falls outside the upper tolerance set on the failure envelope then scale down the applied force increment such that the stress is between the upper and lower tolerances.
6. If the maximum number of iteration cycles has been reached go to step 7; otherwise go to step 1.
7. Unload the excess layer stresses and compute the corresponding fictitious force vector if applicable (Ref. to Chapter 3).
8. If the current total stress level has exceeded the lower tolerance on the failure envelope set the codes for newly cracked or crushed concrete layers and newly yielded steel layers.

9. Compute the total stress, strain, displacement, and force vectors by adding together the old totals and the current increments.
10. Apply a new force increment and go to step 1.

An initial stress and displacement increment of zero is chosen for each load step. Thus the first iteration within a load step uses an elasticity matrix based on the stress level of the previous load cycle.

If the incremental solution option is chosen, then steps 4, 5 and 6 are not employed and iteration within a load step does not take place. As the size of the fixed load increment used is reduced the incremental solution will approach that of the incremental-iterative solution. The advantage of the incremental solution procedure over the incremental-iterative procedure lies in the fact that less solution time is needed for the former than the latter. The disadvantage of the incremental solution procedure is that judgment and experience must be used in selection of the size of the fixed load increment.

3. MATERIAL BEHAVIOR

Structural analysis techniques require that some relation be made between stress and strain. This chapter will present the stress-strain relationships employed in the reported analysis scheme. The elasticity matrix, $[D]$, introduced in the previous chapter is populated using the stress-strain relationships developed in this chapter. As noted in Section 2.9, the theoretical analysis presented in Chapter 2 is actually applied in an incremental fashion. The stress-strain relations discussed in this chapter will sometimes involve both total stresses and strains and incremental stresses and strains. Incremental quantities will be distinguished by a dot over the appropriate symbol.

The material stress-strain relations, $[D]$, must be defined for both the steel reinforcing bars and the concrete before computing the element stiffness matrices. Concrete is a heterogeneous mixture of solids and gel with strength properties influenced by age, time under load, humidity, and temperature to name a few (Ref. 33). The behavior of concrete is also dependent on the state of stress existing within the material. Discontinuities due to micro-cracking and shrinkage cracks may be present in the concrete continuum even before load is applied to the structure (Refs. 14 and 33). Thus, any attempt to define the material stress-strain properties of concrete over a specified region of the structure should be considered as an idealized approximation and by no means exact.

Steel, on the other hand, can be considered to be a homogeneous material. The physical properties of steel are less dependent on environmental conditions than those of concrete.

3.1 Concrete Stress-Strain Relationships

A beam may be idealized as a one dimensional structural element in which bending about one axis produces a uniaxial state of stress. A slab on the other hand should be considered as a two dimensional structural element in which bending about two axes produces a biaxial state of stress (Fig. 4A). A limited number of experimental investigations of concrete behavior in the biaxial stress state have been carried out (Refs. 24, 27 and 32). These studies have covered the entire biaxial principal stress space consisting of the compression-compression region, the tension-tension region, and the compression-tension (or, conversely, tension-compression) region. These regions are shown in Fig. 6.

Equations for the biaxial principal stress-strain relations used in this investigation have been adopted from Liu (Refs. 27 and 28) and were extended to cover the nonlinear compression-tension and tension-compression regions. The idealized biaxial stress-strain curves have two basic forms: the nonlinear form and the linear form. The nonlinear equation is used for biaxial stress states where compression is dominant while the linear expression is used for biaxial stress states where tension is dominant. General nonlinear and linear stress-strain curves are indicated in Fig. 7. Figure 8 shows the approximate regions in the biaxial stress plane where the nonlinear and linear equations are applicable.

3.1.1 Nonlinear Stress-Strain Equation for Concrete

The nonlinear stress-strain curve for concrete assumed to apply in the reported study has the following form:

$$\sigma = \frac{A + B \epsilon E_c}{(1 - \nu\alpha)(1 + C\epsilon + D\epsilon^2)} \quad (3.1)$$

Where: σ = the stress in the principal direction of interest
 ϵ = the strain in direction of interest
 ν = Poisson ratio (taken to be 0.2 but other choices are also permissible)
 α = the ratio of the principal stress in the orthogonal direction to the principal stress in the direction of interest
 E_c = initial tangent modulus in uniaxial loading

A,B,C,D = curve parameters to be determined

A positive stress from Eq. 3.1 denotes compression, and likewise positive strain denotes contraction.

The parameters A,B,C,D are determined by considering the basic shape of the nonlinear stress-strain curve shown in Fig. 7. It can be observed that for the nonlinear case:

1. The curve passes through the point of zero stress and zero strain (i.e., the origin).

2. Under a biaxial state of stress (i.e., a stress ratio, α , not equal to zero) and at a zero stress-zero strain level, the initial slope of the stress-strain curve can be defined as $E_c / (1 - \nu\alpha)$ by employing Hooke's Law for multiaxial stress states. E_c can be obtained by performing a standard compression cylinder test or through an accepted formula such as the ACI equation (Ref. 49), the Jensen equation (Ref. 16), the Hognestad equation (Ref. 27), or the Saenz equation (Ref. 36). These equations are listed below in the order mentioned.

$$E_c = w^{1.5} 33 \sqrt{f'_c} \quad (\text{ACI})$$

$$E_c = \frac{6 \times 10^6}{1 + \frac{2000}{f'_c}} \quad (\text{Jensen})$$

$$E_c = 1.8 \times 10^6 \times 460 f'_c \quad (\text{Hognestad})$$

$$E_c = \frac{10^5 \sqrt{f'_c}}{1 + 0.006 \sqrt{f'_c}} \quad (\text{Saenz})$$

In the equations above f'_c is the 6" x 12" cylinder strength in (28 days) in psi, w is the unit weight in pounds per cubic feet and E_c has the units psi.

3. The curve passes through a peak stress-strain point (σ_p, ϵ_p) .
4. The slope at the peak stress-strain point is E_p .

The parameters A, B, C, D can be determined by enforcing these curve characteristics. Solution for the parameters leads to the following:

$$A = 0$$

$$B = 1$$

$$C = \frac{E_c}{\sigma_p (1 - \nu\alpha)} - \frac{2}{\epsilon_p} + \frac{E_p E_c \epsilon_p}{(1 - \nu\alpha) \sigma_p^2} \quad (3.2)$$

$$D = \frac{1}{\epsilon_p^2} - \frac{E_p E_c}{(1 - \nu\alpha) \sigma_p^2}$$

If the peak slope, E_p , were to be zero as in the case for the compression-compression region the curve parameters would reduce to those presented by Liu (Ref. 27):

$$A = 0$$

$$B = 1$$

$$C = \frac{E_c}{\sigma_p (1 - \nu\alpha)} - \frac{2}{\epsilon_p} \quad (3.3)$$

$$D = \frac{1}{\epsilon_p^2}$$

The tangent modulus, i.e. instantaneous slope, of the stress-strain curve may be obtained by differentiating Eq. 3.1 resulting in:

$$\frac{d\sigma}{d\epsilon} = \frac{E_c (1 - D\epsilon^2)}{(1 - \nu\alpha) (1 + C\epsilon + D\epsilon^2)^2} \quad (3.4)$$

Where $A = 0$

$B = 1$

Some advantage may be gained from the computer programming standpoint if the tangent modulus is defined in terms of only the principal stresses rather than in terms of stresses and strains. This change can be accomplished simply by solving Eq. 3.1 for the strain in terms of stress then substituting into Eq. 3.4. Care must be exercised in using the correct sign for the square root term in the resulting expression.

The tangent modulus of the stress-strain curve given in Eq. 3.4 can be used to relate the incremental stress in a principal direction to the incremental strain in that same direction. Thus the instantaneous slopes of the stress-strain curves for the two principal directions can be expressed as:

$$E_{1b} = \frac{d\sigma_1}{d\varepsilon_1} = \frac{E_c}{(1 - \nu\alpha_1)} \frac{(1 - D_1 \varepsilon_1^2)}{(1 + C_1 \varepsilon_1 + D_1 \varepsilon_1^2)^2} \quad (3.5a)$$

$$E_{2b} = \frac{d\sigma_2}{d\varepsilon_2} = \frac{E_c}{(1 - \nu\alpha_2)} \frac{(1 - D_2 \varepsilon_2^2)}{(1 + C_2 \varepsilon_2 + D_2 \varepsilon_2^2)^2} \quad (3.5b)$$

Where: E_{1b} and E_{2b} are the tangent moduli in the two principal directions 1 and 2 respectively.

$$\alpha_1 = \sigma_2 / \sigma_1$$

$$\alpha_2 = \sigma_1 / \sigma_2$$

D_1 and C_1 are the D and C curve parameters evaluated for the "one" principal direction using Eq. 3.2.

D_2 and C_2 are the D and C curve parameters evaluated for the "two" principal directions using Eq. 3.2.

Thus the incremental stress-incremental strain relation can be defined as:

$$\begin{aligned}\dot{\sigma}_1 &= E_{1b} \dot{\epsilon}_1 \\ \dot{\sigma}_2 &= E_{2b} \dot{\epsilon}_2\end{aligned}\tag{3.6a}$$

or in matrix form:

$$\begin{Bmatrix} \dot{\sigma}_1 \\ \dot{\sigma}_2 \end{Bmatrix} = \begin{bmatrix} E_{1b} & 0 \\ 0 & E_{2b} \end{bmatrix} \begin{Bmatrix} \dot{\epsilon}_1 \\ \dot{\epsilon}_2 \end{Bmatrix}\tag{3.6b}$$

The curve parameters C and D, which are presented in Eq. 3.2, can be determined if the following quantities are known: E_c , ν , α , σ_p , ϵ_p , and E_p . The first three quantities, Young's Modulus, Poisson's ratio and the stress ratio have been previously defined in this section. The latter three quantities (i.e. the peak stress, the peak strain and the peak slope) will be defined in Sections 3.1.3, 3.1.4 and 3.1.5.

3.1.2 Linear Stress-Strain Equation for Concrete

The linear stress-strain equation for concrete has the general form shown below.

$$\sigma = A + B \epsilon\tag{3.7}$$

The curve parameter A and B may be defined by forcing the curve to pass through the zero stress-zero strain point, i.e., origin, and also through the peak stress-strain point, as shown in Fig. 7. The curve parameters are thus defined as:

$$A = 0$$

$$B = \frac{\sigma_p}{\epsilon_p} \quad (3.8)$$

The following stress-strain equation is determined by substituting Eq. 3.8 into Eq. 3.7

$$\sigma = \frac{\sigma_p}{\epsilon_p} \epsilon \quad (3.9)$$

A constant tangent modulus is obtained by differentiating the stress-strain equation:

$$\frac{d\sigma}{d\epsilon} = \frac{\sigma_p}{\epsilon_p} \quad (3.10)$$

The incremental stress - incremental strain relationship follows from Eq. 3.10 as:

$$\begin{Bmatrix} \dot{\sigma}_1 \\ \dot{\sigma}_2 \end{Bmatrix} = \begin{bmatrix} E_{1b} & 0 \\ 0 & E_{2b} \end{bmatrix} \begin{Bmatrix} \dot{\epsilon}_1 \\ \dot{\epsilon}_2 \end{Bmatrix} \quad (3.11a)$$

Where:

$$E_{1b} = \frac{d\sigma_1}{d\epsilon_2} = \frac{\sigma_{p1}}{\epsilon_{p1}}$$

$$E_{2b} = \frac{d\sigma_2}{d\epsilon_2} = \frac{\sigma_{p2}}{\epsilon_{p2}} \quad (3.11b)$$

σ_{p1} and σ_{p2} denote the peak stress for the "one" and "two" directions respectively and ϵ_{p1} and ϵ_{p2} denote the peak strains in those directions. The linear stress-strain curve can be evaluated if the peak stress and peak strain values are known.

In the particular case of the tension-tension region the initial slope of $E_c/(1 - \nu\alpha)$ is maintained. Thus, if the peak stress and peak slope are known, the peak strain in this region can be defined as

$$\varepsilon_p = \sigma_p (1 - \nu\alpha) / E_c.$$

3.1.3 Biaxial Failure Envelope - Definition of σ_p

Non-dimensional experimental peak stress envelopes for concrete strengths of 2700 psi and 4450 psi are shown in Fig. 9 (Ref. 24). The close agreement between the two curves indicate that the basic shape of the failure envelope is essentially fixed and only the size of the envelope will change with concrete strength. The true envelope can be approximated by a series of straight lines as shown in Fig. 9. The maximum increase in biaxial compressive strength over the uniaxial compressive strength for the idealized failure envelope is 20%. This corresponds to a value of 1.2 on the non-dimensional plot in Fig. 9.

The characteristic points used to define the peak stress envelope are shown in Fig. 10 and enumerated in the table below:

<u>Point</u>	σ_{p1}	σ_{p2}
A	f'_c	0.0
B	Rf'_c	$\alpha_B Rf'_c$
C	Rf'_c	Rf'_c
D	Rf'_c/α_D	Rf'_c
E	0.0	f'_c
F	σ_{2F}/α_F	σ_{2F}
G	$-f_t$	0.0
H	$-f_t$	$-f_t$
I	0.0	$-f_t$
J	σ_{1J}	$\alpha_J \sigma_{1J}$

The terms used in the table above and on Fig. 10 are defined as:

f'_c = uniaxial compressive strength from 6" x 12" cylinder test
(28 days)

f_t = direct tensile strength

σ_1 = principal stress in direction 1

σ_2 = principal stress in direction 2

$\alpha = \sigma_2/\sigma_1$

σ_{p1} = peak stress in direction 1

σ_{p2} = peak stress in direction 2

σ_{ij} = stress in direction i at point j

$$\alpha_j = \text{stress ratio } \sigma_{2j} / \sigma_{1j}$$

R = increase in strength due to the biaxial compressive stress state

The following values were used in all test examples included in this report. These values were selected to provide an acceptable approximation to experimentally observed biaxial stress states (Refs. 24 and 27).

$$R = 1.2$$

$$\alpha_B = \frac{1}{\alpha_D} = \nu = 0.2$$

$$\alpha_F = \frac{1}{\alpha_J} = -19.2$$

$$\sigma_{2F} = \sigma_{1J} = 0.85 f'_c$$

Equations 3.12 to 3.21 were used to describe the line segments defining the biaxial failure envelope shown in Fig. 10. The equations have been left in general form so as to accommodate use of different values than those used in this study.

I. The Compression-Compression Stress States

1. Point-A to point-B ($0 \leq \alpha \leq \alpha_B$)

$$\sigma_{p1} = \frac{f'_c}{1 - \frac{\alpha}{\alpha_B} + \frac{\alpha}{\alpha_B R}} \quad (3.12)$$

2. Point-B to point-C ($\alpha_B \leq \alpha \leq 1$)

$$\sigma_{p1} = R f'_c \quad (3.13)$$

3. Point-C to point-D ($1 \leq \alpha \leq \alpha_D$)

$$\sigma_{p1} = \frac{R f'_c}{\alpha} \quad (3.14)$$

4. Point-D to point-E ($\alpha_D \leq \alpha \leq \infty$)

$$\sigma_{p1} = \frac{f'_c}{\alpha + \frac{\alpha_D}{R} - \alpha_D} \quad (3.15)$$

II. Tension-Compression Stress State

1. Point-E to point-F ($-\infty \leq \alpha \leq \alpha_F$)

$$\sigma_{p1} = \frac{f'_c}{\alpha_F \frac{f'_c}{\alpha_{2F}} - \alpha_F + \alpha} \quad (3.16)$$

2. Point-F to point-G ($\alpha_F \leq \alpha \leq 0$)

$$\sigma_{p1} = \frac{f_t}{\frac{\alpha}{\alpha_F} + \frac{\alpha f_t}{\alpha_{2F}} - 1} \quad (3.17)$$

III. Tension-Tension Stress State

1. Point-G to point-H ($0 \leq \alpha \leq 1$)

$$\sigma_{p1} = -f_t \quad (3.18)$$

2. Point-H to point-I ($1 \leq \alpha \leq \infty$)

$$\sigma_{p1} = -\frac{f_t}{\alpha} \quad (3.19)$$

IV. Compression-Tension Stress States

1. Point-I to point-J ($-\infty \leq \alpha \leq \alpha_J$)

$$\sigma_{p1} = \frac{1}{\frac{\alpha_J}{f_t} - \frac{\alpha}{f_t} + \frac{1}{\sigma_{1J}}} \quad (3.20)$$

2. Point-J to point-A ($\alpha_J \leq \alpha \leq 0$)

$$\sigma_{p1} = \frac{f'_c}{1 + \frac{\alpha f'_c}{\sigma_{1J} \alpha_J} - \frac{\alpha}{\alpha_J}} \quad (3.21)$$

3.1.4 Peak Strain Envelope - Definition of ε_p

The nondimensional peak strain envelope shown in Fig. 11 is idealized as a series of straight lines passing through, or very near to, the experimental peak strain points indicated in the figure (Refs. 24 and 27). Peak strain is defined as that strain corresponding to peak stress. Figure 12 shows the peak strain envelope including the characteristic points. The characteristic points used to define the peak strain envelope are listed below:

<u>Point</u>	$\frac{\sigma}{P1}$	$\frac{\epsilon}{P1}$
A'	f'_c	ϵ_c
B'	Rf'_c	ϵ_c
C'	σ_v	0
D'	0	$-\nu\epsilon_c$
E'	$-f_t$	$-\epsilon_t$
F'	0	$\nu\epsilon_t$
G'	σ_{ct}	ϵ_{ct}

R, f'_c , ν and f_t are defined in the previous section. The following additional terms used in the table above are defined as:

σ_v = peak compressive stress at an $\alpha = 1/\nu$ as obtained from the peak stress envelope of Section 3.1.3

$\sigma_{ct}, \epsilon_{ct}$ = a peak stress-strain value defining point G'

ϵ_c = peak strain for uniaxial compression

ϵ_t = peak strain for uniaxial tension

The following values were used for all test examples in this report.

They were selected to provide an acceptable approximation to experimentally observed peak strains in biaxial stress states,

$$R = 1.2$$

$$\nu = 0.2$$

$$\sigma_{ct} = 0.8 f'_c$$

$$\epsilon_{ct} = 1150 \text{ microstrain}$$

$$\epsilon_c = 2500 \text{ microstrain}$$

$$\epsilon_t = \text{tensile strength divided by Young's modulus}$$

As in the case of the peak stress envelope Eqs. 3.22 to 3.28 which define the line segments used to describe the peak strain envelope will be left in general form.

I. Compression-Compression Stress State

1. Point-A' to point-B' ($0 \leq \alpha \leq 1$)

$$\epsilon_{p1} = \epsilon_c \quad (3.22)$$

2. Point-B' to point-C' ($1 \leq \alpha \leq 1/v$)

$$\epsilon_{p1} = \frac{\epsilon_c (\sigma_{p1} - \sigma_v)}{R f'_c - \sigma_v} \quad (3.23)$$

3. Point-C' to point-D' ($1/v \leq \alpha \leq \infty$)

$$\epsilon_{p1} = \frac{v\epsilon_c (\sigma_{p1} - \sigma_v)}{\sigma_v} \quad (3.24)$$

II. Tension-Compression Stress State

1. Point-D' to point-E' ($-\infty \leq \alpha \leq 0$)

$$\epsilon_{p1} = (\epsilon_t - v\epsilon_c) \left(\frac{\sigma_{p1}}{f_t} + 1 \right) - \epsilon_t \quad (3.25)$$

III. Tension-Tension Stress State

1. Point-E' to point-F' ($0 \leq \alpha \leq 1$)

$$\epsilon_{p1} = \frac{\sigma_{p1} (1 - \nu\alpha)}{E_c} \quad (3.26)$$

IV. Compression-Tension Stress State

1. Point-F' to point-G' ($-\alpha \leq \alpha \leq \alpha_{ct}$)

$$\epsilon_{p1} = (\epsilon_{ct} - \nu\epsilon_t) \frac{\sigma_{p1}}{\sigma_{ct}} + \nu\epsilon_t \quad (3.27)$$

2. Point-G' to point-A' ($\alpha_{ct} \leq \alpha \leq 0$)

$$\epsilon_{p1} = \epsilon_c + \frac{(\epsilon_c - \epsilon_{ct}) (\sigma_{p1} - f'_c)}{(f'_c - \sigma_{ct})} \quad (3.28)$$

3.1.5 Peak Slope - Definition of E_p

The peak slope is defined as the tangent of the nonlinear stress-strain curve evaluated at the peak stress. According to experimental observation the peak slope for the compression-compression stress region has a value of zero (Refs. 24, 27 and 32). In the tension-compression regions the peak slope may range from a value of zero for stress states near uniaxial compression to a value equal to the σ_p/ϵ_p for stress states near uniaxial tension. In this study the ratio of peak slope to initial slope in that region has been assumed to vary linearly with respect to the stress ratio, α . The peak slope ratio has a value of zero for stress states near uniaxial compression and ranges to a value of 1.0 for stress states near uniaxial tension.

Two peak slope ratios necessary to define the aforementioned linear variation were scaled from the experimental stress-strain curves

designated as A and C in Fig. 16, and are listed below along with the values of α associated with those curves.

Point	α	$\frac{\text{Peak Slope}}{\text{Initial Slope}}$
I	-0.203	1.000
II	-0.052	0.125
I'	-4.900	1.000
II'	-19.200	0.125

Points I and II, located in the compression-tension region, were obtained by measuring the peak slope ratio for curves C and A respectively. Points I' and II', located in the tension-compression region, were obtained by computing the reciprocals of the values associated with points I and II respectively.

Points I, II, I', and II' and a plot of the ratio of peak slope to initial slope as a function of the stress ratio, α , are presented in Fig. 13. The peak slope function is represented as a series of straight line segments. These straight line segments and corresponding biaxial stress plane regions are indicated by the letters A through E in Fig. 13. The corresponding biaxial stress plane regions designate where that particular straight line segment is applicable. The letters C+ and E+ indicate that the curve extends to a stress ratio of plus infinity while the letters C- and E- indicate that the curve extends to negative infinity at the indicated points on the failure envelope. The straight line segments delineated by the points E-, I, II, A and C+ reflect the peak slope ratios for the compression-tension region through the compression-compression region. The straight line segments associated with the points C-, II', I', D and E+ describe the peak slope relationship for the tension-compression region through the tension-tension region.

3.1.6 Stress-Strain Curves for Concrete

The nonlinear stress-strain relation used in this investigation, Eq. 3.1, reduces to the Saenz equation for the uniaxial compression stress state for which E_p and α are both equal to zero (Ref. 36). The Saenz equation is given below.

$$\sigma = \frac{\epsilon E_c}{1 + \left(\frac{E_c \epsilon_p}{\sigma_p} - 2 \right) \left(\frac{\epsilon}{\epsilon_p} \right) + \left(\frac{\epsilon}{\epsilon_p} \right)^2} \quad (3.29)$$

Figure 14 compares experimental (Ref. 38) and analytical uniaxial compression stress-strain curves for concretes of various strengths. The agreement between the curves is quite good and confirms the applicability of the uniaxial stress-strain equation to a wide range of concrete strengths.

Figures 15, 16 and 17 compare the idealized and experimental biaxial stress-strain curves (Ref. 24). Curves A, B, and C in each figure corresponds to the specific stress ratios listed on the figures. Two curves are plotted for each stress ratio. One corresponds to σ_1/σ_0 versus ϵ_1 and the other to σ_1/σ_0 versus ϵ_2 . σ_1 and σ_2 are the principal stress as shown in the inset of each figure while σ_0 is the uniaxial compressive strength. ϵ_1 and ϵ_2 are the strains in the first and second principal stress directions respectively.

Analytic stress-strain curves corresponding to an unlimited number of stress ratios covering the entire biaxial stress space can be generated using the method presented herein. Figures 20, 21, 22 and 23 show the idealized stress-strain curves corresponding to the selected values of stress ratios indicated in Fig. 18 and enumerated in Fig. 19. These figures show the wide range of biaxial stress-strain curves which are possible for given values of the stress ratio, α .

3.1.7 Stress-Strain Relationships for Concrete

The incremental stress-strain relationship for concrete in terms of principal stresses is represented by Eq. 3.30 in which the subscripts 1 and 2 identify the principal stress directions and the dots indicate incremental quantities.

$$\begin{Bmatrix} \dot{\sigma}_1 \\ \dot{\sigma}_2 \\ \dot{\tau}_{12} \end{Bmatrix} = [\bar{D}] \begin{Bmatrix} \dot{\epsilon}_1 \\ \dot{\epsilon}_2 \\ \dot{\gamma}_{12} \end{Bmatrix} \quad (3.30)$$

Needless to say the in-plane shear stress $\dot{\tau}_{12}$, will be zero but its presence is required in the principal stress vector so as to include the shearing stiffness term in the $[\bar{D}]$ matrix. This is necessary so that transformation of the $[\bar{D}]$ matrix from principal axes to global x-y axes results in the proper elasticity relationships. The $[\bar{D}]$ matrix is the stress-strain relationship for the principal stress plane. The $[\bar{D}]$ matrix can be determined by using the stress-strain relationship for anisotropic materials (Ref. 27).

$$\begin{Bmatrix} \dot{\epsilon}_1 \\ \dot{\epsilon}_2 \\ \dot{\gamma}_{12} \end{Bmatrix} = \begin{bmatrix} \frac{1}{E'_{1b}} & \frac{-\nu_2}{E'_{2b}} & 0 \\ \frac{-\nu_1}{E'_{1b}} & \frac{1}{E'_{2b}} & 0 \\ 0 & 0 & \frac{E'_{1b} + E'_{2b} + 2\nu_1 E'_{2b}}{E'_{1b} E'_{2b}} \end{bmatrix} \begin{Bmatrix} \dot{\sigma}_1 \\ \dot{\sigma}_2 \\ \dot{\tau}_{12} \end{Bmatrix} \quad (3.31)$$

E'_{1b} and E'_{2b} are the tangent moduli in the first and second principal stress directions respectively and ν_1 and ν_2 are the Poisson's ratios in the indicated directions. In the equation above it is assumed that $\nu_1/E'_{1b} = \nu_2/E'_{2b}$. Inversion of the above stress-strain relationship leads to the $[\bar{D}]$ matrix used in Eq. 3.30:

$$[\bar{D}] = \begin{bmatrix} \frac{E'_{1b}}{1 - \nu_1 \nu_2} & \frac{\nu_2 E'_{1b}}{1 - \nu_1 \nu_2} & 0 \\ \frac{\nu_1 E'_{2b}}{1 - \nu_1 \nu_2} & \frac{E'_{2b}}{1 - \nu_1 \nu_2} & 0 \\ 0 & 0 & \frac{E'_{1b} E'_{2b}}{E'_{1b} + E'_{2b} + 2\nu_1 E'_{2b}} \end{bmatrix} \quad (3.32)$$

The analytic stress-strain curves of Section 3.1.1 relate the stress in a particular principal direction to the strain in that same direction and only that direction. Thus, as indicated by Eq. 3.6a and 3.11a, relationships of the following form are defined:

$$\begin{aligned} \dot{\sigma}_1 &= E_{1b} \dot{\epsilon}_1 \\ \dot{\sigma}_2 &= E_{2b} \dot{\epsilon}_2 \end{aligned} \quad (3.33)$$

Where E_{1b} and E_{2b} are the effective tangent moduli for the principal stress plane obtained by differentiating the analytic stress-strain curves of Sections 3.1.1 and 3.1.2. The terms in the $[\bar{D}]$ matrix of Eq. 3.32 must now be related to the known moduli, E_{1b} and E_{2b} in order to use the stress-strain equation given in general form by Eq. 3.1.

The unknown terms in the stress-strain relations may be expressed as functions of the known E_{1b} and E_{2b} values by diagonalizing the stress-strain relations of Eq. 3.31. E_{1b} and E_{2b} are computed from the current total stress state. Diagonalized relations may be obtained by eliminating $\dot{\sigma}_1$ and $\dot{\sigma}_2$ from the first and second algebraic equations, respectively, represented by the matrix equation, Eq. 3.31. This is done by substituting for $\dot{\sigma}_1$ and $\dot{\sigma}_2$ the relations given by Eqs. 3.34. The α 's are also based on the current total stress state so as to be consistent with E_{1b} and E_{2b} .

$$\dot{\sigma}_2 = \dot{\sigma}_1 \alpha_1 \quad (3.34)$$

$$\dot{\sigma}_1 = \dot{\sigma}_2 \alpha_2$$

The above substitution leads to Eqs. 3.35a and 3.35b:

$$\dot{\epsilon}_1 = \dot{\sigma}_1 \left[\frac{1}{E'_{1b}} - \frac{\nu_2 \alpha_1}{E'_{2b}} \right] \quad (3.35a)$$

$$\dot{\epsilon}_2 = \dot{\sigma}_2 \left[\frac{1}{E'_{2b}} - \frac{\nu_1 \alpha_2}{E'_{1b}} \right] \quad (3.35b)$$

The relation $\nu_2/E'_{2b} = \nu_1/E'_{1b}$ allow Eqs. 3.35 to be expressed as:

$$\dot{\epsilon}_1 = \frac{\dot{\sigma}_1}{E'_{1b}} (1 - \nu_1 \alpha_1) \quad (3.36a)$$

$$\dot{\epsilon}_2 = \frac{\dot{\sigma}_2}{E'_{2b}} (1 - \nu_2 \alpha_2) \quad (3.36b)$$

Rearranging Eqs. 3.36a and 3.36b leads to the diagonalized stress-strain relations given by Eqs. 3.37a and 3.37b:

$$\dot{\sigma}_1 = \left(\frac{E'_{1b}}{1 - \nu_1 \alpha_1} \right) \dot{\epsilon}_1 \quad (3.37a)$$

$$\dot{\sigma}_2 = \left(\frac{E'_{2b}}{1 - \nu_2 \alpha_2} \right) \dot{\epsilon}_2 \quad (3.37b)$$

Comparison of Eqs. 3.37a and 3.37b with Eqs. 3.33 shows that the tangent moduli relating principal stresses to strains in the corresponding directions are given by Eqs. 3.38a and 3.38b:

$$E_{1b} = \frac{E'_{1b}}{1 - \nu_1 \alpha_1} \quad (3.38a)$$

$$E_{2b} = \frac{E'_{2b}}{1 - \nu_2 \alpha_2} \quad (3.38b)$$

Rearranging Eqs. 3.38a and 3.38b leads to 3.39a and 3.39b which define the moduli E'_{1b} and E'_{2b} , needed in Eq. 3.32

$$E'_{1b} = E_{1b} (1 - \nu_1 \alpha_1) \quad (3.39a)$$

$$E'_{2b} = E_{2b} (1 - \nu_2 \alpha_2) \quad (3.39b)$$

E_{1b} and E_{2b} are defined in Eqs. 3.5a and 3.5b, respectively, for the nonlinear case and in Eq. 3.11b for the linear case. The curve parameters C and D in the aforementioned expressions, are given by Eq. 3.2.

ν_1 and ν_2 in Eq. 3.32 must still be obtained. The relation $\nu_2/E'_{2b} = \nu_1/E'_{1b}$ leads to the following equations.

$$\nu_A = \nu \quad (3.40a)$$

$$\nu_B = \frac{1.}{\frac{E_{Ab} (1 - \nu_A \alpha_A)}{E_{Bb} \nu_A} + \alpha_B} \quad (3.40b)$$

where subscripts (A,B) correspond to directions (1,2) or (2,1) whichever is applicable. Applicability was determined by selecting the combination that resulted in positive values for both ν_1 and ν_2 . The reported study has used the value of 0.2 for ν_A . The range of values for ν_B , resulting from the application of Eqs. 3.40a and 3.40b for various combinations of cylinder strength, stress ratios and stress levels, was approximately 0.16 to 0.24, or about 80% to 120% of the value assumed for ν_A .

All terms of Eq. 3.32 can be defined using Eqs. 3.5a, 3.5b, 3.11b, 3.39a, 3.39b, 3.40a and 3.40b. The resulting $[\bar{D}]$ matrix is the constitutive relationship for the particular layer expressed in principal stress directions. Before computing the contribution of this layer to the element stiffness matrix, the $[\bar{D}]$ matrix must be transformed into an elasticity matrix, $[D]$, relating stress and strain in the x-y coordinate system of the element:

$$\begin{Bmatrix} \dot{\sigma}_x \\ \dot{\sigma}_y \\ \dot{\tau}_{xy} \end{Bmatrix} = [D] \begin{Bmatrix} \dot{\epsilon}_x \\ \dot{\epsilon}_y \\ \dot{\gamma}_{xy} \end{Bmatrix} \quad (3.41)$$

This transformation is carried out in the following manner (Ref. 12,48):

$$[D] = [T] [\bar{D}] [T]^T \quad (3.42)$$

where the transformation matrix, [T] is defined by Eq. 3.43:

$$[T] = \begin{bmatrix} \cos^2\theta & \sin^2\theta & -2 \cos\theta \sin\theta \\ \sin^2\theta & \cos^2\theta & 2 \cos\theta \sin\theta \\ \cos\theta \sin\theta & -\cos\theta \sin\theta & \cos^2\theta - \sin^2\theta \end{bmatrix} \quad (3.43)$$

The angle θ is defined as the angle between the 1 direction and the x direction. This angle is positive when measured in a clockwise direction from the positive x axis.

3.1.8 Concrete Failure Modes

Concrete exhibits physically distinct types of failure modes which are dependent upon the applied stress ratio as shown in Fig. 24A. Figures 24A and 24B each show one-half of a symmetric region. Four distinct failure modes can be described as follows (Ref. 32):

- I. In the tension-tension region and up to a tensile stress/compressive stress ratio of $-1/30$ failure occurs by the formation of one crack perpendicular to the largest tensile force and perpendicular to the free plane, i.e., unloaded plane, of the specimen. For a stress ratio of equal tension in both directions there is no preferred crack direction (Ref. 24). This will be called a Type I failure.

- II. For stress ratios between $-1/30$ and $-1/100$ numerous cracks are formed instead of just a single crack as was the case for the previous region. These cracks are also perpendicular to the tensile force and the free plane of the specimen. This will be called a Type II failure.
- III. From a stress ratio of $-1/100$ in the compression-tension region to a stress ratio of $3/10$ in the compression-compression region, cracks are not only formed perpendicular to the applied tensile force and free surface of the specimen but also cleavage planes occur parallel to the free surface of the specimen. This will be called a Type III failure.
- IV. For stress ratios between $3/10$ and $1/1$ in the compression-compression region only cleavage cracks parallel to the free plane of the specimen occur. This will be called a Type IV failure.

Kupfer, Hildsorf, and Rusch (Ref. 24) report two general types of failure modes. They are a Type IV crushing failure for stress ratios occurring between $1/1$ and $-1/15$ ($-1/30$ according to Ref. 32) and a Type I cracking failure for stress ratios from $-1/15$ to $-1/-1$.

The idealized failure modes used in this report are depicted in Fig. 24B. From the tension-tension region to a stress ratio of $-1/15$ a cracking failure mode is assumed to occur. The direction of the crack(s) is assumed to be perpendicular to the largest tensile force and to the free surface of the specimen. From the compression-compression region to

the stress ratio of $-1/15$ crushing failure mode is assumed to occur. The direction of crushing is assumed to be perpendicular to the largest compressive stress and perpendicular to the free surface of the specimen.

3.1.9 Cracked or Crushed Concrete

Cracking or crushing of the concrete is deemed to occur when the principal stress has exceeded the peak stress as defined in Fig. 9. The direction of cracking or crushing is assumed to be perpendicular to the direction of the corresponding principal tensile or compressive stress, whichever is appropriate. The concrete layer is assumed to have stiffness only in the uncracked or uncrushed direction. For example, the constitutive stress-strain relation for a concrete layer which has experienced a failure caused by the stress in direction 2 would be

$$\begin{Bmatrix} \dot{\sigma}_1 \\ \dot{\sigma}_2 \\ \dot{\tau}_{12} \end{Bmatrix} = \begin{bmatrix} E'_{1b} & 0 & 0 \\ 0 & 0 & 0 \\ 0 & 0 & 0 \end{bmatrix} \cdot \begin{Bmatrix} \dot{\epsilon}_1 \\ \dot{\epsilon}_2 \\ \dot{\gamma}_{12} \end{Bmatrix} \quad (3.44)$$

The first principal direction is still effective in contributing stiffness to the element. The elasticity matrix, $[\bar{D}]$ would then be rotated from the principal stress coordinate axis to the x-y coordinate system. The layer stiffnesses are then computed and used in the summation process for the element stiffness formulation.

3.1.10 Unloading of Cracked and Crushed Concrete Layers

After cracking or crushing of the concrete layer, the layer will be incapable of sustaining the stress that caused the failure. This stress must be reduced to zero within the layer while still maintaining equilibrium between the external forces and internal stresses. Thus, unloading of the layer stress to zero necessitates the adjustment of the internal stress field of the slab. This adjustment or redistribution is accomplished through the use of fictitious forces which are statically equivalent to the amount of stress to be redistributed to the slab. A solution of the stiffness equations corresponding to these forces will cause a redistribution of stresses within the slab.

Recent experimental evidence indicates that after attainment of peak strength, either tension or compression, the concrete stress strain curve has a downward leg, i.e., unloading (Refs. 5, 15, 24 and 27). It is assumed that this downward portion is a straight line and has a slope of some finite value (Refs. 19 and 26). Thus unloading proceeds at some finite rate determined by the slope of the downward portion of the stress-strain curve.

This unloading branch can also be used to model the tension stiffening effect due to the gradual transfer of load from the cracked concrete to the steel reinforcing bars (Ref. 26).

The fictitious force vector can be computed using Eq. 3.45

$$\{F_c\} = \int_{vol} \left[[B_u] \quad z [B_\phi] \right]^T \{\dot{\sigma}_r\} dvol \quad (3.45)$$

where the vector $\{\dot{\sigma}_r\}$ is the increment of stress in the x-y coordinate system to be redistributed and $\{F_c\}$ is the resulting vector of fictitious forces. The fictitious force vector can be separated into terms involving only in-plane fictitious forces, $\{F_{uc}\}$ and terms involving bending fictitious forces, $\{F_{\phi c}\}$ as shown in Eq. 3.46:

$$\begin{Bmatrix} F_{uc} \\ F_{\phi c} \end{Bmatrix} = \begin{Bmatrix} \int [B_u]^T \{\dot{\sigma}_r\} dvol \\ \int [B_\phi]^T \{\dot{\sigma}_r\} z dvol \end{Bmatrix} \quad (3.46)$$

If it is assumed that the stress to be unloaded is constant through the thickness of a layer, integration of Eq. 3.46 with respect to the z direction over the thickness of the layer results in Eqs. 3.47a and 3.47b

$$\{F_{uc}\} = \left[\int \int_{yx} [B_u]^T dx dy \right] \{\dot{\sigma}_r\} (Z_{i+1} - Z_i) \quad (3.47a)$$

$$\{F_{\phi c}\} = \left[\int \int_{yx} [B_\phi]^T dx dy \right] \{\dot{\sigma}_r\} \frac{Z_{i+1}^2 - Z_i^2}{2} \quad (3.47b)$$

The amount of stress to be redistributed, $\{\dot{\sigma}_r\}$, for a particular load cycle can be computed in principal stress plane by multiplying the unloading modulus, (Ref. 19), by the appropriate integrated average strain increment. Transformation of the stress vector from the principal to the x-y global coordinate system is necessary before substituting into Eqs. 3.47a and 3.47b.

3.2 Stress-Strain Relationship for Steel

The steel reinforcing bars are considered to be in a uniaxial state of stress. The steel stress-strain curve is assumed to follow the Ramberg-Osgood formulation (Refs. 19 and 35) given by Eq. 3.48

$$\epsilon = \frac{\sigma}{E_s} + \left(\frac{1-m}{m} \right) \frac{\sigma_y}{E_s} \left(\frac{\sigma}{\sigma_y} \right)^n \quad (3.48)$$

Where: σ = stress

ϵ = strain

E_s = initial modulus of elasticity

σ_y = yield strength

n = a constant assumed to be approximately equal to 100 for mild steel

m = a constant defining a line of slope $m.E_s$ on the stress-strain plot and taken to be .7 for metals

The tangent modulus can be found by differentiating the stress-strain equation as follows:

$$\frac{d\sigma_1}{d\epsilon_1} = \frac{E_s}{1 + n \frac{(1-m)}{m} \left(\frac{\sigma_1}{\sigma_y} \right)^{n-1}} \quad (3.49)$$

The stress-strain matrix for reinforcing bars is given below:

$$\begin{Bmatrix} \dot{\sigma}_1 \\ \dot{\sigma}_2 \\ \dot{\tau}_{12} \end{Bmatrix} = \begin{bmatrix} \bar{D}_{11} & 0 & 0 \\ 0 & 0 & 0 \\ 0 & 0 & 0 \end{bmatrix} \begin{Bmatrix} \dot{\epsilon}_1 \\ \dot{\epsilon}_2 \\ \dot{\gamma}_{12} \end{Bmatrix} \quad (3.50)$$

Where: $\bar{D}_{11} = d\sigma_1 / d\epsilon_1$

The $[\bar{D}]$ matrix is then transformed from the principal stress direction of the reinforcing bars to the x-y axes as shown in Eq. 3.42 where $[T]$ is as previously defined by Eq. 3.43. The angle θ is the angle between the x-axis and the longitudinal direction of the reinforcing bars.

Mathematical distinction between yielded and non-yielded steel need not be made since the Ramberg-Osgood formulation provides a continuous stress-strain curve. Proper selection of the curve parameters can produce an almost perfectly plastic plateau as would be the case for mild steel. This plateau will have some finite slope but its value will be so small that for all practical purposes its effect on the structural behavior can be considered negligible.

3.3 Additional Considerations

Several further considerations could be incorporated into the present analysis procedure of reinforced concrete slabs to attack more general problems. Possible items that could be considered are:

1. Shear Retention Factor
2. Dowel Action (in-plane)
3. Transverse Shear, i.e. normal to the slab
4. Bond Slip

These considerations were not included in the present analysis scheme due to one or more of the following reasons:

1. It is believed that they have a negligible effect on the structural behavior of the slab at load levels which will not cause substantial damage,
2. The experimental investigations have not demonstrated the need for their inclusion,
3. It has not been demonstrated that manageable analytical methods of proven reliability have been developed for all observed experimental phenomena, and, most importantly,
4. Necessary physical constants for some of the phenomena are not available.

The shear retention factor has been used to model aggregate interlock behavior along the crack face (Refs. 7,11,12,25,26,37). In the present study it was assumed that aggregate interlock failure occurs immediately after cracking or crushing. It has been reported that analytic results for the flexural analysis of slabs are insensitive to the particular value of the shear retention factor chosen (Refs. 11,12,26). This would be expected in the experimental flexural tests since separation of the crack faces occurs after the initiation of the flexural failure, thus reducing the shearing stiffness along the crack face to zero.

Experimental studies on dowel action of reinforcing bars has been carried out and is available in the literature (Ref. 30). These experiments were concerned with investigating dowel action caused by the

shearing deformation of the reinforcing bars in the plane of the slab. The dowel action discussed here should not be confused with the type of dowel action considered when discussing shear perpendicular to the plane of the plate. It was concluded from these studies that after a flexural type of failure in a reinforced concrete slab, the reinforcing bars do not distort across the cracks. This implies that the reinforcing bars do not carry excessive shearing forces. Thus for the analysis procedure reported herein, it was assumed that the steel reinforcing bars have a shearing stiffness of zero. Furthermore, it should be noted that this assumption is consistent with the assumption regarding the stress fields of the reinforcing bars, i.e., uniaxial stressing.

An approximate method to include the transverse shear perpendicular to the plane of the plate in an elastic plate bending analysis has been proposed in Ref. 10. A more exact analysis scheme to include the transverse shear would require a three dimensional elasticity approach. The three dimensional approach would lead to prohibitive solution time and storage requirements as mentioned in Chapter 1.

At high stresses the bond between the concrete and steel may be broken and the steel may slip relative to the concrete. This slippage changes the stress distribution in the reinforcing bars and concrete at the vicinity of the slippage. Slip phenomena has been taken into account in some analytical studies (Refs. 31 and 34). These investigations have employed the continuum approach and used "linkage elements" to model slippage. Bond slip could possibly be incorporated into the present analysis procedure by use of an appropriate concrete strain-steel reinforcing

bar slip relationship. Equilibrium would have to be re-established after the required internal adjustments to the reinforcing bar strain field have been made through an application of the currently used fictitious force vector concept. It must be emphasized that the above procedure has not been implemented or verified. Also the required strain-slip relationship and its dependence on loading, boundary conditions, physical properties and material properties associated with reinforced concrete slabs has not yet been determined. Thus inclusion of bond slip remains hypothetical at this time.

3.4 Limitations

The presented method as reported herein, is applicable only to the reinforced concrete slabs whose predominant mode of response is flexure. The method has been kept general enough to permit various boundary conditions. However, if the support resistance is a function of the deformation of the slab and the loading, then it will be more convenient to treat such problems via the method under development on the overload response of beam-slab bridges (see page 1). It should be noted that the presented method cannot and should not be used if the slab failure is due to shear punch, without any flexural damage. Furthermore the effect of shrinkage and temperature have not been included in the present scheme. It is strongly recommended that prior to the usage of the method presented herein, the assumptions and their implications be reconsidered as far as the problem to be analyzed is concerned.

4. CORRELATION WITH TESTS

A comparison of experimental and analytical results will be presented in this chapter to verify that the developed analytical model accurately represents reinforced concrete slabs. Solutions for the seven test cases listed below will be discussed:

- No. 1: A simply supported reinforced concrete beam (Ref. 50).
- No. 2: A rectangular slab simply supported on two opposite sides and free on the other sides (Ref. 6).
- No. 3: A corner supported square slab (Ref. 17).
- No. 4: A simply supported square slab with orthogonal reinforcement (Ref. 39).
- No. 5: A simply supported square slab with diagonal reinforcement (Ref. 39).
- No. 6: A rectangular slab fixed on two opposite sides and free on the other two (Ref. 40).
- No. 7: A square slab fixed on all edges (Ref. 40).

These examples will show that the analysis technique being reported can handle various boundary conditions and loadings.

The material properties of the test specimens are listed in Table I and are defined as follows:

TABLE I: MATERIAL PROPERTIES

Example	f'_c-4'' (psi)	f'_c (psi)	f_t (psi)	E_c (ksi)	f_y (ksi)	E_s (ksi)
1		5000.*	500.	3450.*	46.3*	30000.
2		5150.*	502.	4330. ^J	50.0*	29000.*
3		5500.*	440.	4150.*	40./50.	30000.
4	5540.*	4600.	391.	4323. ^J	54.5*	30000.
5	5120.*	4250.	370.	4226. ^J	61.0*	30000.
6	4300.*	3600.	324.	3450. ^{A*}	44.3*	30000.
7	5060.*	4200.	375.	3100.*	44.6*	30000.

* Given

J = Jensen

A = ACI

f'_c-4'' = 4" x 4" x 4" cube strength (28 days)

f'_c = 6" x 12" cylinder strength (28 days)

f_t = direct tensile strength (28 days)

E_c = Young's modulus for concrete (at the time of testing)

f_y = yield strength for reinforcing steel

E_s = Young's modulus for reinforcing steel

As noted in Table I, not all material properties needed in the analysis scheme were reported or obtained by the experimenters. In all examples either the 6" x 12" cylinder strength, f'_c , or the 4" x 4" x 4" cube strength, $f'_{c-4''}$, was reported. If the concrete properties f'_t and E_c were not experimentally obtained they were computed from f'_c or $f'_{c-4''}$ in the following manner:

1. If the cube strength is readily available then it can be converted to cylinder strength by any acceptable relationship such as the equation below.

$$f'_c = (0.83) (f'_{c-4''})$$

2. Young's modulus, E_c , was obtained using an acceptable formula such as those mentioned in Section 3.1.1.
3. The direct tensile strength, f'_t , can be obtained from Fig. 25 which indicates a relationship between the cylinder strength and the direct tensile strength. This figure was plotted using values reported in Ref. 33. Examples 1 and 2 used tensile strengths that had been previously used by other investigators and hence Fig. 25 was not used in these two examples.

The following material properties were assumed for all test cases:

Poisson's ratio, $\nu = 0.2$

Compression unloading modulus = 1000 ksi (Ref. 19)

Tension unloading modulus = 800 ksi (Ref. 19)

Material properties needed for steel are the yield strength, Young's modulus and the Ramberg-Osgood parameters discussed in Section 3.2. In all cases except example 3 the yield strength of the steel was reported. For example No. 3 two analyses were carried out, one for a yield strength of 40 ksi and one for a yield strength of 50 ksi. Young's modulus was assumed to be 30×10^6 psi if it was not given.

4.1 Reinforced Concrete Beam

An 11 foot simply supported beam with a 6" x 12" rectangular cross section was subjected to third point loading (Ref. 50). The loading produced a pure moment region in the middle third of the beam. The half beam was discretized into four finite elements as shown in Fig. 26. Reinforcement consisted of six No. 5 deformed round mild steel bars each with a cross sectional area of 0.31 square inches. Three bars were located at a centroidal distance of 8.75" from the top of the beam and three bars were located at a centroidal distance of 10.5". The value of Young's modulus for concrete used in this example was computed from the precracked load-deflection curve of the test beam. The result was 3450. ksi. Two analyses were carried out: one using six concrete layers and two steel layers as shown in Fig. 27 and one using ten concrete layers and two steel layers.

The calculated and experimental load deflection histories are shown in Fig. 28. It can be seen that there is a very good agreement between the experimental and the calculated results. The calculated curves indicate convergence to the experimental ultimate load as the number of concrete layers is increased.

4.2 Simple-Free Slab

This 54" x 40.5" x 4.14" slab (slab B7, Ref. 6) was loaded by a uniformly distributed moment along two opposite sides as shown in Fig. 29. The constant moment region was idealized as one finite element. This is an adequate idealization because the stress field does not, theoretically, vary with position in the plane of the plate. The distributed moment was applied on the short sides which were considered as simply supported. The long sides of the slab were free to displace. Reinforcement consisted of 1/4" diameter deformed bars placed at $\pm 45^\circ$ to the slab edges. The bars closest to the surface of the slab were spaced at 1.5" with a minimum cover of 3/8". The bars in the next layer were spaced at 1.375" with a cover of 5/8".

The slab was divided into ten concrete layers and two steel layers as shown in Fig. 30. T_s in Fig. 30 indicates the steel layer thickness and θ_x indicates the reinforcing bar angle measured from the x-axis. The location of the steel layers in the model corresponds to the centroidal location of the steel reinforcing bars in the test specimen. The experimental and analytical distributed moment versus curvature histories are presented in Fig. 31. The agreement between the experimental and analytic results is quite good with respect to overall shape, formation of collapse mechanism, and ultimate load. Figures 32 and 33 show the applied moment versus concrete compressive strain and the applied moment versus average steel strain histories respectively for both the experimental and analytic models. It is noted that there is significant scatter of experimental strain readings about their average values for some

levels of applied moment. However the general agreement between the experimental and analytic results is quite satisfactory.

4.3 Corner-Supported Slab

This corner-supported 36" x 36" square slab was tested under a center point load. The slab was discretized into sixteen finite elements per quarter section as shown in Fig. 34 (Ref. 17). The slab thickness was 1.75" with an effective depth of 1.31". A steel percentage of 0.85% for both orthogonal directions was used to reinforce the slab. The slab was divided into six concrete layers and two steel layers through the depth as shown in Fig. 35.

The analytical and experimental load-deflection histories are shown in Fig. 36. The analytical load-deflection histories are plotted for node points 5 and 10. The experimental load-deflection history corresponds to point "A" which is indicated in Fig. 34. Point "A" is the closest point to the center of the slab for which experimental results were presented. As seen in Fig. 36 the analytic results for nodes 5 and 10 form a very narrow band in which the analytic result for point "A", had it been obtained, would lie.

4.4 Simply Supported Slab with Orthogonal Reinforcement

The 6' x 6' x 1.75" simply supported slab in this example was loaded using sixteen evenly spaced hydraulic jacks to simulate a uniformly distributed load. The tensile reinforcement, consisting of 3/16" diameter

plain round mild steel bars, was placed according to the following pattern:

Layer #1: spacing = 2.5"	Layer #2: spacing = 2.2"
cover = 0.1875"	cover = 0.375"
$\theta_x = -90^\circ$	$\theta_x = 0^\circ$

The quarter slab was discretized into sixteen finite elements as shown in Fig. 37. The hydraulic jack locations are indicated by the solid squares. The slab was divided into six concrete layers and two steel layers through the depth as indicated in Fig. 38.

The analytical and experimental load deflection histories of the center point (node 5) are presented in Fig. 39. During this particular test series the loading plates became inclined to the hydraulic jacks due to the excessive deflections experienced by the slab. Discrepancies of as much as 10% were reported between the load indicated by the jacks (higher value) and the load indicated by the load cells at the supports (lower value), (Ref. 39). The lower value of load as indicated by the supports was used in plotting Fig. 39. The experimental ultimate load exceeded the ultimate load calculated by the experimenters using the yield line theory by 64%. Possible reasons for this discrepancy, given by the experimenters, were as follows (Ref. 39):

1. A lower bound yield criterion was used in the experimenter's calculations.
2. Strain hardening of the reinforcement was not included.
3. The development of tensile membrane action was ignored.

By observing the steel strains obtained using the analytic method presented in this report it was concluded that strain hardening would effect only the very last portion of the load deflection history. The increase in strength beyond the yield line theory prediction is apparently due, in large measure, to tensile membrane action and non-ideal support or loading conditions. Considering the force exerted by the jacks to be defined as "P" and taking the vertical component as being 90% of P corresponding to that recorded by the load cells at the supports (i.e., a difference of 10%) results in a horizontal force equal to 43.6% of P which must be applied in the plane of the slab. Thus for a maximum discrepancy of 10% at the ultimate load, the slab is under a total vertical force of 26.1 kips, a horizontal in-plane force of 12.6 kips and the resultant force applied by the jacks of 29.0 kips. The magnitude and direction of the individual horizontal in-plane force applied by each individual jack is unknown. Since these in-plane forces are unknown, three models involving different in-plane support conditions were analyzed:

1. No in-plane restraint (ideal loading and support).
2. In-plane restraint of the exterior boundary of the slab.
3. Partial in-plane restraint at selected interior node points of the slab.

Model #1 had no additional in-plane restraints other than those required to maintain the proper boundary conditions at the lines of symmetry and to eliminate rigid body motion. This model produced an ultimate

load which agreed with the ultimate load predicted by the yield line theory but which underestimated the experimental ultimate load considerably.

Model #2 resulted in an ultimate load 17% higher than the experimental value. Tensile membrane cracks developed on top of the slab during test loading (Ref. 39). These crack patterns indicated that the tension field which caused the crack patterns was located in the center portion of the slab. Both models #2 and #3 would tend to produce a tension field within the slab. Since model #2 resulted in an overestimation of the experimental ultimate load it was decided to restrain the jack locations which correspond to nodes 7, 9, 17, and 19 from in-plane movement. This model, designated as model #3, would lead to a tension field limited to a more centralized region of the slab as compared to model #2. Thus the apparent stiffness of model #3 would be lower than model #2. The resulting load deflection history from model #3 is presented in Fig. 39. The ultimate load computed is within 1.5% of the experimental ultimate load. The analytic load at which crushing of the concrete and yielding of the steel occurs is indicated in the above figure. Figure 39 shows that, despite the many assumptions and approximations which had to be made in this comparative example, good agreement between experimental and analytic results has been attained.

4.5 Simply Supported Slab with Diagonal Reinforcement

A second slab from the same test series as the previous example and loaded in the same way was also analyzed to further demonstrate the reliability of the analysis technique. The slab dimensions were

6' x 6' x 2". The reinforcement consisted of 3/16" diameter plain round mild steel bars and were placed according to the following pattern:

Layer #1: spacing = 3.5"	Layer #2: spacing = 3.0"
cover = 0.1875"	cover = 0.375"
$\theta_x = + 45^\circ$	$\theta_x = - 45^\circ$

The quarter slab was discretized into sixteen finite elements as shown in Fig. 37. Six concrete layers and two steel layers were used as shown in Fig. 40. The experimental ultimate load exceeded the yield line collapse load by 73% in this example. The behavior of this slab was influenced by the same factors as discussed previously in Section 4.4. To account for the tensile membrane action the in-plane displacement components of nodes 3 and 13 in the x-direction and the in-plane displacement component of nodes 15 and 13 in the y-direction were restrained.

The analytic and experimental load deflection histories for the center point are plotted in Fig. 41. The analytic loads at which yielding of the steel and crushing of the concrete begin are also indicated in that figure. The agreement between the experimental and analytic curves is comparable to that attained in the last section. As in the previous example, the in-plane restraints were used to approximate the second order phenomena arising from the substantial deformations. Limited observations reported from the actual experiment make accurate determination of the magnitude and direction of these effects almost impossible.

4.6 Fixed-Free Rectangular Slab

Two almost identical 12' x 6' x 4" rectangular slabs were tested under a concentrated center point load (Ref. 40). The load was applied through a 9" x 9" steel bearing plate. The long sides of the slab were fixed against all deformations while the short sides were left free, i.e., unsupported. Reinforcement consisted of 1/4" and 3/8" diameter mild steel bars orthogonal to the slab edges. Both top and bottom tension reinforcement was used since tensile stresses are developed on both the top and the bottom surface of the slab because of the boundary conditions. Although the distribution of reinforcing varied throughout the plate, it is believed that an adequate model was developed by using a constant thickness for each steel layer. There is, however, no analytic difficulty in extending this formulation to consider a steel layer whose thickness varies from element to element.

The experimental slab No. 1 was selected for the analytic study. Material properties are listed in Table I. A quarter of the slab was discretized into sixteen finite elements as shown in Fig. 42. The depth was divided into six concrete layers and four steel layers as indicated in Fig. 43.

The load deflection histories for the two experimental slabs and the analytic model for slab No. 1 are shown in Fig. 44. Shear punch failure occurred during the experimental tests and caused premature collapse of the slabs before their full flexural capacity could be developed. Since the analytic model considers only the flexural action, the shear

punch type of failure could not be obtained analytically. Enlarged portions of experimental and analytic load deflection histories up to the occurrence of shear punch failure are shown in Fig. 45. The figure indicates that when flexural action is dominant a close agreement between experimental and computed results is obtained.

The analytic and experimental crack patterns for the top surface of the quarter slab are shown in Figs. 46A and 46B respectively. The experimental crack pattern was not perfectly symmetric but it had essentially the same general form for all quadrants of the slab. The bottom surface crack patterns are shown in Figs. 47A and 47B. The center portion of the slab exhibited extensive cracking due to the shear punch failure. As would be expected, the analytic model did not reflect those cracks due to the shear punch failure. Good agreement was obtained between the experimental and analytic crack patterns that were caused primarily by the flexural action in the slab. Both experimental and analytic results indicated a fan shape crack pattern radiating from the center point of the slab on the bottom surface and extensive cracking on the top surface along the fixed edge.

The fact that these experimental slabs failed by shear punch action does not reduce the value of the flexural analysis presented here when applied to the bridge overload problem. Work currently underway (Ref. 18) substantiates former conclusions that punching shear failures are very unlikely in bridge decks subjected to vehicular loadings.

4.7 Fixed-Fixed Square Slab

Two 6' x 6' x 6" square slabs were tested as part of the same experimental study as the two rectangular slabs mentioned in Section 4.6. The slabs were fixed on all four sides and loaded by a concentrated center point load applied through a 9" x 9" steel plate. As before, 1/4" and 3/8" diameter mild steel bars were placed orthogonal to the slab edges.

The analytic model was developed using the material properties of the first experimental slab of this pair. These properties are listed in Table 1. A quarter of the slab was discretized into sixteen finite elements as shown in Fig. 48. The depth was divided into six concrete layers and four steel layers as indicated in Fig. 49.

The experimental load deflection histories for the two almost identical test slabs along with the analytic results are shown in Fig. 50. As was the case for the rectangular slabs of the previous section, a shear punch failure occurred before the flexural capacity of the slab was developed. The load deflection history up to the initiation of the shear punch failure is plotted to a larger scale in Fig. 51. The slight difference between the analytic and experimental load deflection histories may be attributed to the lack of total fixity observed by the experimenters. It was estimated that the fixed edge supports were 90% effective. The analytic work assumes full restraint along the edges in question. Thus the analytic model should produce a load deflection history which is stiffer than that obtained experimentally.

The analytic and experimental top surface and bottom surface crack patterns are presented in Figs. 52 and 53 respectively. Both the analytic and experimental bottom surface crack patterns developed into a fan shape pattern radiating from the center point. The top surface crack patterns in both the experimental and analytic cases developed into a concentric circle-like pattern around the center of the slab.

5. SUMMARY AND CONCLUSIONS

The reported work deals with the inelastic flexural analysis of reinforced concrete slabs. This analysis technique provides a method by which the load deflection response up to a flexural collapse of a reinforced concrete slab can be obtained. The state of flexural stress and strain are also obtained for various load levels.

This work has been performed as a subset of a larger investigation dealing with the overload response of beam-slab highway bridges. The method presented in this report will eventually be interfaced with a completed study on the inelastic analysis of prestressed concrete beams (Ref. 19) so as to model a complete bridge superstructure (Ref. 23).

The finite element method was used as the basic analysis technique. The slab is discretized into a mesh of rectangular finite elements connected at the node points. These finite elements are further divided into a series of layers through the depth. The elements provide a means to monitor the spread of nonlinear behavior through the plane of the plate, and the layers monitor nonlinear behavior through the depth of the plate. The following material nonlinearities have been considered:

1. Nonlinear stress-strain behavior of concrete,
2. Cracking and crushing of concrete, and
3. Yielding of reinforcing steel.

These nonlinearities have been incorporated into the analysis scheme via:

1. A nonlinear biaxial stress-strain curve for concrete,
2. A biaxial failure criteria for concrete,
3. A Ramberg-Osgood stress-strain curve for reinforcing steel, and,
4. A piecewise linear tangent stiffness incremental iterative solution technique.

The method has been applied to one beam and six slabs from experimental studies available in the literature. Experimental and analytical load deflection curves were compared for all problems, and crack patterns and strain histories were compared where available. Good agreement was observed between the analytical predictions and experimental tests for slabs which failed in flexure. The following conclusions can be drawn:

1. The rectangular finite element with coupling can be used in an inelastic flexural analysis of reinforced concrete slabs.
2. Previous work on biaxial stress-strain relations for concrete has been extended and applied to reinforced concrete slabs. The results have indicated that this idealization is adequate for the flexural problems.
3. As was previously observed, a nonlinear Ramberg-Osgood stress-strain curve can be used for reinforcing steel.
4. The steel reinforcing bars placed at different angles and depths within the slab can be modeled as a system of uniaxially stressed layers.

5. The downward portion of the stress-strain curve for concrete can be used to produce a globally adequate redistribution of the effects of cracking and crushing. The effect of the downward portion of the tensile stress-strain curve has been called tension stiffening by some authors.
6. Gross crack patterns can be obtained through the use of the presented analysis.
7. The load deflection history up to a flexural collapse can be obtained. If the basic response is flexural and the failure mode is punching shear, then the developed method can accurately predict the load-deflection history up to the initiation of the shear punch failure.
8. It can be concluded from the example problems in Chapter 4 that a variety of complex support conditions and loadings can be handled in the analysis technique which has been presented.

6. APPENDIX

ELEMENT STIFFNESS MATRICES

A.1 Introduction

This appendix is a supplement to Sections 2.3 through 2.7. The previous development of stiffness matrices will be expanded upon so that explicit evaluation can be performed. The resulting explicit matrices will be presented as an aid to those who may carry the work further. It will be assumed that the reader has read Chapter 2 in detail.

A.2 Displacement Functions

The displacement functions chosen in this analysis were presented as Eq. 2.11 and Eq. 2.12. Substitution of these equations into Eq. 2.13 yields:

$$[P_u(x,y)] = \begin{bmatrix} 1 & x & y & xy & 0 & 0 & 0 & 0 \\ 0 & 0 & 0 & 0 & 1 & x & y & xy \end{bmatrix} \quad (A.1)$$

$$[P_\phi(x,y)] = \begin{bmatrix} 1 & x & y & x^2 & xy & y^2 & x^3 & x^2y & xy^2 & y^3 & x^3y & xy^3 \\ 0 & 0 & 1 & 0 & x & 2y & 0 & x^2 & 2xy & 3y^2 & x^3 & 3xy^2 \\ 0 & -1 & 0 & -2x & -y & 0 & -3x^2 & -2xy & -y^2 & 0 & -3x^2y & -y^3 \end{bmatrix} \quad (A.2)$$

The $W(x,y)$ displacement function will be non-dimensionalized to facilitate the inversion of the $[C_\phi]$ matrix introduced in Eq. 2.21b and

shown inverted in Eq. 2.22a. This is carried out by substituting the non-dimensionalized coordinates (\bar{x}, \bar{y}) into $W(x, y)$ defined in Eq. 2.11. Thus

$$W(\bar{x}, \bar{y}) = [1 \quad \bar{x} \quad \bar{y} \quad \bar{x}^2 \quad \bar{x}\bar{y} \quad \bar{y}^2 \quad \bar{x}^3 \quad \bar{x}^2\bar{y} \quad \bar{x}\bar{y}^2 \quad \bar{y}^3 \quad \bar{x}^3\bar{y} \quad \bar{x}\bar{y}^3] \quad (\text{A.3})$$

$$W(x, y) = [W(\bar{x}, \bar{y})] \cdot [R] \cdot \{A\} \quad (\text{A.4})$$

Where: $x = a\bar{x}$

$y = b\bar{y}$

[R] is a 12 x 12 diagonal matrix (i.e. all off diagonal elements are zero) where the diagonal terms consist of the following values: 1, a, b, a^2 , ab, b^2 , a^3 , a^2b , ab^2 , b^3 , a^3b , and ab^3 . The quantities a and b are element half lengths in the x-direction and the y-direction respectively and are shown in Fig. 3. The three bending displacements are given by Eq. 2.10. The derivatives in Eq. 2.10 may now be written as, for example:

$$\frac{\partial W}{\partial y} = \frac{\partial W(x, y)}{\partial y} = \frac{\partial W(x, y)}{\partial \bar{y}} \frac{\partial \bar{y}}{\partial y} = \frac{\partial}{\partial \bar{y}} [W(\bar{x}, \bar{y})] \frac{\partial \bar{y}}{\partial y} [R] \{A\} \quad (\text{A.5})$$

Using Eq. 2.14, it is possible to write

$$\Delta_{\phi}(x, y) = [\bar{\Gamma}_{\phi}(x, y)] [W(x, y)] \{A\} = [P_{\phi}(x, y)] \{A\} \quad (\text{A.6a})$$

$[\bar{\Gamma}_{\phi}(x, y)]$ is a matrix containing the differential operators indicated in Eq. 2.13. Substitution of Eq. A.4 yields

$$\Delta_{\phi}(x, y) = [\bar{\Gamma}_{\phi}(x, y)] [W(\bar{x}, \bar{y})] [R] \{A\} \quad (\text{A.6b})$$

Employing the chain rule of differentiation as indicated in Eq. A.5 results in

$$\Delta_{\phi}(x,y) = [t] [\bar{\Gamma}_{\phi}(\bar{x},\bar{y})] [W(\bar{x},\bar{y})] [R] \{A\} = [t] [P_{\phi}(\bar{x},\bar{y})] [R] \{A\} \quad (A.7)$$

Where:

$$[t] = \begin{bmatrix} 1 & 0 & 0 \\ 0 & \partial\bar{y}/\partial y & 0 \\ 0 & 0 & \partial\bar{x}/\partial x \end{bmatrix} = \begin{bmatrix} 1 & 0 & 0 \\ 0 & 1/b & 0 \\ 0 & 0 & 1/a \end{bmatrix}$$

The $[C_u]$ and $[C_{\phi}]$ matrices can now be obtained by substituting the nodal point coordinates (x_n, y_n) into Eq. A.1 for $[C_u]$ and (\bar{x}_n, \bar{y}_n) into Eq. A.7 for $[C_{\phi}]$. (x_n, y_n) consists of the set of I, J, K and L nodal point coordinates $(-a,b)$, $(-a,-b)$, (a,b) , $(a,-b)$. (\bar{x}_n, \bar{y}_n) consists of the set of non-dimensionalized nodal point coordinates $(-1,1)$, $(-1,-1)$, $(1,1)$ and $(1,-1)$. The resulting $[C_{\phi}]$ and $[C_u]$ matrices are given as:

$$[C_{\phi}] = \begin{bmatrix} 1 & -1 & 1 & 1 & -1 & 1 & -1 & 1 & -1 & 1 & -1 & -1 \\ 0 & 0 & 1 & 0 & -1 & 2 & 0 & 1 & -2 & 3 & -1 & -3 \\ 0 & -1 & 0 & 2 & -1 & 0 & -3 & 2 & -1 & 0 & -3 & -1 \\ 1 & -1 & -1 & 1 & 1 & 1 & -1 & -1 & -1 & -1 & 1 & 1 \\ 0 & 0 & 1 & 0 & -1 & -2 & 0 & 1 & 2 & 3 & -1 & -3 \\ 0 & -1 & 0 & 2 & 1 & 0 & -3 & -2 & -1 & 0 & 3 & 1 \\ 1 & 1 & 1 & 1 & 1 & 1 & 1 & 1 & 1 & 1 & 1 & 1 \\ 0 & 0 & 1 & 0 & 1 & 2 & 0 & 1 & 2 & 3 & 1 & 3 \\ 0 & -1 & 0 & -2 & -1 & 0 & -3 & -2 & -1 & 0 & -3 & -1 \\ 1 & 1 & -1 & 1 & -1 & 1 & 1 & -1 & 1 & -1 & -1 & -1 \\ 0 & 0 & 1 & 0 & 1 & -2 & 0 & 1 & -2 & 3 & 1 & 3 \\ 0 & -1 & 0 & -2 & 1 & 0 & -3 & 2 & -1 & 0 & 3 & 1 \end{bmatrix} \quad (A.8)$$

$$[C_u] = \begin{bmatrix} 1 & -a & b & -ab & 0 & 0 & 0 & 0 \\ 0 & 0 & 0 & 0 & 1 & -a & b & -ab \\ 1 & -a & -b & ab & 0 & 0 & 0 & 0 \\ 0 & 0 & 0 & 0 & 1 & -a & -b & ab \\ 1 & a & b & ab & 0 & 0 & 0 & 0 \\ 0 & 0 & 0 & 0 & 1 & a & b & ab \\ 1 & a & -b & -ab & 0 & 0 & 0 & 0 \\ 0 & 0 & 0 & 0 & 1 & a & -b & -ab \end{bmatrix} \quad (A.9)$$

Thus the nodal point displacements are:

$$\{\delta_u^e\} = [\Delta_u(x_n, y_n)] = [C_u] \{B\} \quad (A.10)$$

$$\{\delta_\phi^e\} = [\Delta_\phi(\bar{x}_n, \bar{y}_n)] = [T] [C_\phi] [R] \{A\} \quad (A.11)$$

Where:

$$[T] = \begin{bmatrix} [t] & 0 & 0 & 0 \\ 0 & [t] & 0 & 0 \\ 0 & 0 & [t] & 0 \\ 0 & 0 & 0 & [t] \end{bmatrix} \quad (A.12)$$

and $[t]$ is defined in Eq. A.7.

A.3 Strains

Appropriate terms must be included in Eq. 2.18 to reflect the fact that the bending displacement function has been non-dimensionalized. Applying the chain rule again results in:

$$\begin{Bmatrix} -\frac{\partial^2 W}{\partial x^2} \\ -\frac{\partial^2 W}{\partial y^2} \\ -2\frac{\partial^2 W}{\partial x \partial y} \end{Bmatrix} = [S] \begin{Bmatrix} -\frac{\partial^2 W}{\partial \bar{x}^2} \\ -\frac{\partial^2 W}{\partial \bar{y}^2} \\ -2\frac{\partial^2 W}{\partial \bar{x} \partial \bar{y}} \end{Bmatrix} \quad (\text{A.13})$$

Where:

$$[S] = \begin{bmatrix} \frac{\partial \bar{x}}{\partial x} \frac{\partial \bar{x}}{\partial x} & 0 & 0 \\ 0 & \frac{\partial \bar{y}}{\partial y} \frac{\partial \bar{y}}{\partial y} & 0 \\ 0 & 0 & \frac{\partial \bar{x}}{\partial x} \frac{\partial \bar{y}}{\partial y} \end{bmatrix} \quad (\text{A.14a})$$

or:

$$[S] = \begin{bmatrix} \frac{1}{a^2} & 0 & 0 \\ 0 & \frac{1}{b^2} & 0 \\ 0 & 0 & \frac{1}{ab} \end{bmatrix} \quad (\text{A.14b})$$

Thus Eq. 2.18 is modified to reflect the non-dimensionalized coordinates in the following manner. Substitution of Eqs. 2.12 and Eq. A.4 into Eq. 2.18 leads to:

$$\{\epsilon_z\} = [Q_u] \{B\} + z [S] [Q_\phi] [R] \{A\} \quad (\text{A.15})$$

in which:

$$[Q_u] = \begin{bmatrix} 0 & 1 & 0 & y & 0 & 0 & 0 & 0 \\ 0 & 0 & 0 & 0 & 0 & 0 & 1 & x \\ 0 & 0 & 1 & x & 0 & 1 & 0 & y \end{bmatrix} \quad (A.16)$$

$$[Q_\phi] = \begin{bmatrix} 0 & 0 & 0 & -2 & 0 & 0 & -6\bar{x} & -2\bar{y} & 0 & 0 & -6\bar{x}\bar{y} & 0 \\ 0 & 0 & 0 & 0 & 0 & -2 & 0 & 0 & -2\bar{x} & -6\bar{y} & 0 & -6\bar{x}\bar{y} \\ 0 & 0 & 0 & 0 & -2 & 0 & 0 & -4\bar{x} & -4\bar{y} & 0 & -6\bar{x}^2 & -6\bar{y}^2 \end{bmatrix} \quad (A.17)$$

The constants {A} and {B} can be found as indicated in Eqs. 2.22 if care is taken to include the new matrices which result from non-dimensionalizing the bending displacement function.

Thus: $\{B\} = [C_u^{-1}] \{\delta_u^e\} \quad (A.18)$

$$\{A\} = [R^{-1}] [C_\phi^{-1}] [T^{-1}] \{\delta_\phi^e\} \quad (A.19)$$

Inversion of $[C_u]$ and $[C_\phi]$ results in the following matrices.

$$[C_{\phi}]^{-1} = \frac{1}{8} \begin{bmatrix} 2 & -1 & -1 & 2 & 1 & -1 & 2 & -1 & 1 & 2 & 1 & 1 \\ -3 & 1 & 1 & -3 & -1 & 1 & 3 & -1 & 1 & 3 & 1 & 1 \\ 3 & -1 & -1 & -3 & -1 & 1 & 3 & -1 & 1 & -3 & -1 & -1 \\ 0 & 0 & 1 & 0 & 0 & 1 & 0 & 0 & -1 & 0 & 0 & -1 \\ -4 & 1 & 1 & 4 & 1 & -1 & 4 & -1 & 1 & -4 & -1 & -1 \\ 0 & 1 & 0 & 0 & -1 & 0 & 0 & 1 & 0 & 0 & -1 & 0 \\ 1 & 0 & -1 & 1 & 0 & -1 & -1 & 0 & -1 & -1 & 0 & -1 \\ 0 & 0 & 1 & 0 & 0 & -1 & 0 & 0 & -1 & 0 & 0 & 1 \\ 0 & -1 & 0 & 0 & 1 & 0 & 0 & 1 & 0 & 0 & -1 & 0 \\ -1 & 1 & 0 & 1 & 1 & 0 & -1 & 1 & 0 & 1 & 1 & 0 \\ 1 & 0 & -1 & -1 & 0 & 1 & -1 & 0 & -1 & 1 & 0 & 1 \\ 1 & -1 & 0 & -1 & -1 & 0 & -1 & 1 & 0 & 1 & 1 & 0 \end{bmatrix}$$

(A.20)

$$[C_u]^{-1} = \frac{1}{4} \begin{bmatrix} 1 & 0 & 1 & 0 & 1 & 0 & 1 & 0 \\ -\frac{1}{a} & 0 & -\frac{1}{a} & 0 & \frac{1}{a} & 0 & \frac{1}{a} & 0 \\ \frac{1}{b} & 0 & -\frac{1}{b} & 0 & \frac{1}{b} & 0 & -\frac{1}{b} & 0 \\ -\frac{1}{ab} & 0 & \frac{1}{ab} & 0 & \frac{1}{ab} & 0 & -\frac{1}{ab} & 0 \\ 0 & 1 & 0 & 1 & 0 & 1 & 0 & 1 \\ 0 & -\frac{1}{a} & 0 & -\frac{1}{a} & 0 & \frac{1}{a} & 0 & \frac{1}{a} \\ 0 & \frac{1}{b} & 0 & -\frac{1}{b} & 0 & \frac{1}{b} & 0 & -\frac{1}{b} \\ 0 & -\frac{1}{ab} & 0 & \frac{1}{ab} & 0 & \frac{1}{ab} & 0 & -\frac{1}{ab} \end{bmatrix}$$

(A.21)

Substitution of Eqs. A.18 and A.19 into Eq. A.15 defines the strains as a function of the nodal point displacements:

$$\{\varepsilon\}_z = [Q_u] [C_u]^{-1} \{\delta_u^e\} + z [S] [Q_\phi] [R] [R]^{-1} [C_\phi]^{-1} [T]^{-1} \{\delta_\phi^e\} \quad (\text{A.22})$$

After performing the multiplication of the [R] matrices,

$$\{\varepsilon\}_z = [Q_u] [C_u]^{-1} \{\delta_u^e\} + z [S] [Q_\phi] [C_\phi]^{-1} [T]^{-1} \{\delta_\phi^e\} \quad (\text{A.23})$$

Comparison of Eq. A.23 with Eqs. 2.24 shows that the $[B_u]$ and $[B_\phi]$ matrices can be defined as:

$$[B_u] = [Q_u] [C_u]^{-1} \quad (\text{A.24a})$$

$$[B_\phi] = [S] [Q_\phi] [C_\phi]^{-1} [T]^{-1} \quad (\text{A.24b})$$

A.4 Element Stiffness Matrices

Evaluation of the inplane, coupling and bending stiffness matrices given in Eqs. 2.33 can now proceed. Substitution of Eqs. A.24a and A.24b into Eqs. 2.33 gives:

$$[k_{uu}] = [C_u]^{-1T} \iint_{yx} [Q_u]^T [D_{uu}] [Q_u] dx dy [C_u]^{-1} \quad (\text{A.25})$$

$$[k_{u\phi}] = [C_u]^{-1T} \iint_{yx} [Q_u]^T [D_{u\phi}] [S] [Q_\phi] dx dy [C_\phi]^{-1} [T]^{-1} \quad (\text{A.26})$$

$$[k_{\phi\phi}] = [T]^{-1T} [C_\phi]^{-1T} \iint_{yx} [Q_\phi]^T [S]^T [D_{\phi\phi}] [S] [Q_\phi] dx dy [C_\phi]^{-1} [T]^{-1} \quad (\text{A.27})$$

$[D_{uu}]$, $[D_{u\phi}]$ and $[D_{\phi\phi}]$ are the rigidities introduced in Section 2.7 and given in Eq. 2.32. The evaluation of the integrals in Eqs. A.25 to A.27 can be simplified by considering only one element of the rigidity matrix to be nonzero at a time. This reduces one very laborious evaluation of each of the three stiffness matrices to six much simpler problems. For each matrix the results are then summed up in the following form:

$$[k_{uu}] = [C_u]^{-1T} \left[D_{11} [K_1] + D_{12} [K_2] + D_{13} [K_3] + D_{22} [K_4] + D_{23} [K_5] + D_{33} [K_6] \right]_{uu} [C_u]^{-1} \quad (A.28)$$

$$[k_{u\phi}] = [C_u]^{-1T} \left[D_{11} [K_1] + D_{12} [K_2] + D_{13} [K_3] + D_{22} [K_4] + D_{23} [K_5] + D_{33} [K_6] \right]_{u\phi} [C_\phi]^{-1} [T]^{-1} \quad (A.29)$$

$$[k_{\phi\phi}] = [T]^{-1T} [C_\phi]^{-1T} \left[D_{11} [K_1] + D_{12} [K_2] + D_{13} [K_3] + D_{22} [K_4] + D_{23} [K_5] + D_{33} [K_6] \right]_{\phi\phi} [C_\phi]^{-1} [T]^{-1} \quad (A.30)$$

The submatrices pertaining to the inplane stiffness matrix are evaluated by employing Eq. A.25 as follows:

$$\left(D_{11} [K_1] \right)_{uu} = \iint_{yx} [Q_u]^T \begin{bmatrix} D_{11} & 0 & 0 \\ 0 & 0 & 0 \\ 0 & 0 & 0 \end{bmatrix} [Q_u] \, dx dy \quad (\text{A.31a})$$

$$\left(D_{12} [K_2] \right)_{uu} = \iint_{yx} [Q_u]^T \begin{bmatrix} 0 & D_{12} & 0 \\ D_{21} & 0 & 0 \\ 0 & 0 & 0 \end{bmatrix} [Q_u] \, dx dy \quad (\text{A.31b})$$

$$\left(D_{13} [K_3] \right)_{uu} = \iint_{yx} [Q_u]^T \begin{bmatrix} 0 & 0 & D_{13} \\ 0 & 0 & 0 \\ D_{31} & 0 & 0 \end{bmatrix} [Q_u] \, dx dy \quad (\text{A.31c})$$

$$\left(D_{22} [K_4] \right)_{uu} = \iint_{yx} [Q_u]^T \begin{bmatrix} 0 & 0 & 0 \\ 0 & D_{22} & 0 \\ 0 & 0 & 0 \end{bmatrix} [Q_u] \, dx dy \quad (\text{A.31d})$$

$$\left(D_{23} [K_5] \right)_{uu} = \iint_{yx} [Q_u]^T \begin{bmatrix} 0 & 0 & 0 \\ 0 & 0 & D_{23} \\ 0 & D_{32} & 0 \end{bmatrix} [Q_u] \, dx dy \quad (\text{A.31e})$$

$$\left(D_{33} [K_6] \right)_{uu} = \iint_{yx} [Q_u]^T \begin{bmatrix} 0 & 0 & 0 \\ 0 & 0 & 0 \\ 0 & 0 & D_{33} \end{bmatrix} [Q_u] \, dx dy \quad (\text{A.31f})$$

The $(D_{ij})_{uu}$ terms in the above equations correspond to elements of the inplane rigidities given in Eq. 2.32a. Explicit expressions for Eq. A.31 can be developed by utilizing Eq. A.16. This has been done to generate the following formulae:

$$[K_1]_{uu} = \begin{bmatrix} 0 & & & & & & & & \\ 0 & 1 & & & & & & & \\ 0 & 0 & 0 & & & & & & \\ 0 & 0 & 0 & \frac{b^2}{3} & & & & & \\ 0 & 0 & 0 & 0 & 0 & & & & \\ 0 & 0 & 0 & 0 & 0 & 0 & & & \\ 0 & 0 & 0 & 0 & 0 & 0 & 0 & & \\ 0 & 0 & 0 & 0 & 0 & 0 & 0 & 0 & \end{bmatrix} \quad \begin{matrix} 4ab \\ (A.32a) \end{matrix}$$

$$[K_2]_{uu} = \begin{bmatrix} 0 & & & & & & & & \\ 0 & 0 & & & & & & & \\ 0 & 0 & 0 & & & & & & \\ 0 & 0 & 0 & 0 & & & & & \\ 0 & 0 & 0 & 0 & 0 & & & & \\ 0 & 0 & 0 & 0 & 0 & 0 & & & \\ 0 & 1 & 0 & 0 & 0 & 0 & 0 & & \\ 0 & 0 & 0 & 0 & 0 & 0 & 0 & 0 & \end{bmatrix} \quad \begin{matrix} 4ab \\ (A.32b) \end{matrix}$$

$$[K_3]_{uu} = \begin{bmatrix}
 0 & & & & & & & & \\
 0 & 0 & & & & & & & \\
 0 & 1 & 0 & & & & & & \\
 0 & 0 & 0 & 0 & & & & & \\
 0 & 0 & 0 & 0 & 0 & & & & \\
 0 & 1 & 0 & 0 & 0 & 0 & & & \\
 0 & 0 & 0 & 0 & 0 & 0 & 0 & & \\
 0 & 0 & 0 & \frac{b^2}{3} & 0 & 0 & 0 & 0 & \\
 \end{bmatrix} \quad 4ab \quad (A.32c)$$

$$[K_4]_{uu} = \begin{bmatrix}
 0 & & & & & & & & \\
 0 & 0 & & & & & & & \\
 0 & 0 & 0 & & & & & & \\
 0 & 0 & 0 & 0 & & & & & \\
 0 & 0 & 0 & 0 & 0 & & & & \\
 0 & 0 & 0 & 0 & 0 & 0 & & & \\
 0 & 0 & 0 & 0 & 0 & 0 & 0 & & \\
 0 & 0 & 0 & 0 & 0 & 0 & 0 & 1 & \\
 0 & 0 & 0 & 0 & 0 & 0 & 0 & 0 & \frac{a^2}{3} \\
 \end{bmatrix} \quad 4ab \quad (A.32d)$$

$$[K_5]_{uu} = \begin{bmatrix} 0 & & & & & & & \\ 0 & 0 & & & & & & \\ 0 & 0 & 0 & & & & & \\ 0 & 0 & 0 & 0 & & & & \\ 0 & 0 & 0 & 0 & 0 & & & \\ 0 & 0 & 0 & 0 & 0 & 0 & & \\ 0 & 0 & 1 & 0 & 0 & 1 & 0 & \\ 0 & 0 & 0 & \frac{a^2}{3} & 0 & 0 & 0 & 0 \end{bmatrix} \quad \begin{matrix} \\ \\ \\ \\ \\ \\ 4ab \\ \end{matrix} \quad (A.32e)$$

$$[K_6]_{uu} = \begin{bmatrix} 0 & & & & & & & \\ 0 & 0 & & & & & & \\ 0 & 0 & 1 & & & & & \\ 0 & 0 & 0 & \frac{a^2}{3} & & & & \\ 0 & 0 & 0 & 0 & 0 & & & \\ 0 & 0 & 1 & 0 & 0 & 1 & & \\ 0 & 0 & 0 & 0 & 0 & 0 & 0 & \\ 0 & 0 & 0 & 0 & 0 & 0 & 0 & \frac{b^2}{3} \end{bmatrix} \quad \begin{matrix} \\ \\ \\ \\ \\ 4ab \\ \\ \end{matrix} \quad (A.32f)$$

In a similar manner the submatrices for the coupling and bending element stiffness matrices can be developed from Eqs. A.16 and A.17 and Eqs. A.26 and A.27. Care must be exercised to insure that the proper rigidities given in Eqs. 2.32b and 2.32c are employed. The submatrices for the coupling and bending stiffness matrices are presented in Eqs. A.33 and A.34 respectively.

$$[K_1]_{u\phi} = \begin{bmatrix} 0 & 0 & 0 & 0 & 0 & 0 & 0 & 0 & 0 & 0 & 0 & 0 \\ 0 & 0 & 0 & \frac{-8b}{a} & 0 & 0 & 0 & 0 & 0 & 0 & 0 & 0 \\ 0 & 0 & 0 & 0 & 0 & 0 & 0 & 0 & 0 & 0 & 0 & 0 \\ 0 & 0 & 0 & 0 & 0 & 0 & 0 & \frac{-8b^2}{3a} & 0 & 0 & 0 & 0 \\ 0 & 0 & 0 & 0 & 0 & 0 & 0 & 0 & 0 & 0 & 0 & 0 \\ 0 & 0 & 0 & 0 & 0 & 0 & 0 & 0 & 0 & 0 & 0 & 0 \\ 0 & 0 & 0 & 0 & 0 & 0 & 0 & 0 & 0 & 0 & 0 & 0 \\ 0 & 0 & 0 & 0 & 0 & 0 & 0 & 0 & 0 & 0 & 0 & 0 \end{bmatrix} \quad (\text{A.33a})$$

$$[K_2]_{u\phi} = \begin{bmatrix} 0 & 0 & 0 & 0 & 0 & 0 & 0 & 0 & 0 & 0 & 0 & 0 \\ 0 & 0 & 0 & 0 & 0 & \frac{-8a}{b} & 0 & 0 & 0 & 0 & 0 & 0 \\ 0 & 0 & 0 & 0 & 0 & 0 & 0 & 0 & 0 & 0 & 0 & 0 \\ 0 & 0 & 0 & 0 & 0 & 0 & 0 & 0 & 0 & -8a & 0 & 0 \\ 0 & 0 & 0 & 0 & 0 & 0 & 0 & 0 & 0 & 0 & 0 & 0 \\ 0 & 0 & 0 & 0 & 0 & 0 & 0 & 0 & 0 & 0 & 0 & 0 \\ 0 & 0 & 0 & \frac{-8b}{a} & 0 & 0 & 0 & 0 & 0 & 0 & 0 & 0 \\ 0 & 0 & 0 & 0 & 0 & 0 & -8b & 0 & 0 & 0 & 0 & 0 \end{bmatrix} \quad (\text{A.33b})$$

$$[K_3]_{u\phi} =$$

$$\begin{bmatrix} 0 & 0 & 0 & 0 & 0 & 0 & 0 & 0 & 0 & 0 & 0 & 0 \\ 0 & 0 & 0 & 0 & -8 & 0 & 0 & 0 & 0 & 0 & -8 & -8 \\ 0 & 0 & 0 & \frac{-8b}{a} & 0 & 0 & 0 & 0 & 0 & 0 & 0 & 0 \\ 0 & 0 & 0 & 0 & 0 & 0 & -8b & 0 & \frac{-16b}{3} & 0 & 0 & 0 \\ 0 & 0 & 0 & 0 & 0 & 0 & 0 & 0 & 0 & 0 & 0 & 0 \\ 0 & 0 & 0 & \frac{-8b}{a} & 0 & 0 & 0 & 0 & 0 & 0 & 0 & 0 \\ 0 & 0 & 0 & 0 & 0 & 0 & 0 & 0 & 0 & 0 & 0 & 0 \\ 0 & 0 & 0 & 0 & 0 & 0 & 0 & \frac{-8b^2}{3a} & 0 & 0 & 0 & 0 \end{bmatrix}$$

(A.33c)

$$[K_4]_{u\phi} =$$

$$\begin{bmatrix} 0 & 0 & 0 & 0 & 0 & 0 & 0 & 0 & 0 & 0 & 0 & 0 \\ 0 & 0 & 0 & 0 & 0 & 0 & 0 & 0 & 0 & 0 & 0 & 0 \\ 0 & 0 & 0 & 0 & 0 & 0 & 0 & 0 & 0 & 0 & 0 & 0 \\ 0 & 0 & 0 & 0 & 0 & 0 & 0 & 0 & 0 & 0 & 0 & 0 \\ 0 & 0 & 0 & 0 & 0 & 0 & 0 & 0 & 0 & 0 & 0 & 0 \\ 0 & 0 & 0 & 0 & 0 & 0 & 0 & 0 & 0 & 0 & 0 & 0 \\ 0 & 0 & 0 & 0 & 0 & \frac{-8a}{b} & 0 & 0 & 0 & 0 & 0 & 0 \\ 0 & 0 & 0 & 0 & 0 & 0 & 0 & 0 & \frac{-8a^2}{3b} & 0 & 0 & 0 \end{bmatrix}$$

(A.33d)

$$[K_5]_{u\phi} = \begin{bmatrix} 0 & 0 & 0 & 0 & 0 & 0 & 0 & 0 & 0 & 0 & 0 & 0 \\ 0 & 0 & 0 & 0 & 0 & 0 & 0 & 0 & 0 & 0 & 0 & 0 \\ 0 & 0 & 0 & 0 & 0 & \frac{-8a}{b} & 0 & 0 & 0 & 0 & 0 & 0 \\ 0 & 0 & 0 & 0 & 0 & 0 & 0 & 0 & \frac{-8a^2}{3b} & 0 & 0 & 0 \\ 0 & 0 & 0 & 0 & 0 & 0 & 0 & 0 & 0 & 0 & 0 & 0 \\ 0 & 0 & 0 & 0 & 0 & \frac{-8a}{b} & 0 & 0 & 0 & 0 & 0 & 0 \\ 0 & 0 & 0 & 0 & -8 & 0 & 0 & 0 & 0 & 0 & -8 & -8 \\ 0 & 0 & 0 & 0 & 0 & 0 & 0 & \frac{-16a}{3} & 0 & -8a & 0 & 0 \end{bmatrix} \quad (\text{A.33e})$$

$$[K_6]_{u\phi} = \begin{bmatrix} 0 & 0 & 0 & 0 & 0 & 0 & 0 & 0 & 0 & 0 & 0 & 0 \\ 0 & 0 & 0 & 0 & 0 & 0 & 0 & 0 & 0 & 0 & 0 & 0 \\ 0 & 0 & 0 & 0 & -8 & 0 & 0 & 0 & 0 & 0 & -8 & -8 \\ 0 & 0 & 0 & 0 & 0 & 0 & 0 & \frac{-16a}{3} & 0 & 0 & 0 & 0 \\ 0 & 0 & 0 & 0 & 0 & 0 & 0 & 0 & 0 & 0 & 0 & 0 \\ 0 & 0 & 0 & 0 & -8 & 0 & 0 & 0 & 0 & 0 & -8 & -8 \\ 0 & 0 & 0 & 0 & 0 & 0 & 0 & 0 & 0 & 0 & 0 & 0 \\ 0 & 0 & 0 & 0 & 0 & 0 & 0 & 0 & \frac{-16b}{3} & 0 & 0 & 0 \end{bmatrix} \quad (\text{A.33f})$$

$$[K_1]_{\phi\phi} = \frac{16b}{15a^3}$$

0												
0	0											
0	0	0										
0	0	0	15									
0	0	0	0	0								
0	0	0	0	0	0							
0	0	0	0	0	0	0						
0	0	0	0	0	0	0	45					
0	0	0	0	0	0	0	0	5				
0	0	0	0	0	0	0	0	0	0			
0	0	0	0	0	0	0	0	0	0	0		
0	0	0	0	0	0	0	0	0	0	0	15	
0	0	0	0	0	0	0	0	0	0	0	0	0

(A.34a)

$$[K_2]_{\phi\phi} = \frac{16}{15ab}$$

0												
0	0											
0	0	0										
0	0	0	0									
0	0	0	0	0								
0	0	0	15	0	0							
0	0	0	0	0	0	0						
0	0	0	0	0	0	0	0					
0	0	0	0	0	0	0	0	0				
0	0	0	0	0	0	15	0	0				
0	0	0	0	0	0	0	15	0	0			
0	0	0	0	0	0	0	0	0	0	0		
0	0	0	0	0	0	0	0	0	0	0	15	0

(A.34b)

$$[K_3]_{\phi\phi} = \frac{16}{15a^2}$$

0												
0	0											
0	0	0										
0	0	0	0									
0	0	0	15	0								
0	0	0	0	0	0							
0	0	0	0	0	0	0						
0	0	0	0	0	0	30	0					
0	0	0	0	0	0	0	10	0				
0	0	0	0	0	0	0	0	0	0			
0	0	0	15	0	0	0	0	0	0	0		
0	0	0	15	0	0	0	0	0	0	0	0	0

Symmetric

(A.34c)

$$[K_4]_{\phi\phi} = \frac{16a}{15b^3}$$

0												
0	0											
0	0	0										
0	0	0	0									
0	0	0	0	0								
0	0	0	0	0	15							
0	0	0	0	0	0	0						
0	0	0	0	0	0	0	0					
0	0	0	0	0	0	0	0	5				
0	0	0	0	0	0	0	0	0	45			
0	0	0	0	0	0	0	0	0	0	0		
0	0	0	0	0	0	0	0	0	0	0	0	15

Symmetric

(A.34d)

$$[K_5]_{\phi\phi} = \frac{16}{15b^2}$$

0												
0	0											
0	0	0										
0	0	0	0									
0	0	0	0	0								
0	0	0	0	0	15	0						
0	0	0	0	0	0	0	0					
0	0	0	0	0	0	0	0	0				
0	0	0	0	0	0	0	0	10	0			
0	0	0	0	0	0	0	0	0	30	0		
0	0	0	0	0	0	15	0	0	0	0	0	
0	0	0	0	0	0	15	0	0	0	0	0	0

(A.34e)

$$[K_6]_{\phi\phi} = \frac{16}{15ab}$$

0												
0	0											
0	0	0										
0	0	0	0									
0	0	0	0	15								
0	0	0	0	0	0							
0	0	0	0	0	0	0						
0	0	0	0	0	0	0	0	20				
0	0	0	0	0	0	0	0	0	20			
0	0	0	0	0	0	0	0	0	0	0		
0	0	0	0	0	15	0	0	0	0	0	27	
0	0	0	0	0	15	0	0	0	0	0	15	27

(A.34f)

Addition of the submatrices and multiplication by the $[T]^{-1}$, $[C_\phi]^{-1}$ and $[C_u]^{-1}$ matrices shown in Eqs. A.28, A.29 and A.30 are performed in the computer program. The results are the required stiffness matrices.

7. ACKNOWLEDGMENTS

This study was conducted in the Department of Civil Engineering and Fritz Engineering Laboratory, under the auspices of the Lehigh University Office of Research, as a part of a research investigation sponsored by the Pennsylvania Department of Transportation, U. S. Department of Transportation, Federal Highway Administration.

The basic research planning and administrative coordination in this investigation were in cooperation with the following individuals representing the Pennsylvania Department of Transportation: Mr. B. F. Kotalik, Bridge Engineer; Mr. H. P. Koretzky, and Mr. Hans Streibel, all from the Bridge Engineering Division; and Messrs. Leo D. Sandvig, Director; Wade L. Gramling, Research Engineer; Kenneth L. Heilman, Research Coordinator; all from the Bureau of Materials, Testing and Research.

The authors would like to thank the staff of Lehigh University Computing Center for their cooperation.

The manuscript was typed by Mrs. Ruth Grimes, and the figures were prepared by John M. Gera and Mrs. Sharon Balogh.

8. FIGURES

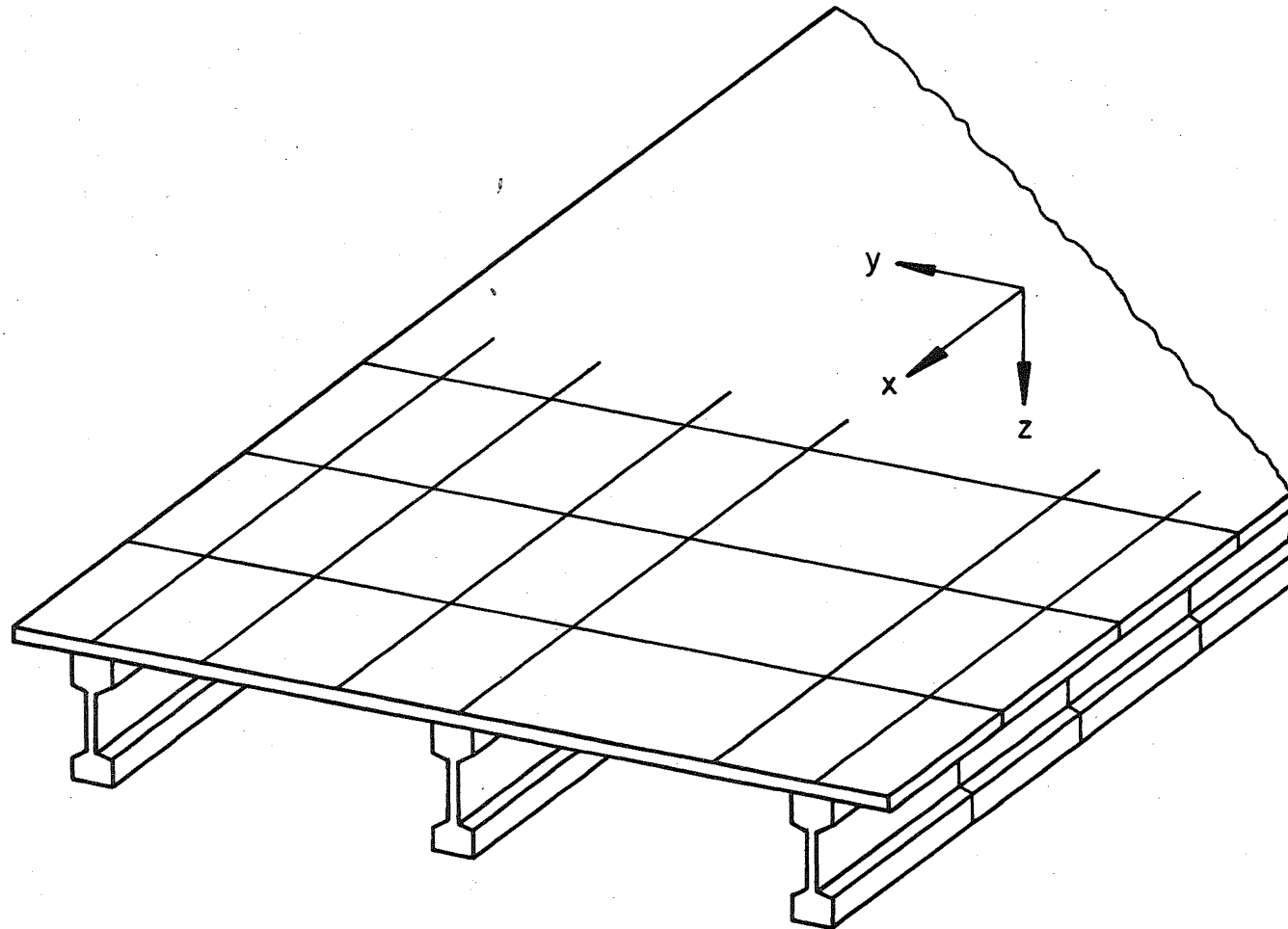


Fig. 1 Typical Beam-Slab Type Bridge and its Structural Idealization by Rectangular Finite Elements

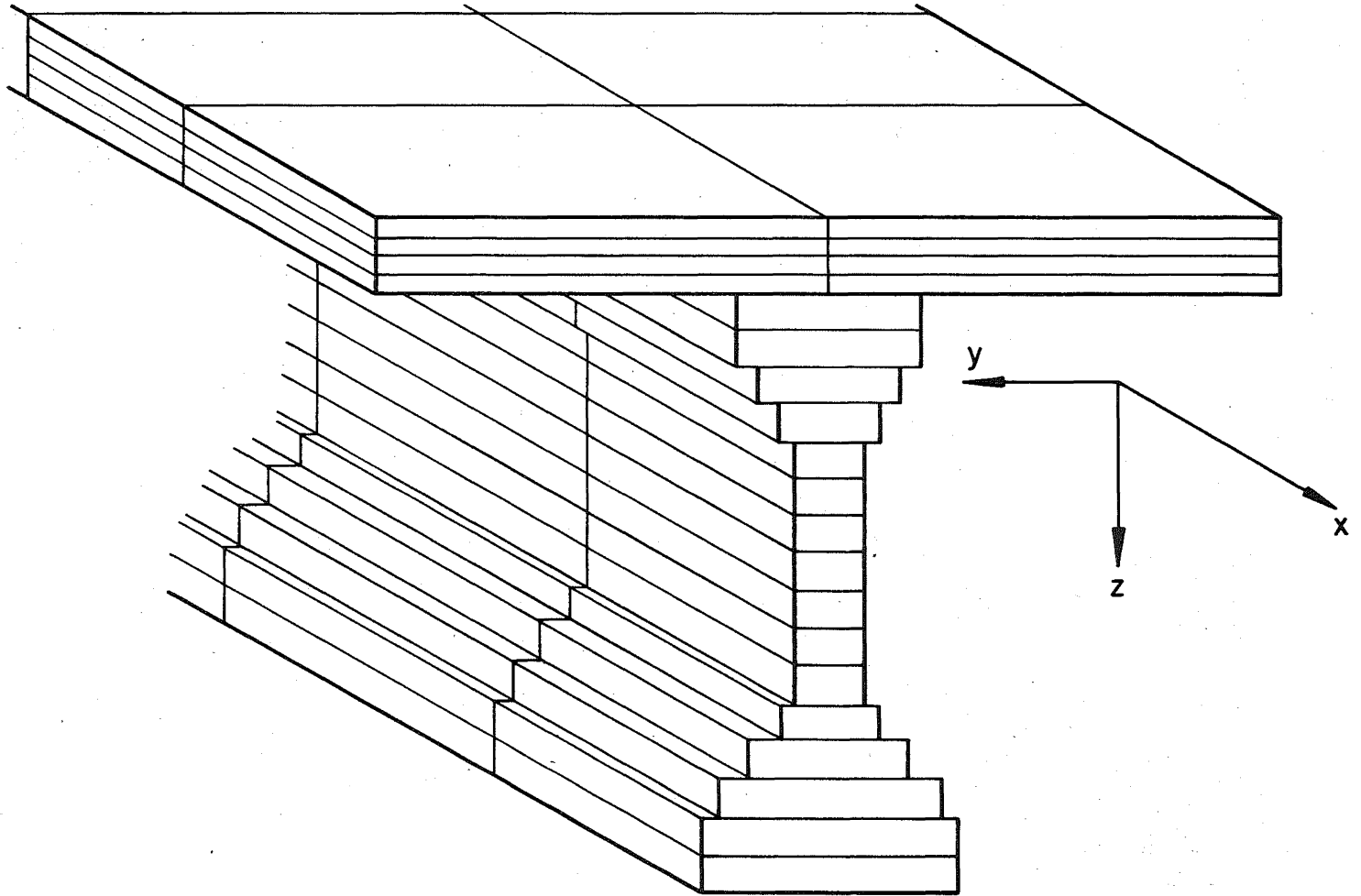


Fig. 2 Layered Elements Used to Idealize a Beam and Slab

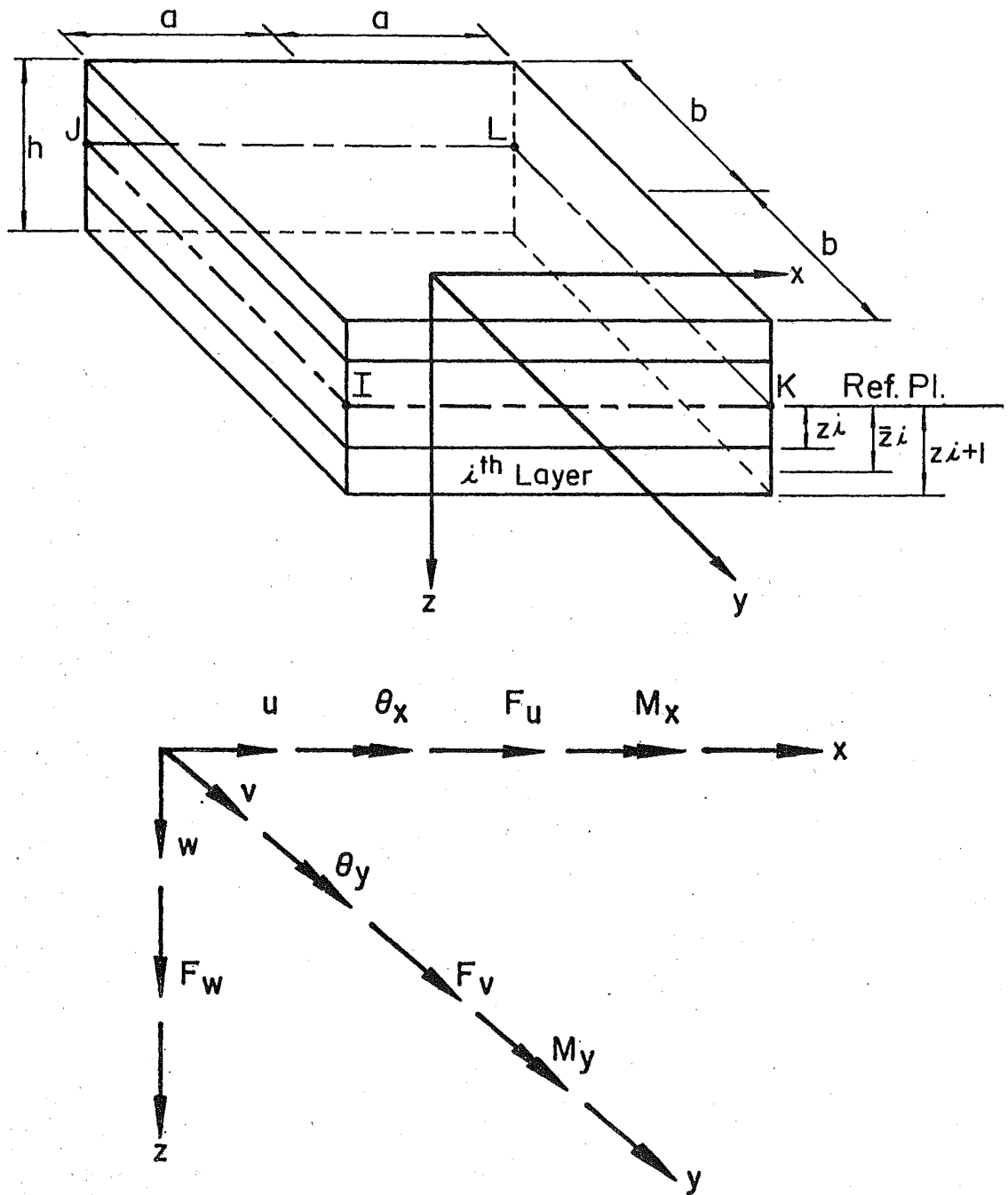
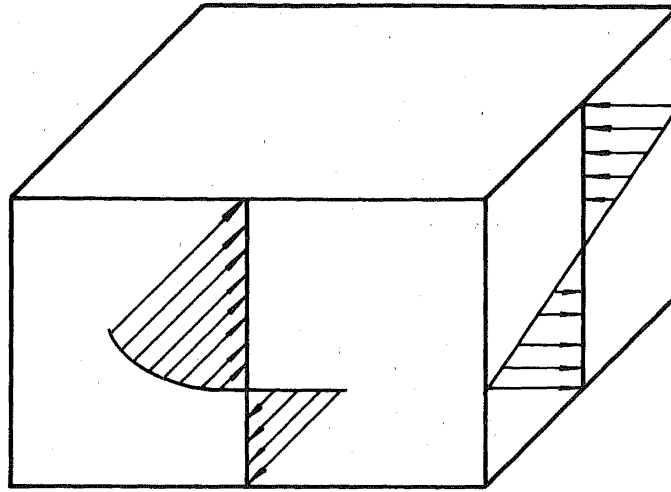
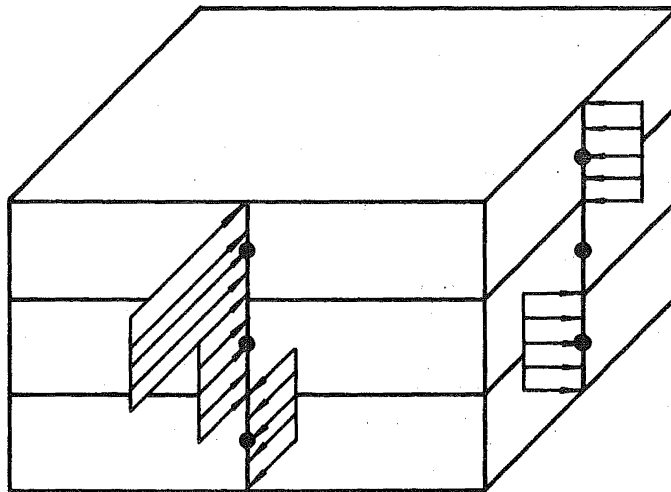


Fig. 3 Rectangular Finite Element for the Slab and Layering; Positive Coordinate Directions and, Force and Deformation Components at a Node



(A)



(B)

Fig. 4 Biaxial Stress Fields:
Continuum Approach (A) and Layer Idealization (B)

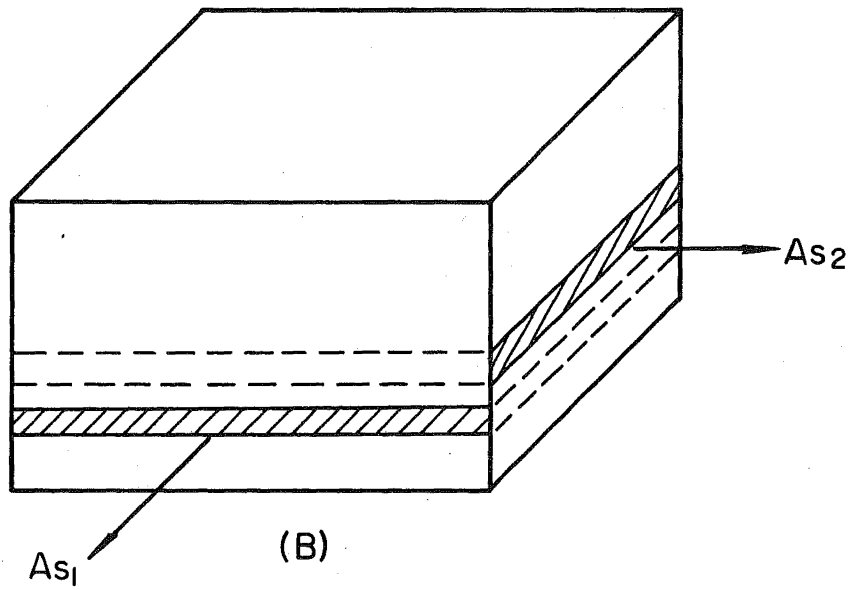
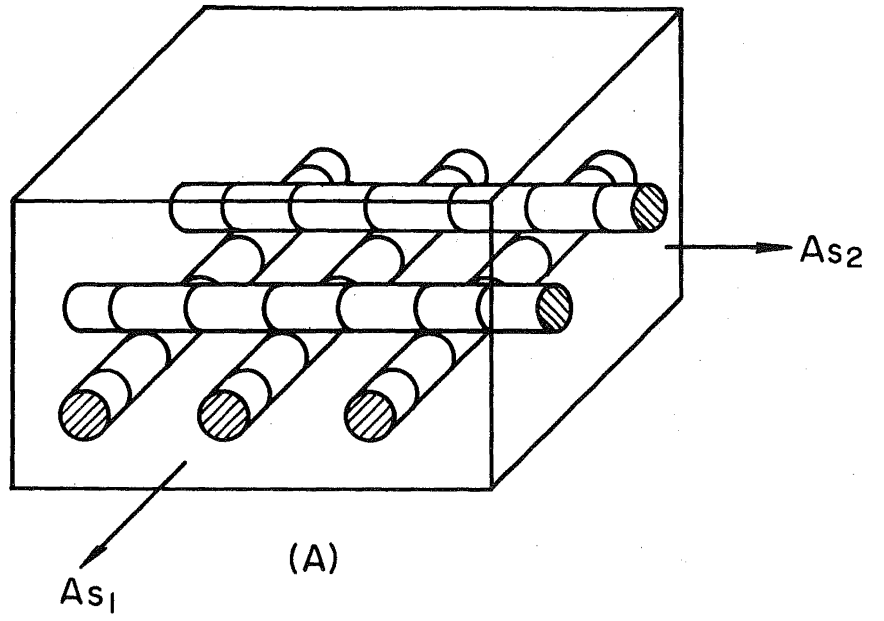


Fig. 5 Steel Reinforcing Bar System:
Actual (A) and Idealized (B)

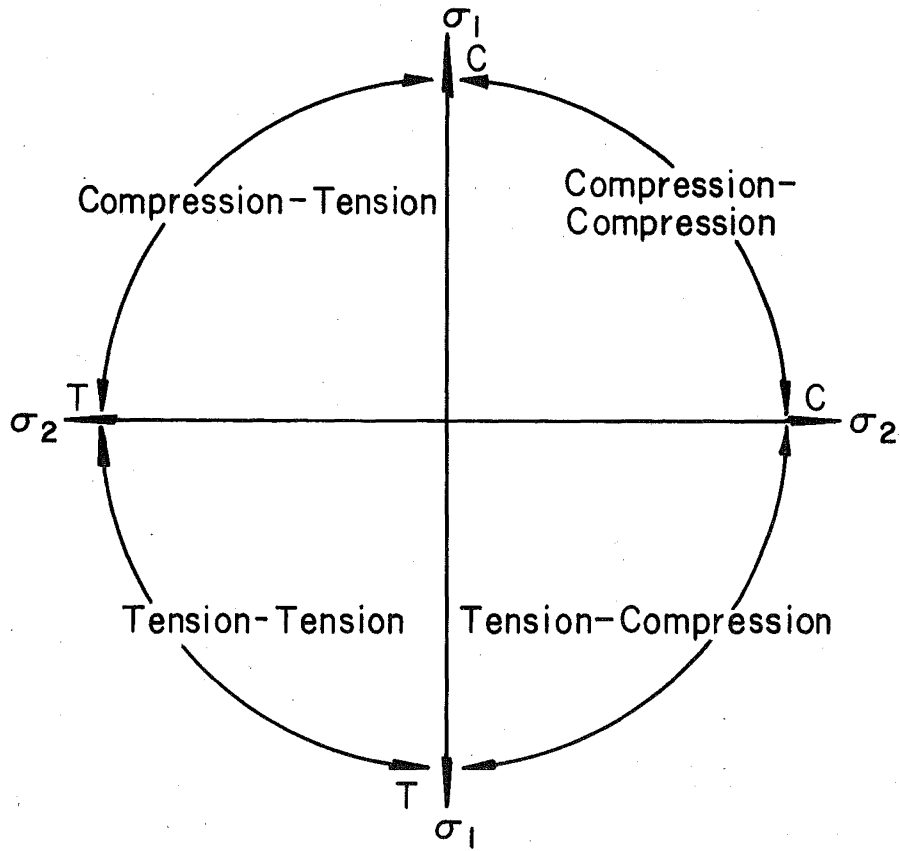


Fig. 6 The Biaxial Stress Plane

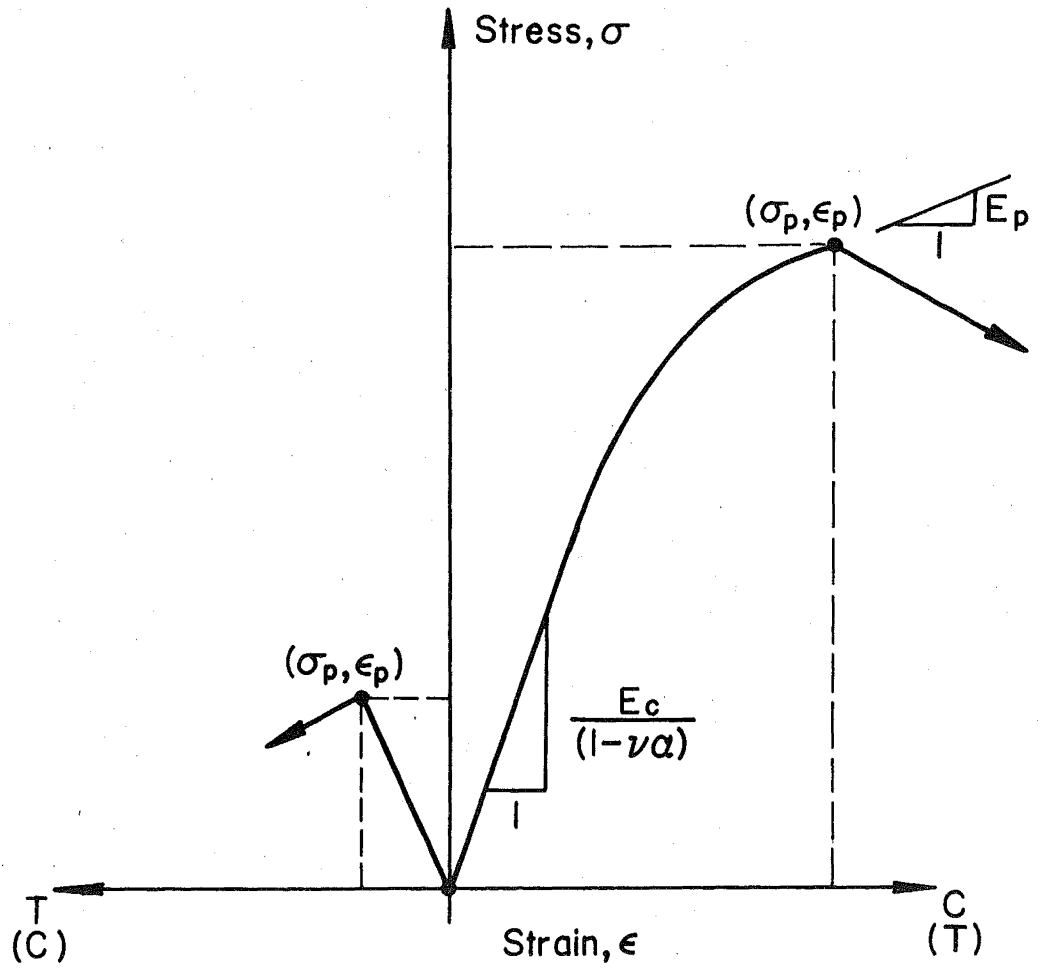


Fig. 7 General Linear and Nonlinear Concrete Stress-Strain Curves

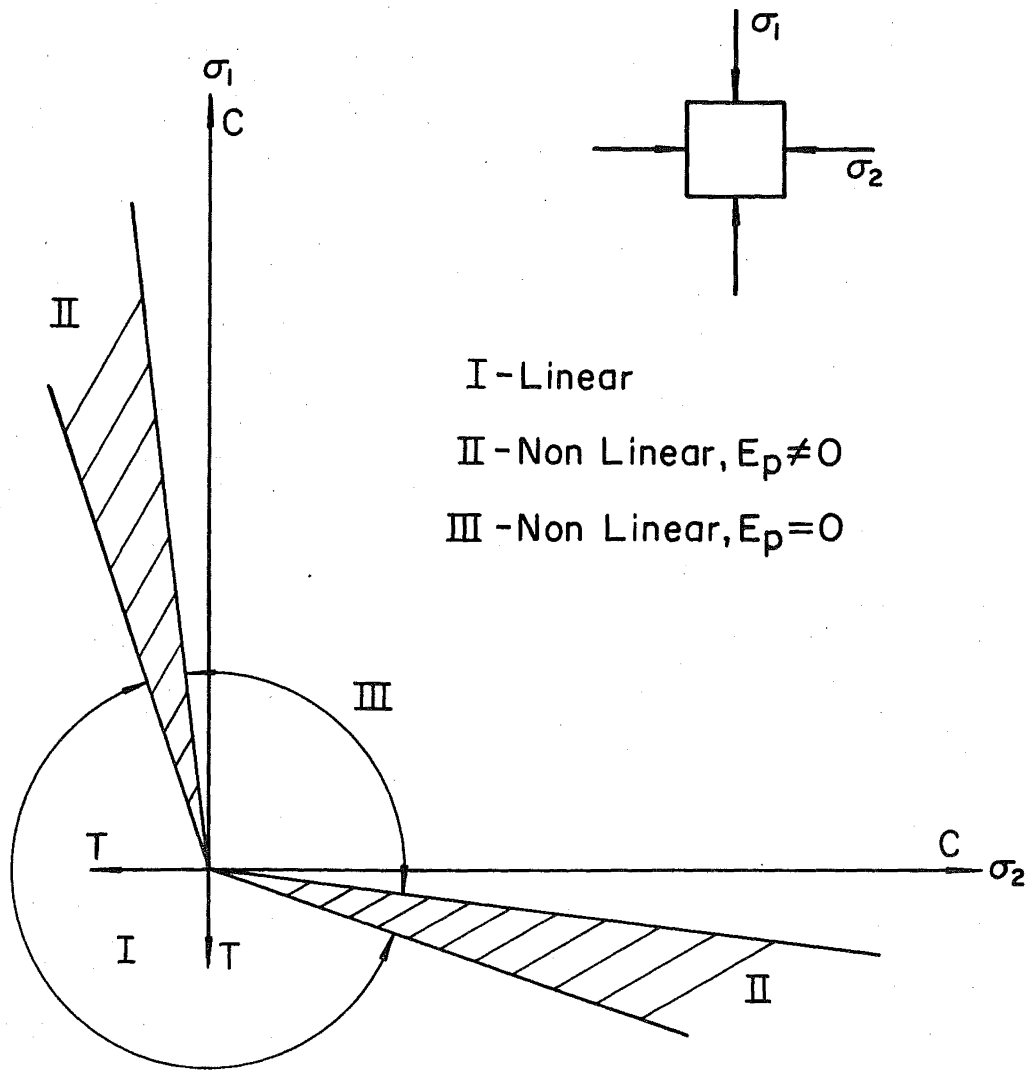


Fig. 8 Biaxial Stress Plane Regions Indicating where the Linear and Nonlinear Concrete Stress-Strain Curves are Applicable

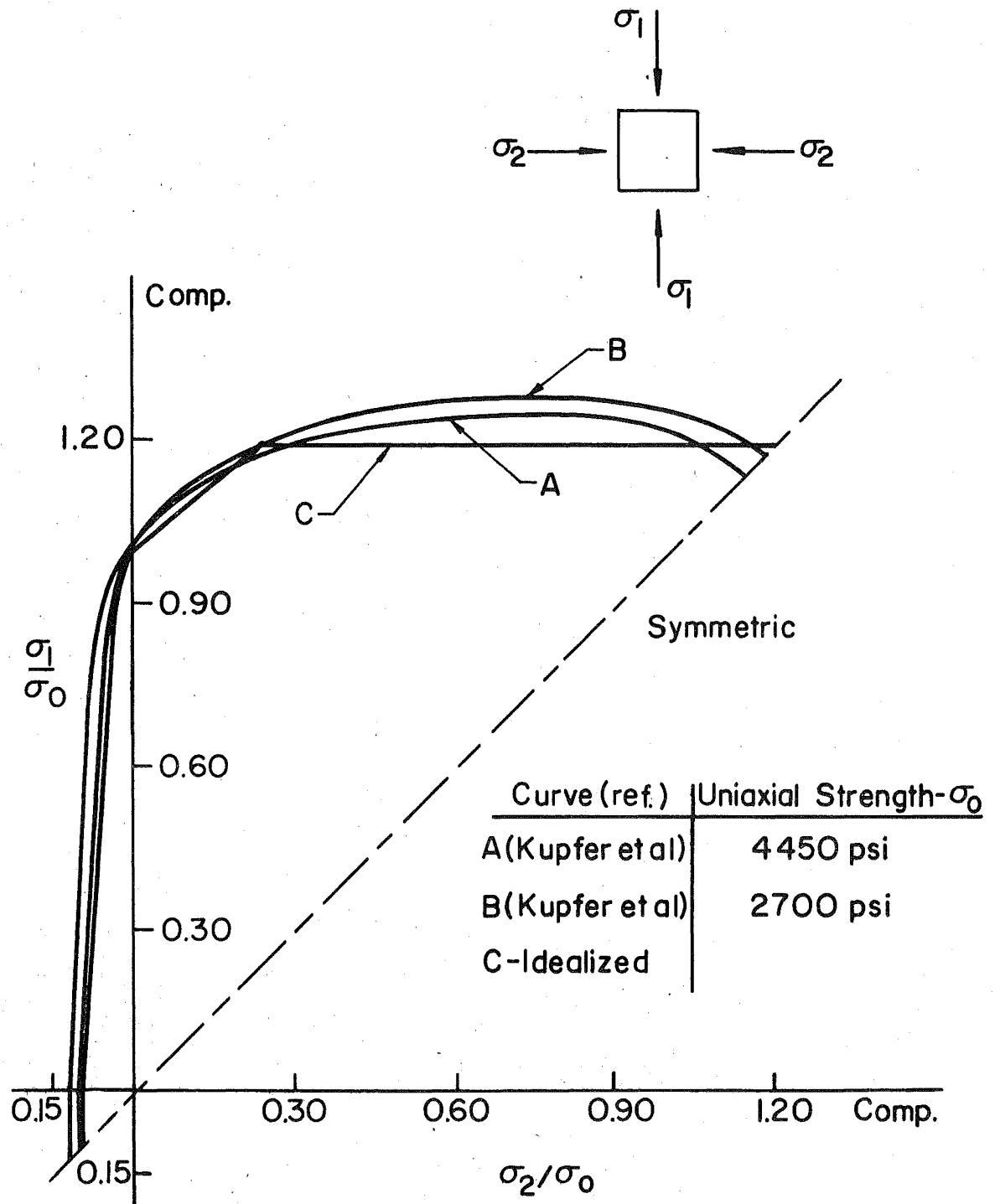


Fig. 9 Concrete Failure Envelopes for the Biaxial Stress Space

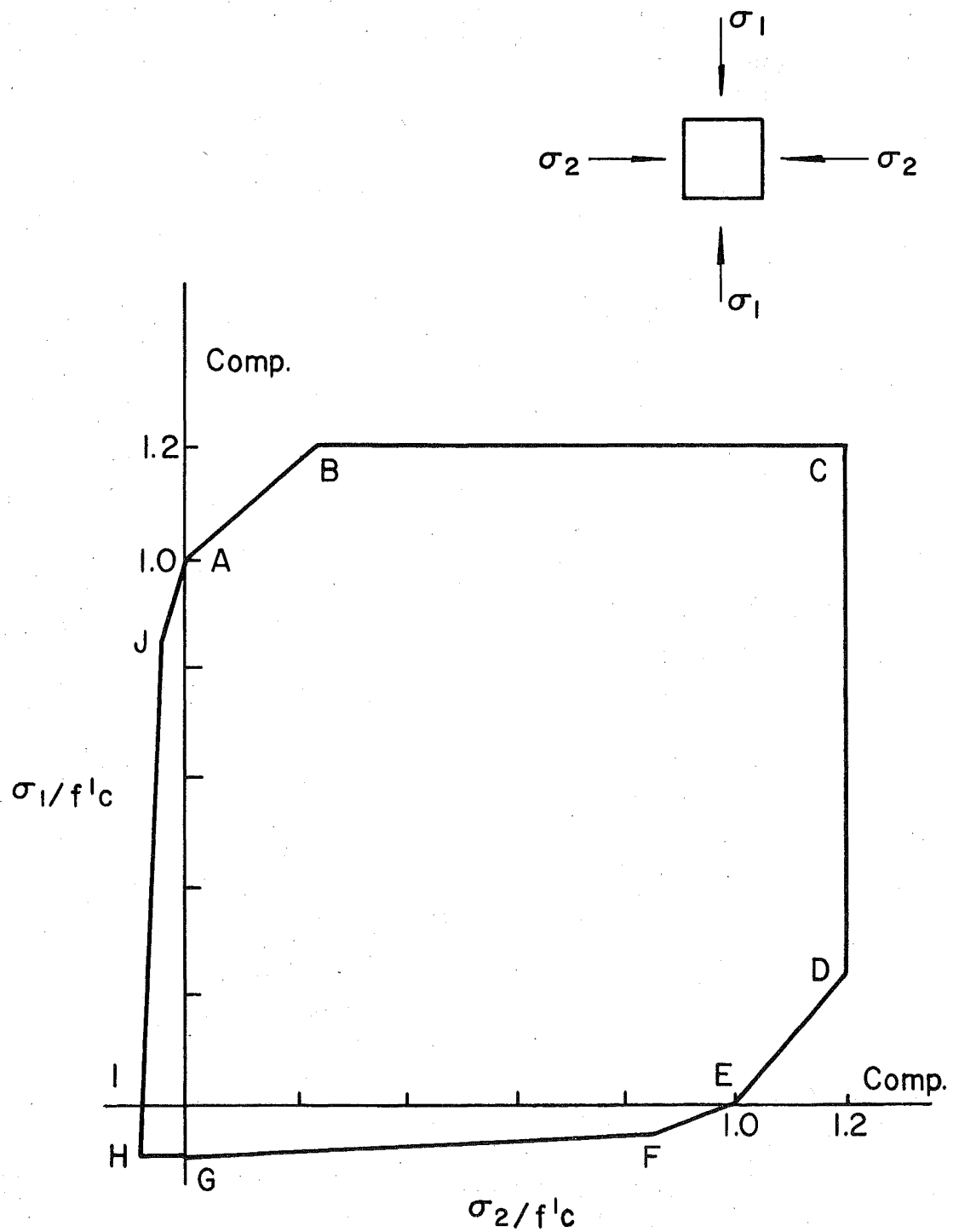


Fig. 10 Idealized Biaxial Failure Envelope with Characteristic Points

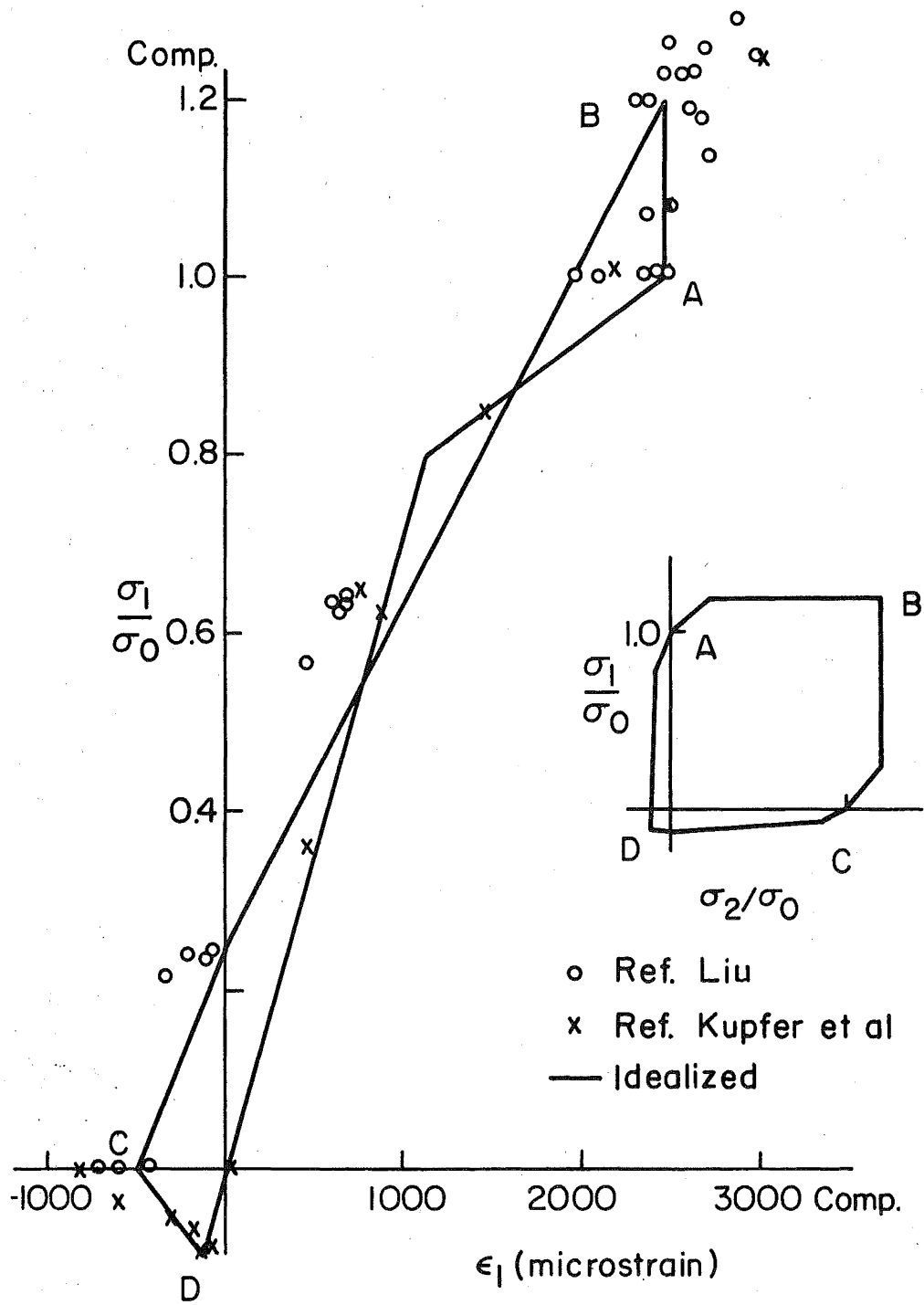


Fig. 11 Peak Strain Envelope

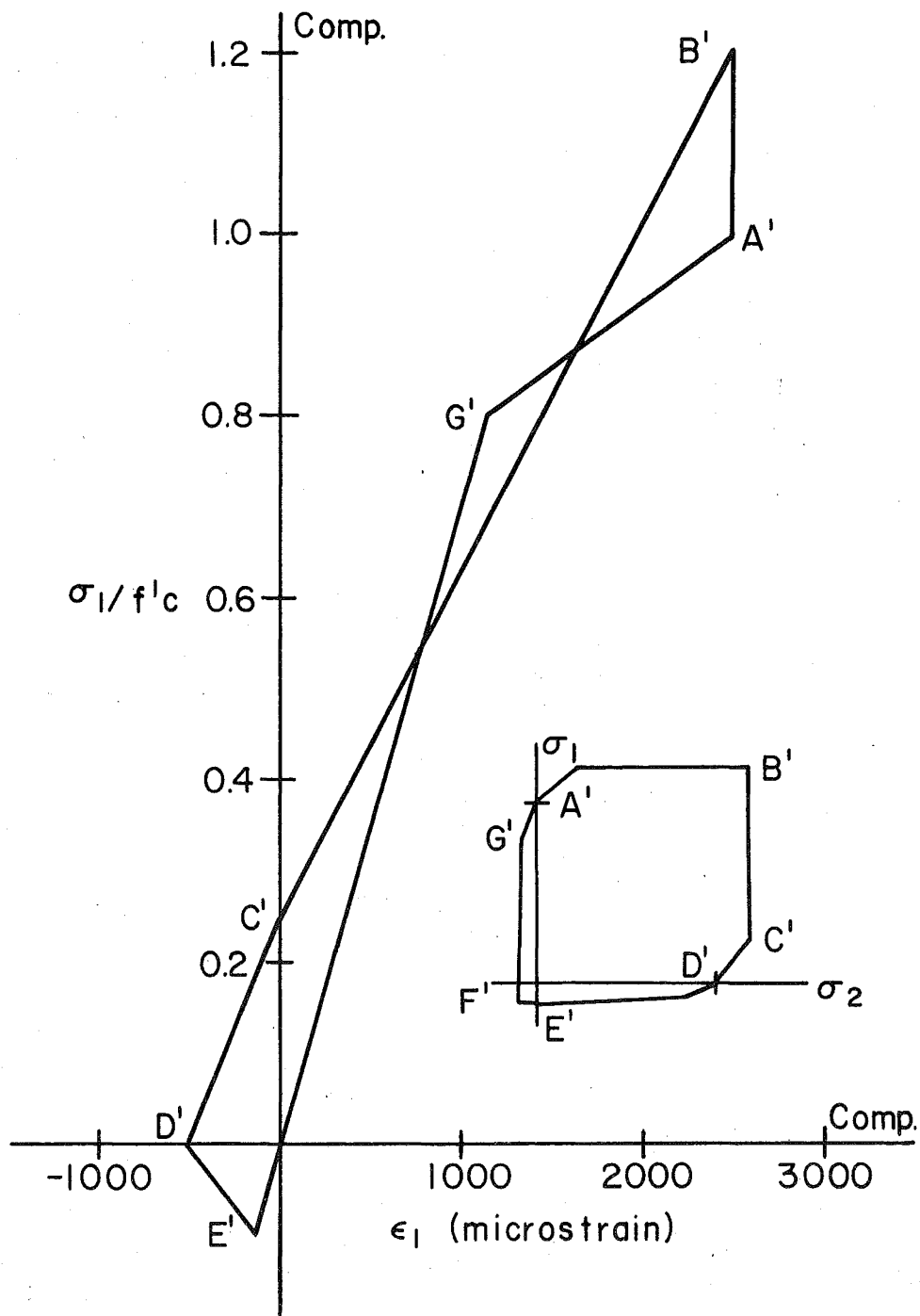


Fig. 12 Peak Strain Envelope with Characteristic Points

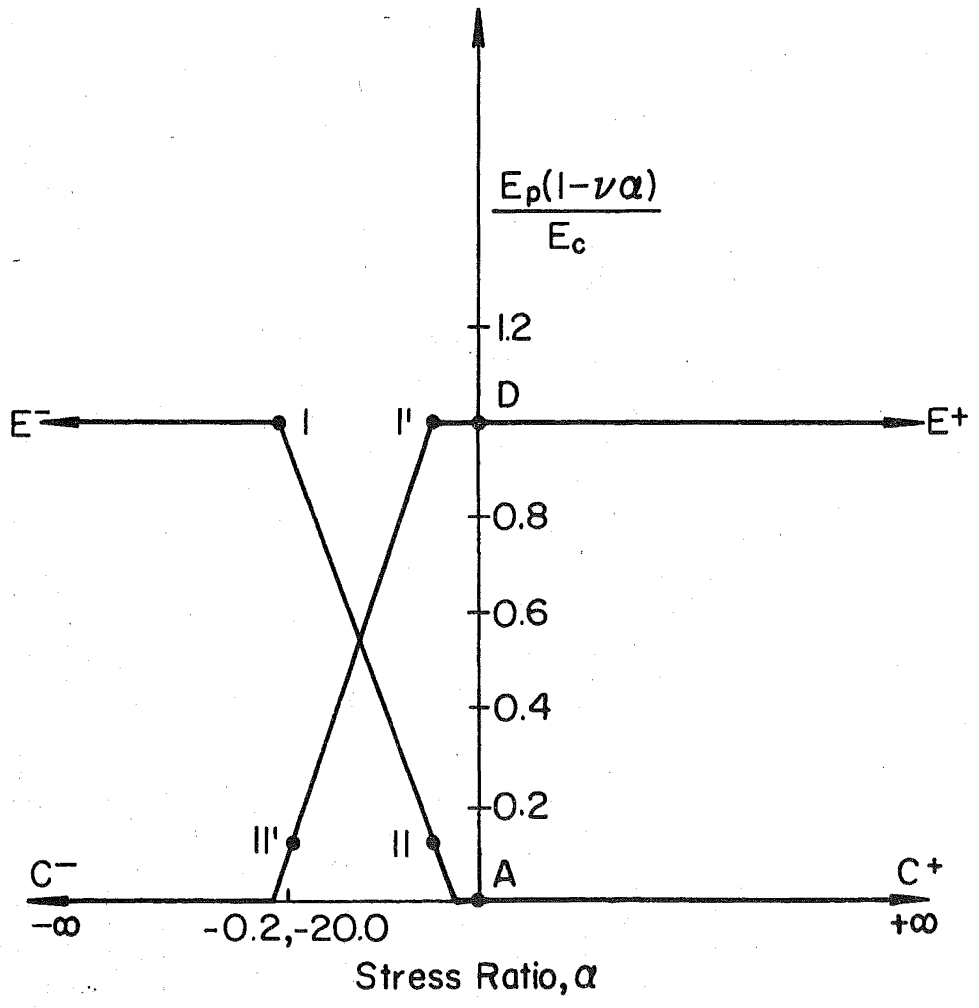
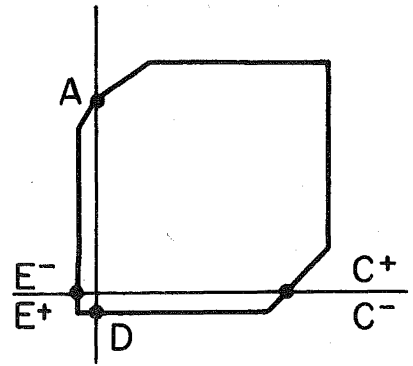


Fig. 13 Ratio of Peak Slope to Initial Slope as a Function of the Stress Ratio

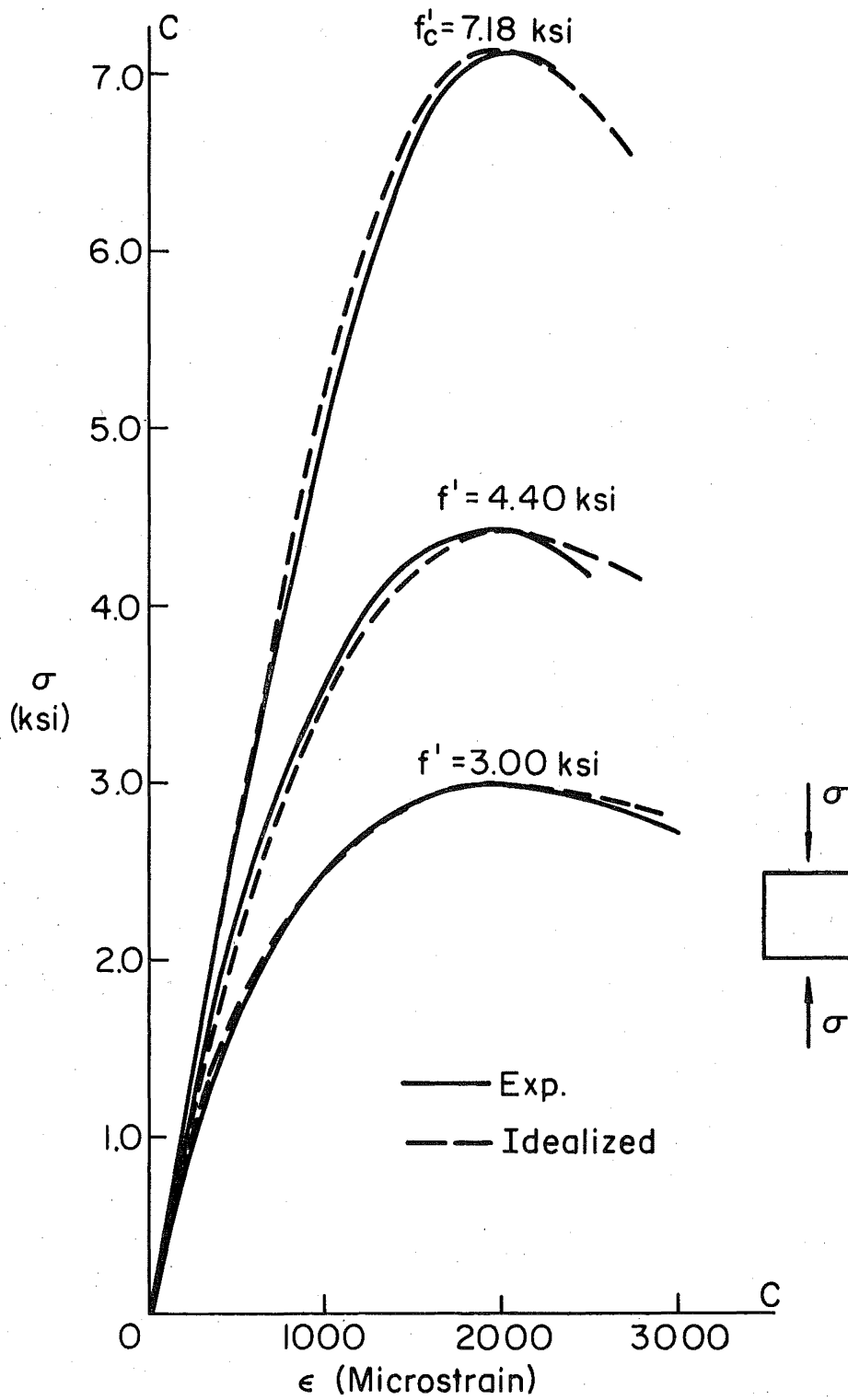


Fig. 14 Uniaxial Stress-Strain Curves for Concrete

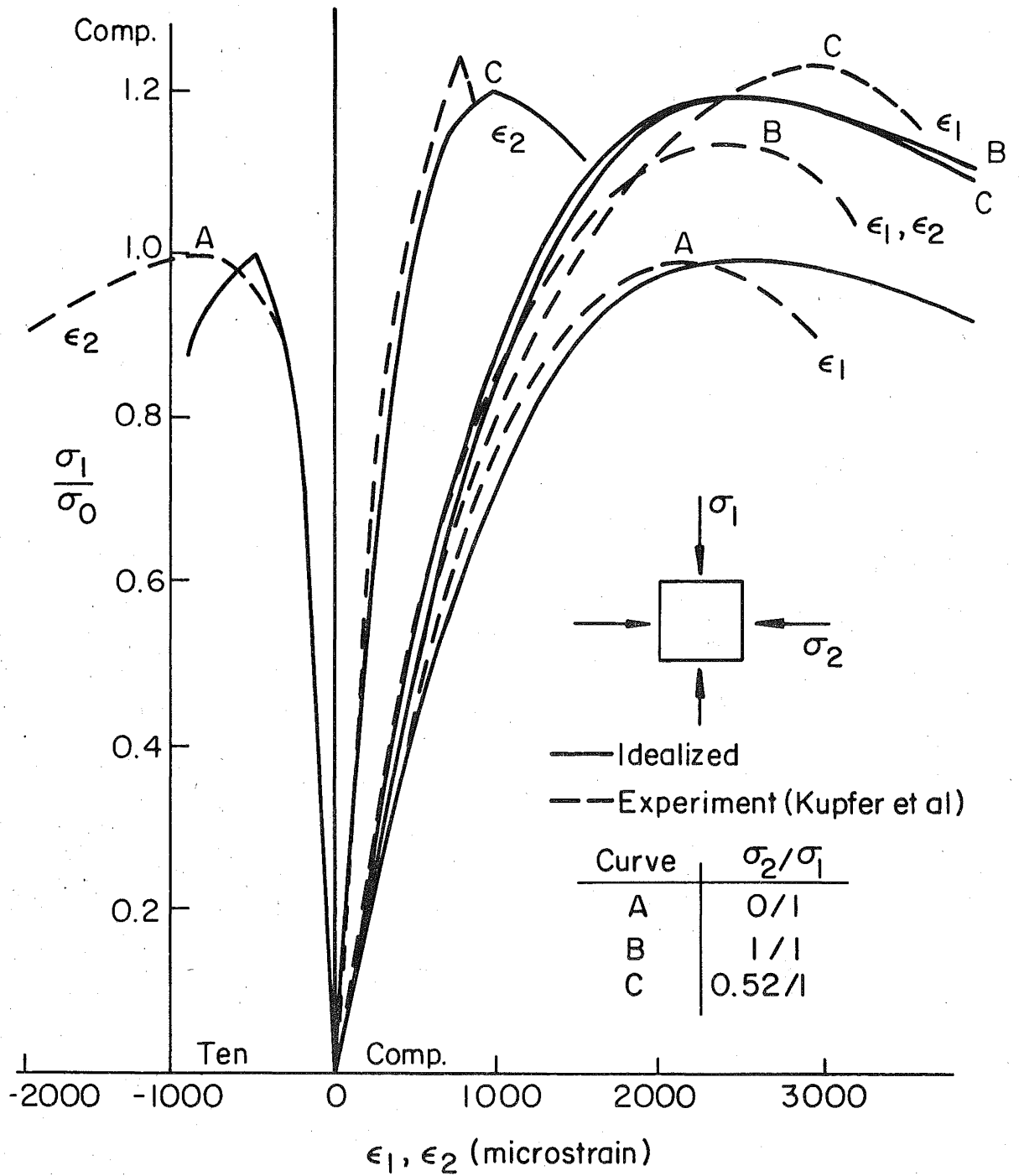


Fig. 15 Concrete Biaxial Stress-Strain Curves:
Compression-Compression Region

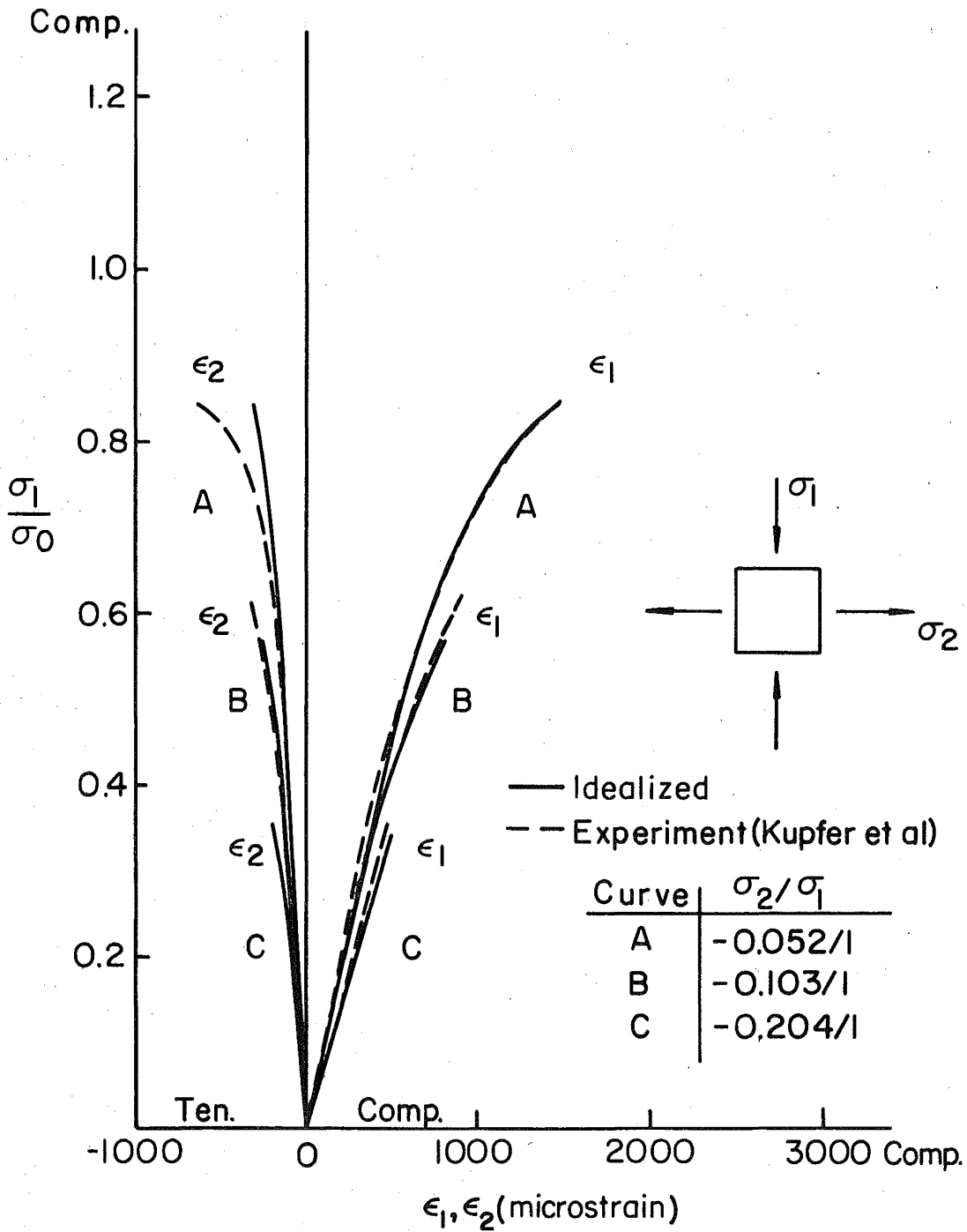


Fig. 16 Concrete Biaxial Stress-Strain Curves: Compression-Tension Region

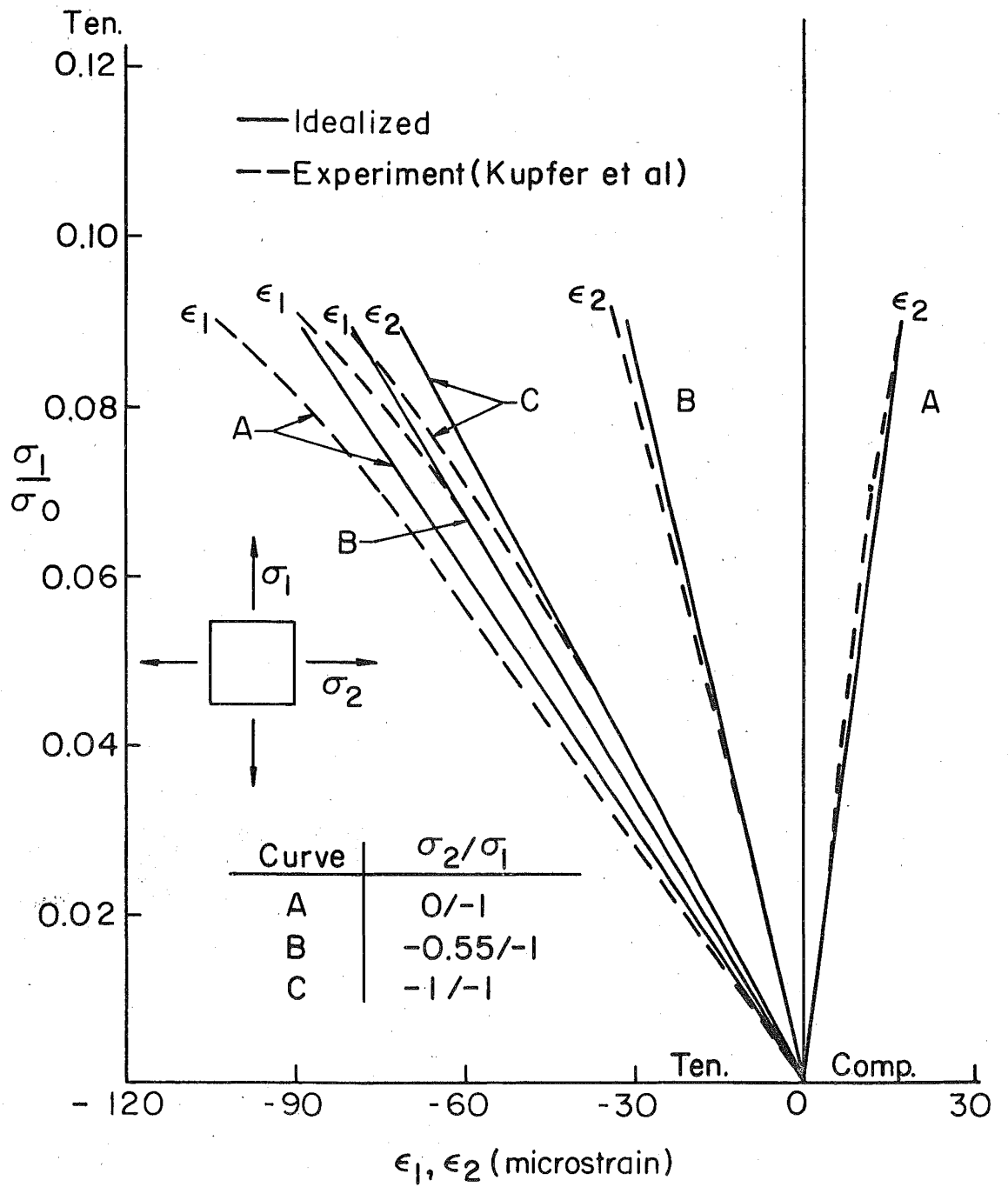


Fig. 17 Concrete Biaxial Stress-Strain Curves: Tension-Tension Region

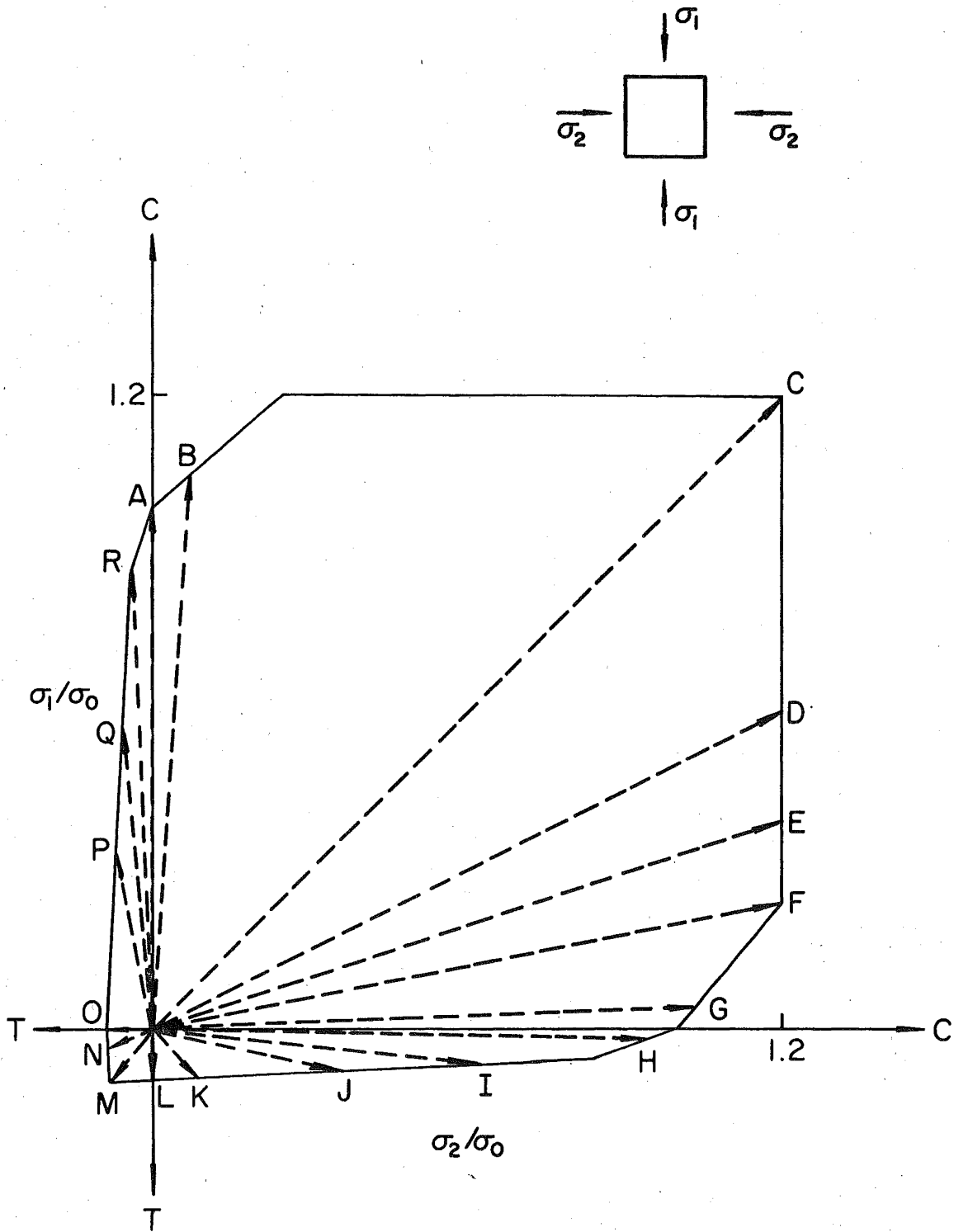


Fig. 18 Stress Paths in the Biaxial Stress Space Corresponding to Selected Values of the Stress Ratio

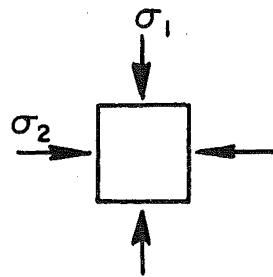
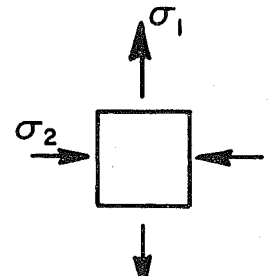
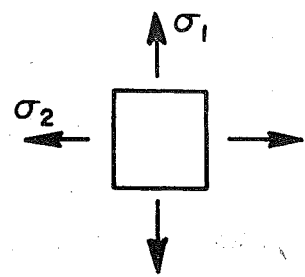
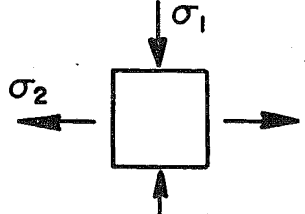
CURVE	σ_2/σ_1	STRESS STATE
A	0/1	
B	1/5	
C	1/1	
D	2/1	
E	3/1	
F	5/1	
G	25/1	
H	40/-1	
I	10/-1	
J	5/-1	
K	1/-1	
L	0/-1	
M	-1/-1	
N	-5/-1	
O	-15/-1	
P	-1/5	
Q	-1/10	
R	-1/25	

Fig. 19 Enumeration of the Selected Values of the Stress Ratio

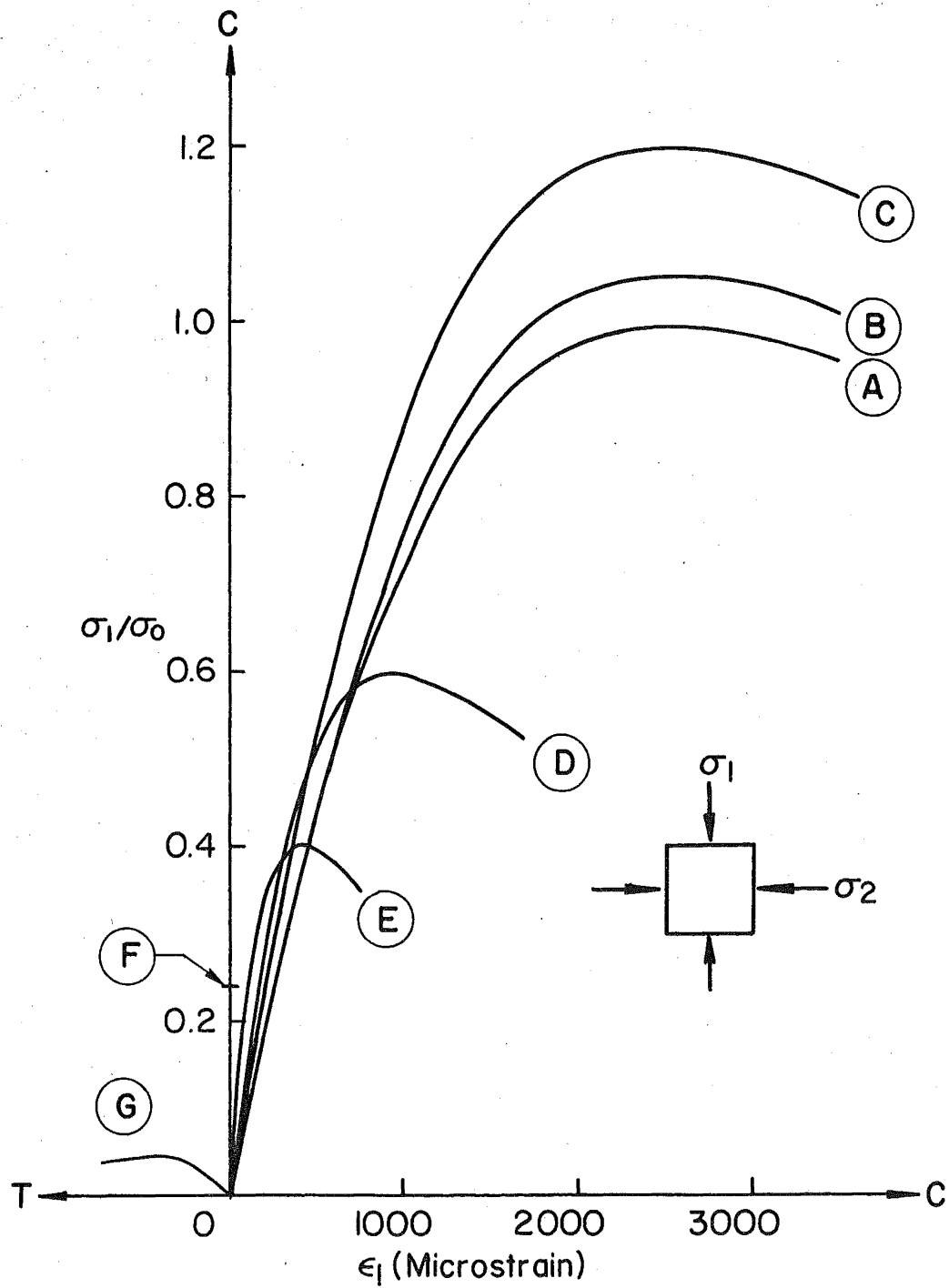


Fig. 20 Idealized Concrete Stress-Strain Curves:
Compression-Compression Region

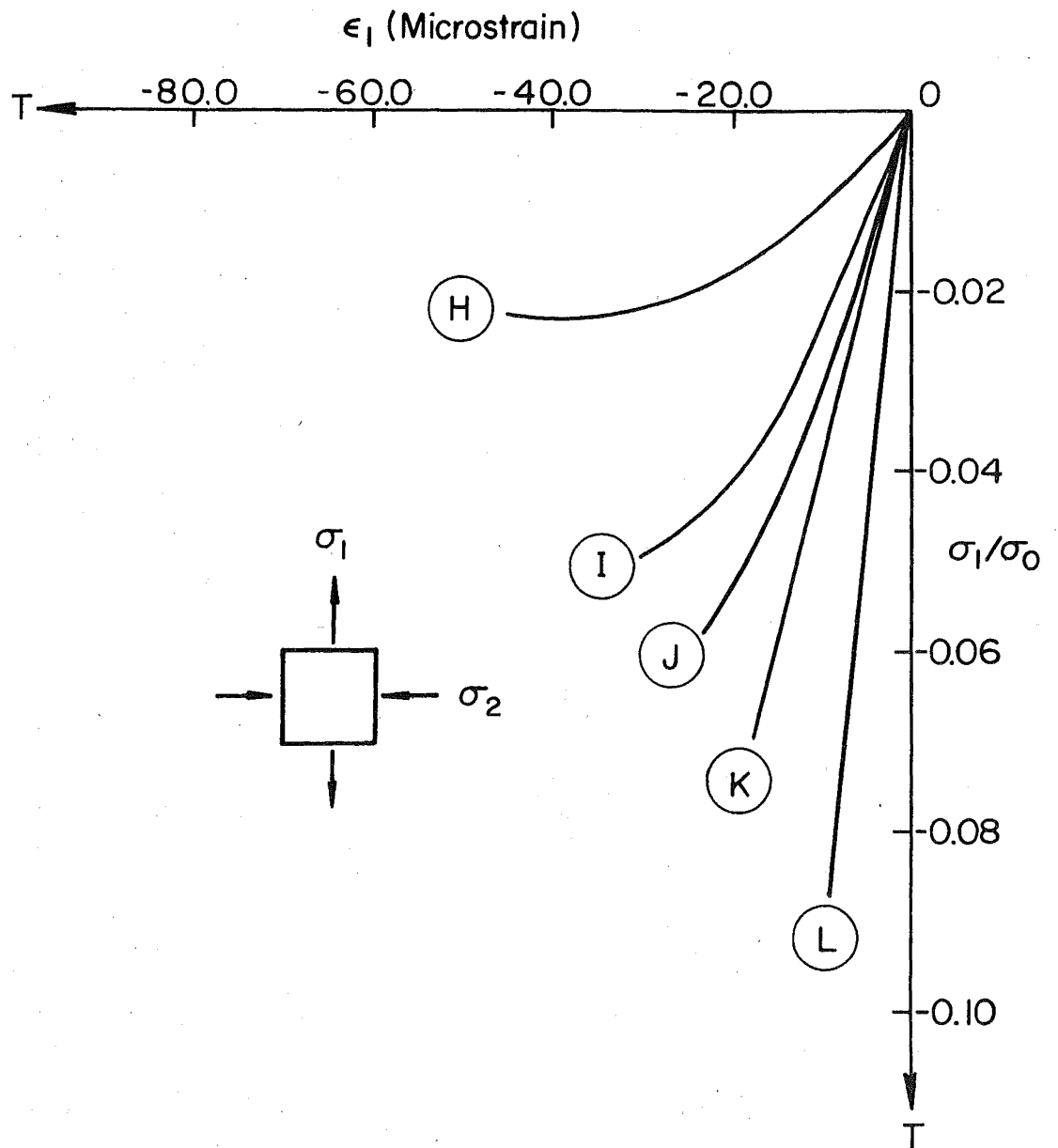


Fig. 21 Idealized Concrete Stress-Strain Curves:
Tension-Compression Region

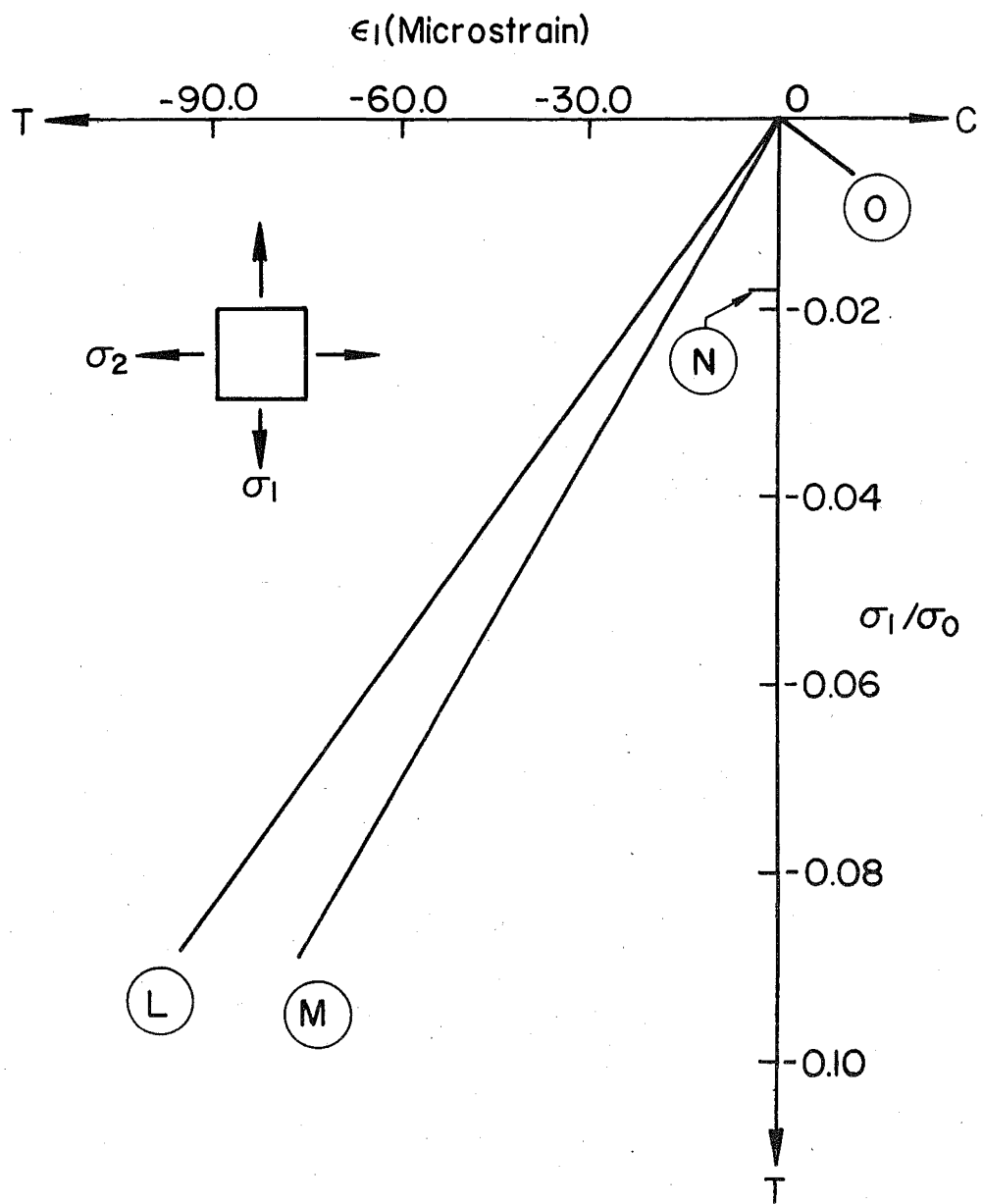


Fig. 22 Idealized Concrete Stress-Strain Curves:
Tension-Tension Region

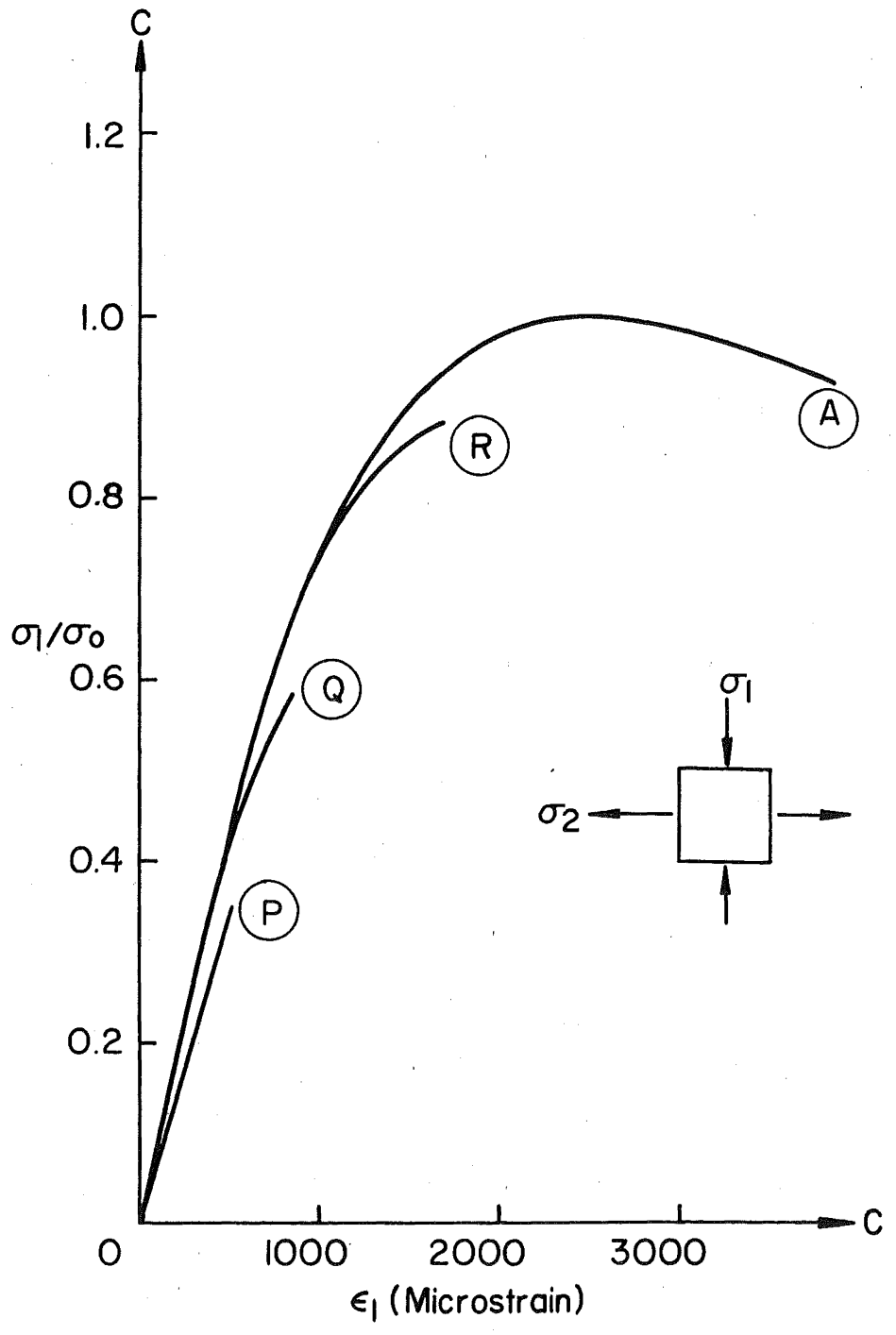


Fig. 23 Idealized Concrete Stress-Strain Curves:
Compression-Tension Region

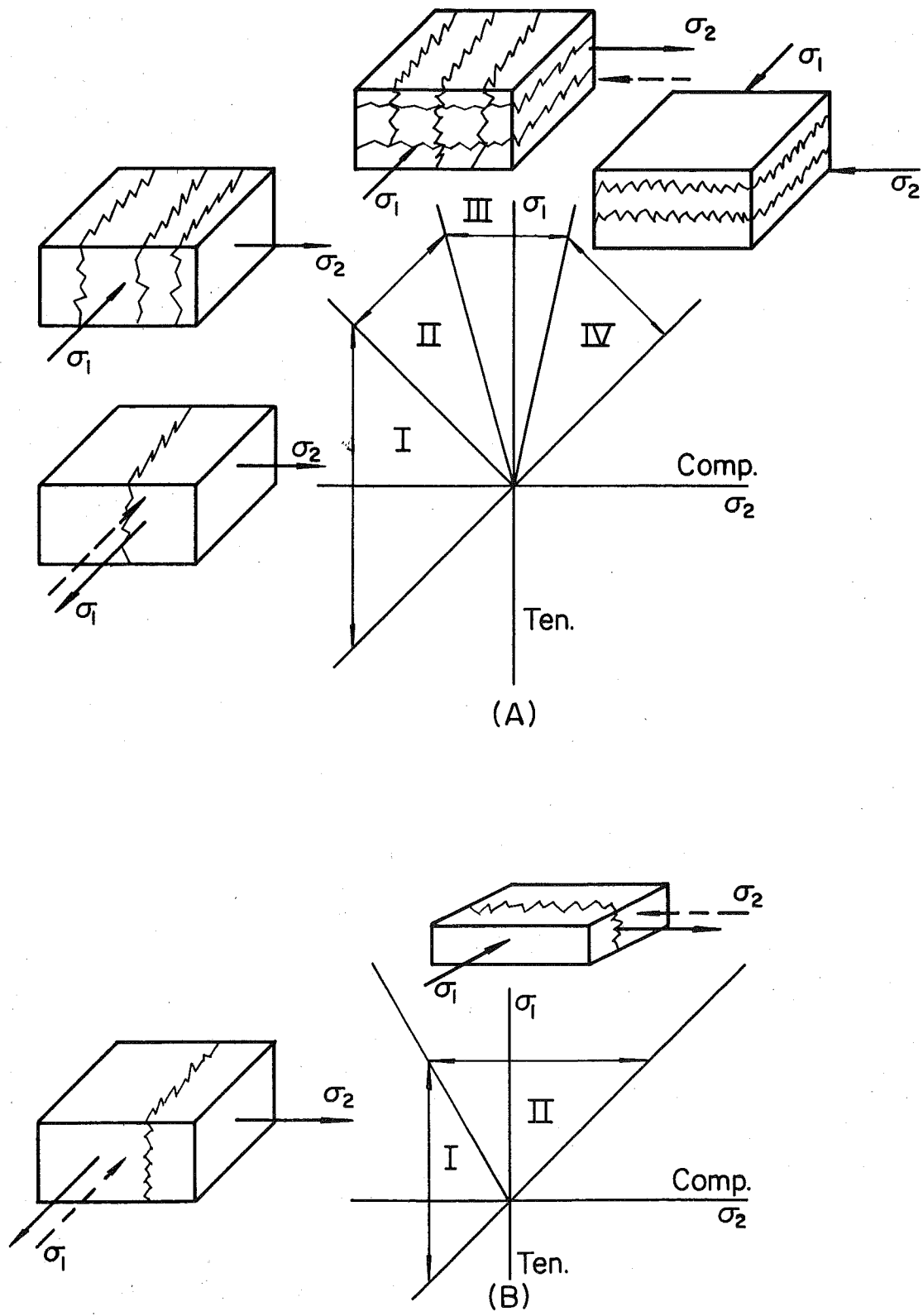


Fig. 24 Actual (A) and Idealized (B) Concrete Failure Modes

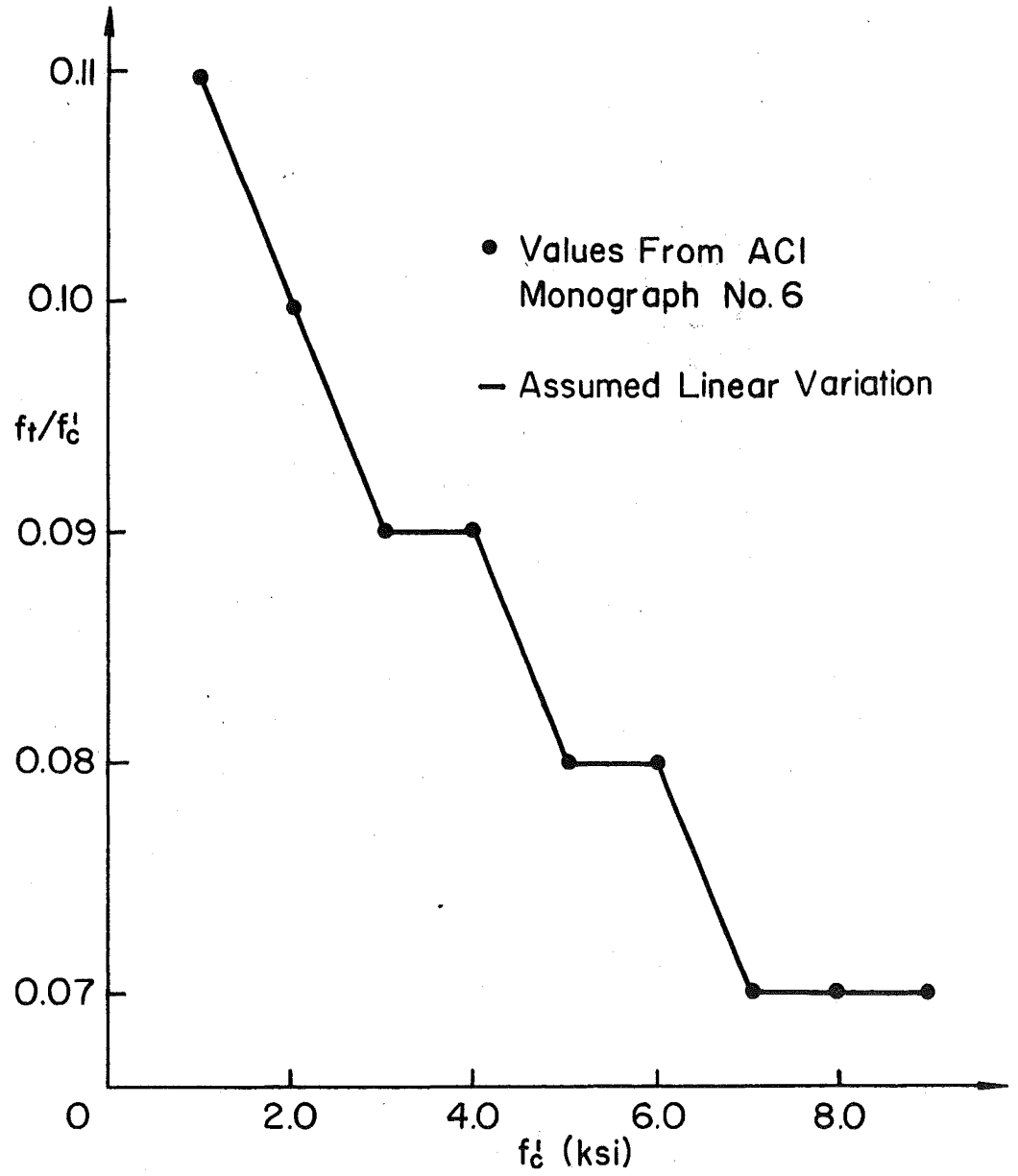


Fig. 25 Direct Tensile Strength vs. Cylinder Strength for Concrete

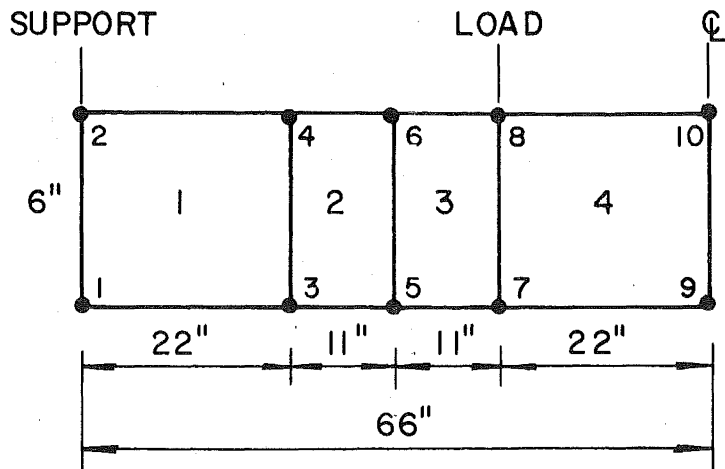


Fig. 26 Plan View of the Finite Element Discretization for the Reinforced Concrete Beam

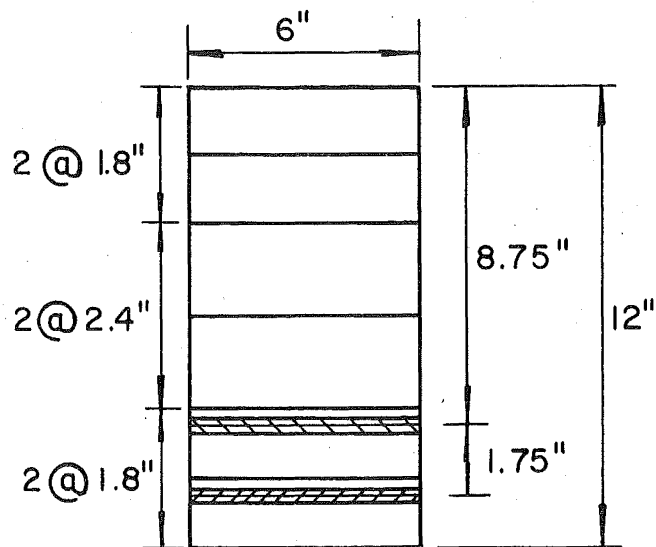


Fig. 27 Layering for the Reinforced Concrete Beam

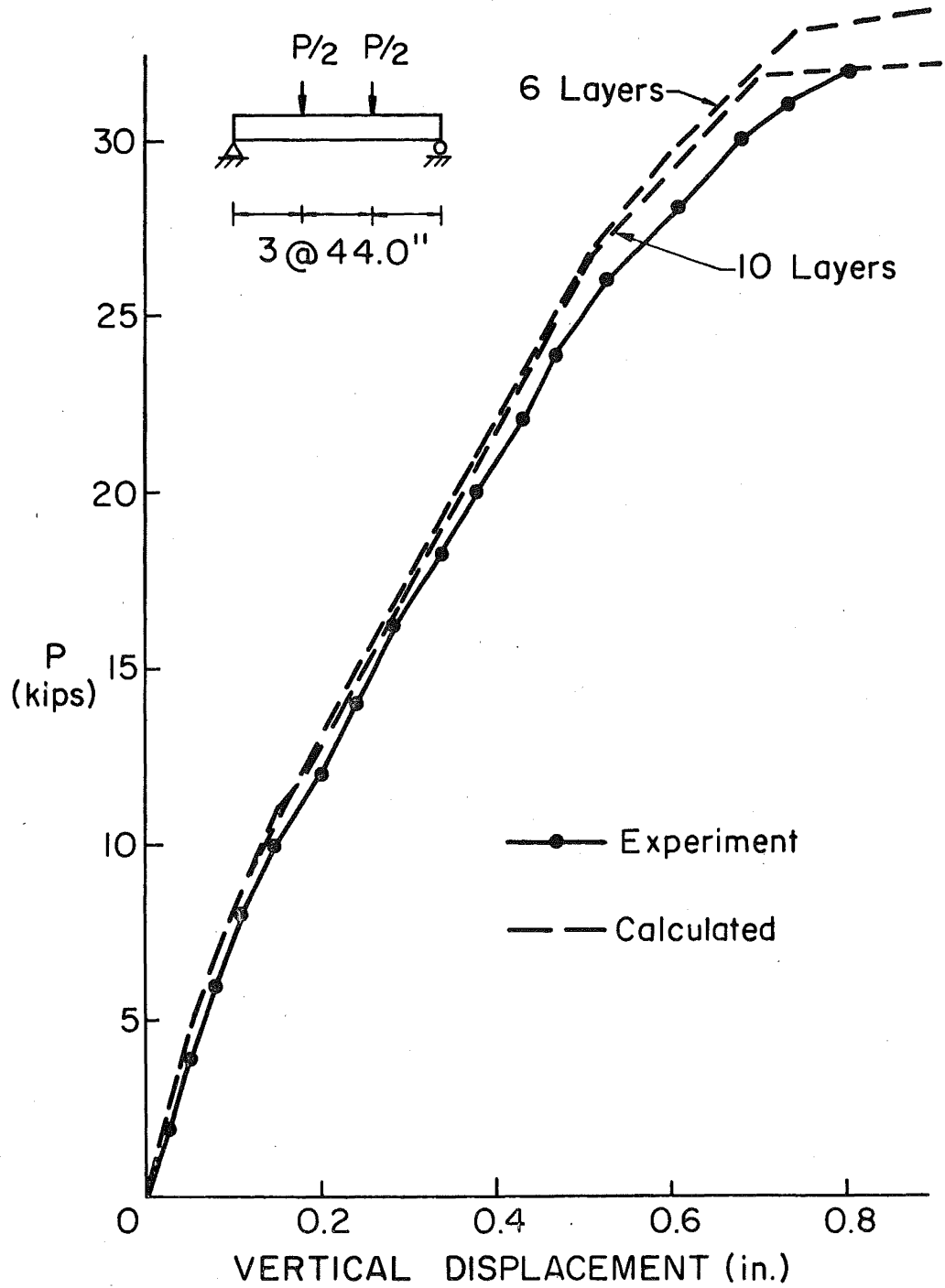


Fig. 28 Load-Deflection Histories for the Reinforced Concrete Beam

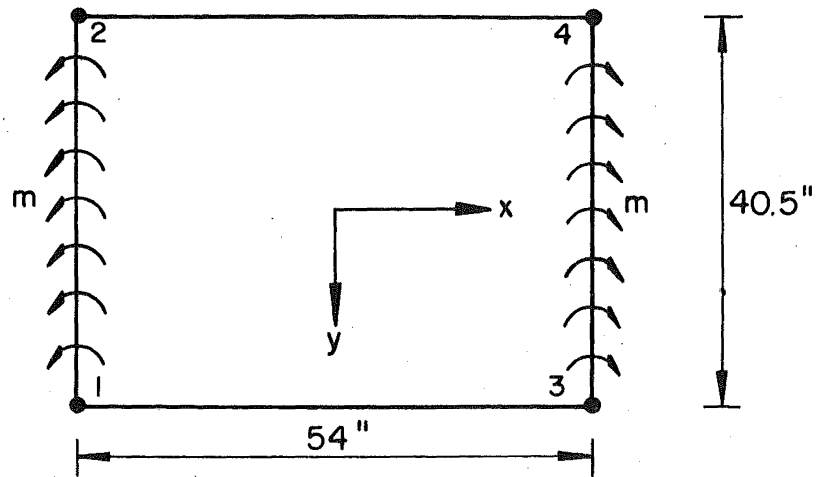


Fig. 29 Discretization and Loading for Simple-Free Slab
(Horizontal Edges Free, Vertical Edges Simply Supported)

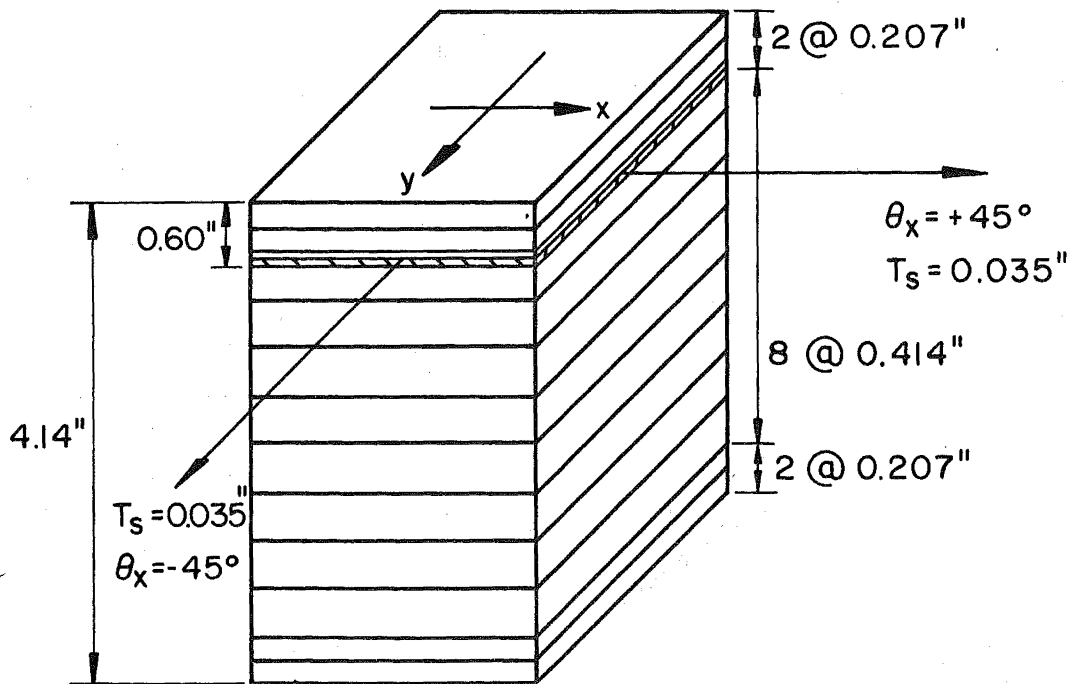


Fig. 30 Layering for the Simple-Free Slab

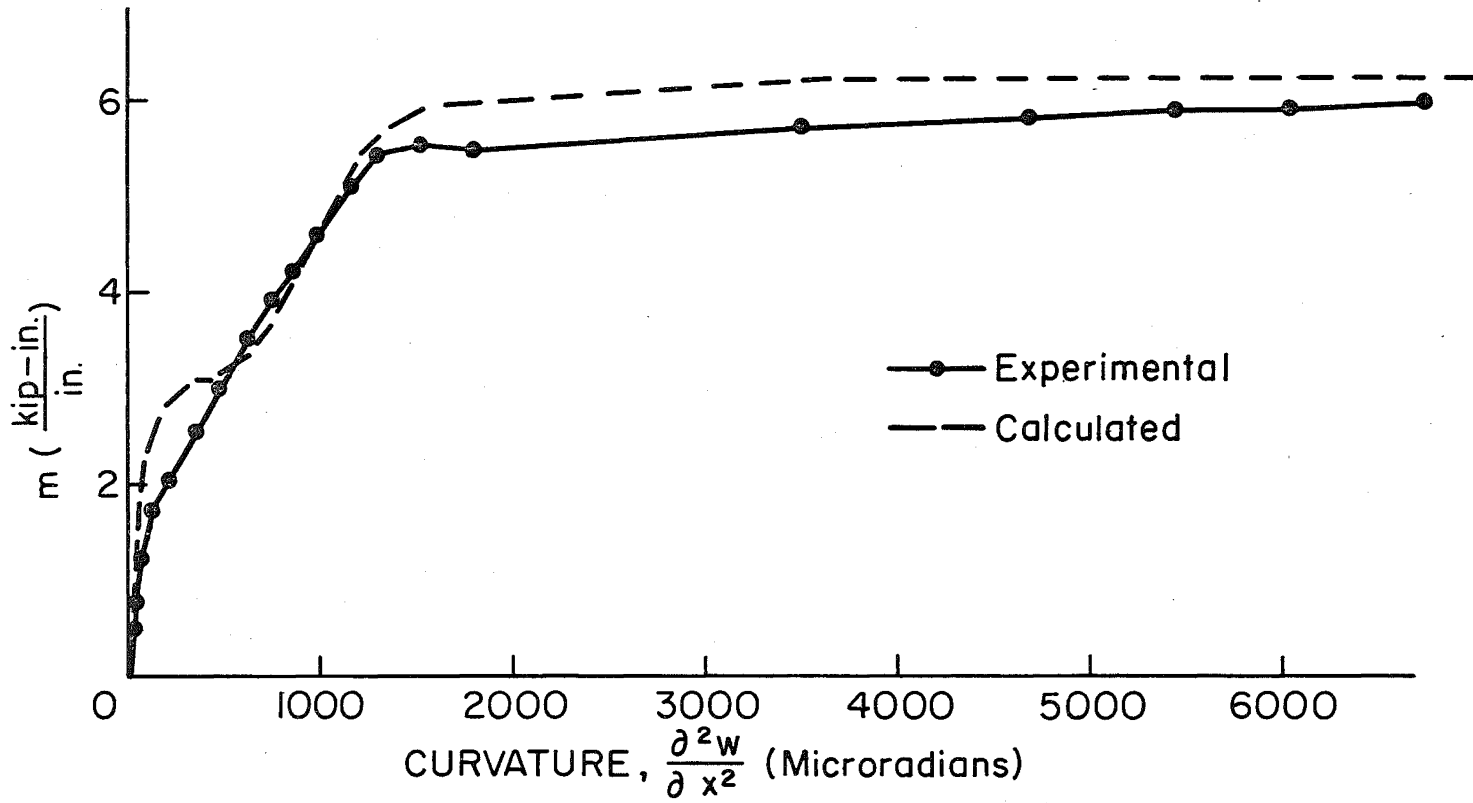


Fig. 31 Moment verses Curvature History for the Simple-Free Slab

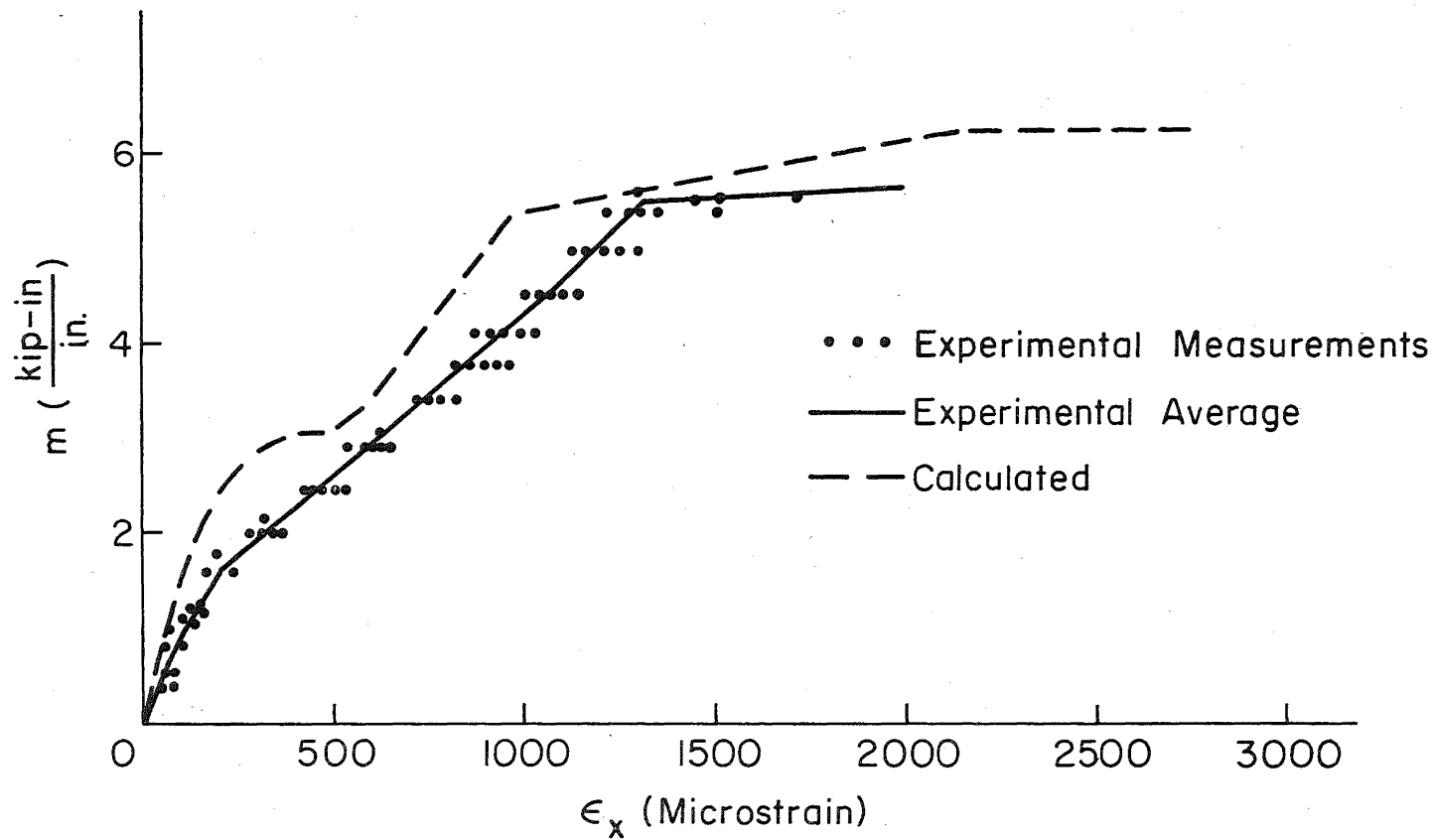


Fig. 32 Moment versus Concrete Compressive Strain for the Simple-Free Slab

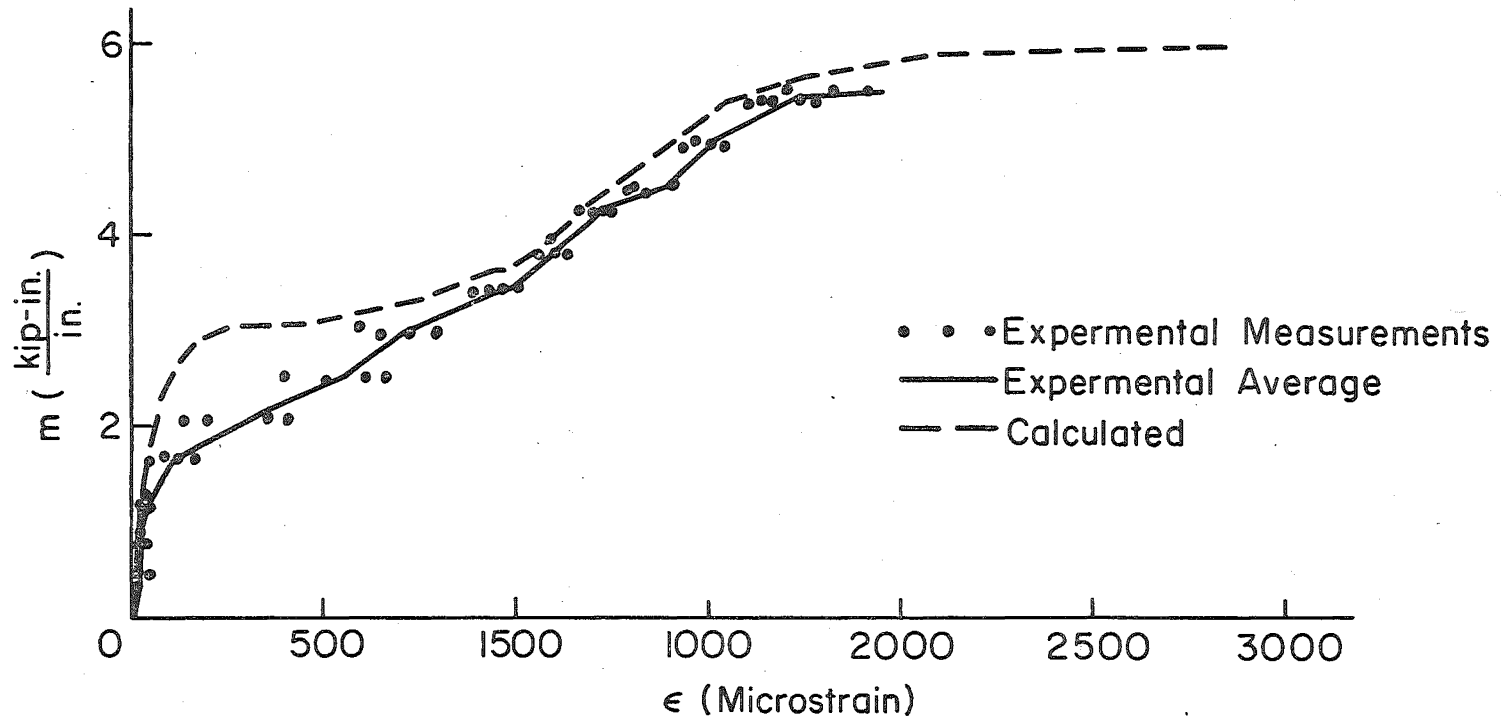


Fig. 33 Moment versus Average Steel Strain for the Simple-Free Slab

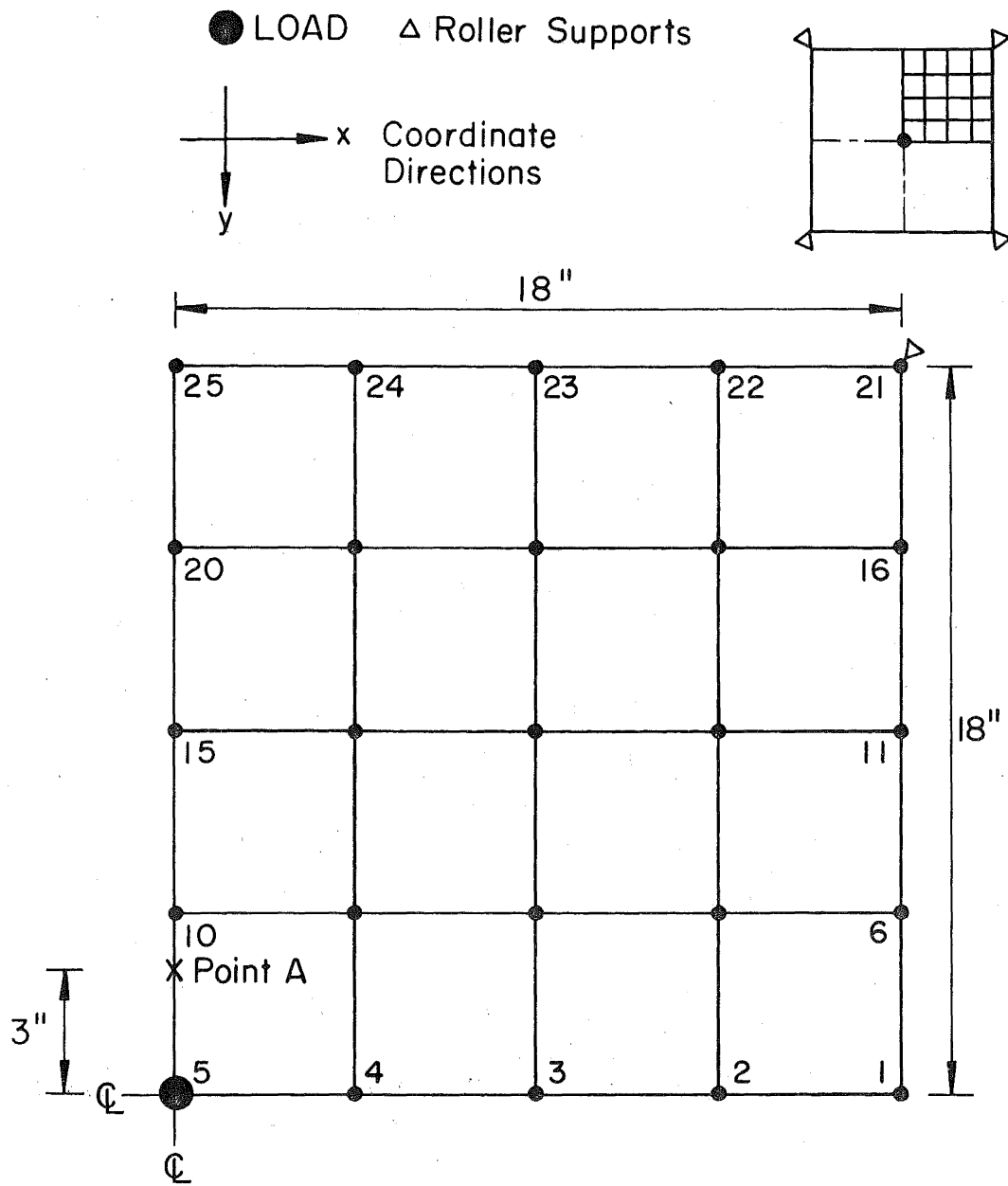


Fig. 34 Discretization and Loading for the Corner-Supported Slab

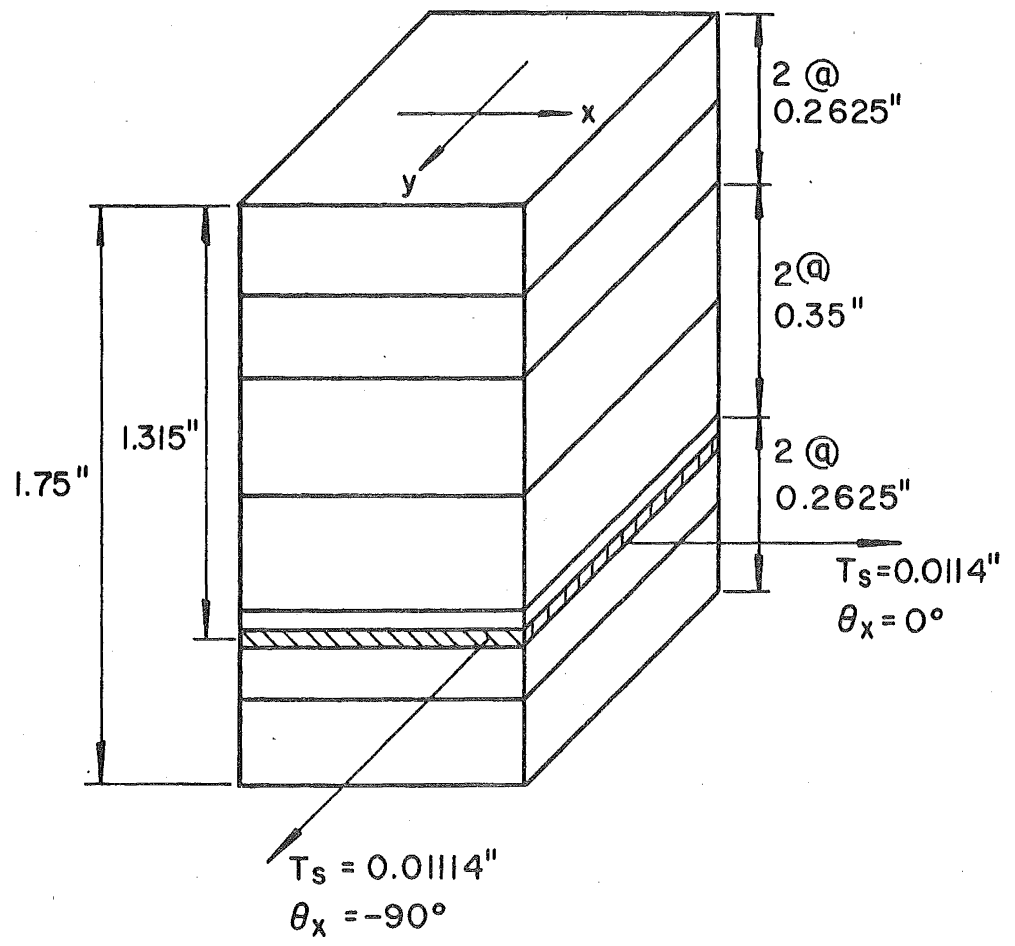


Fig. 35 Layering for the Corner-Supported Slab

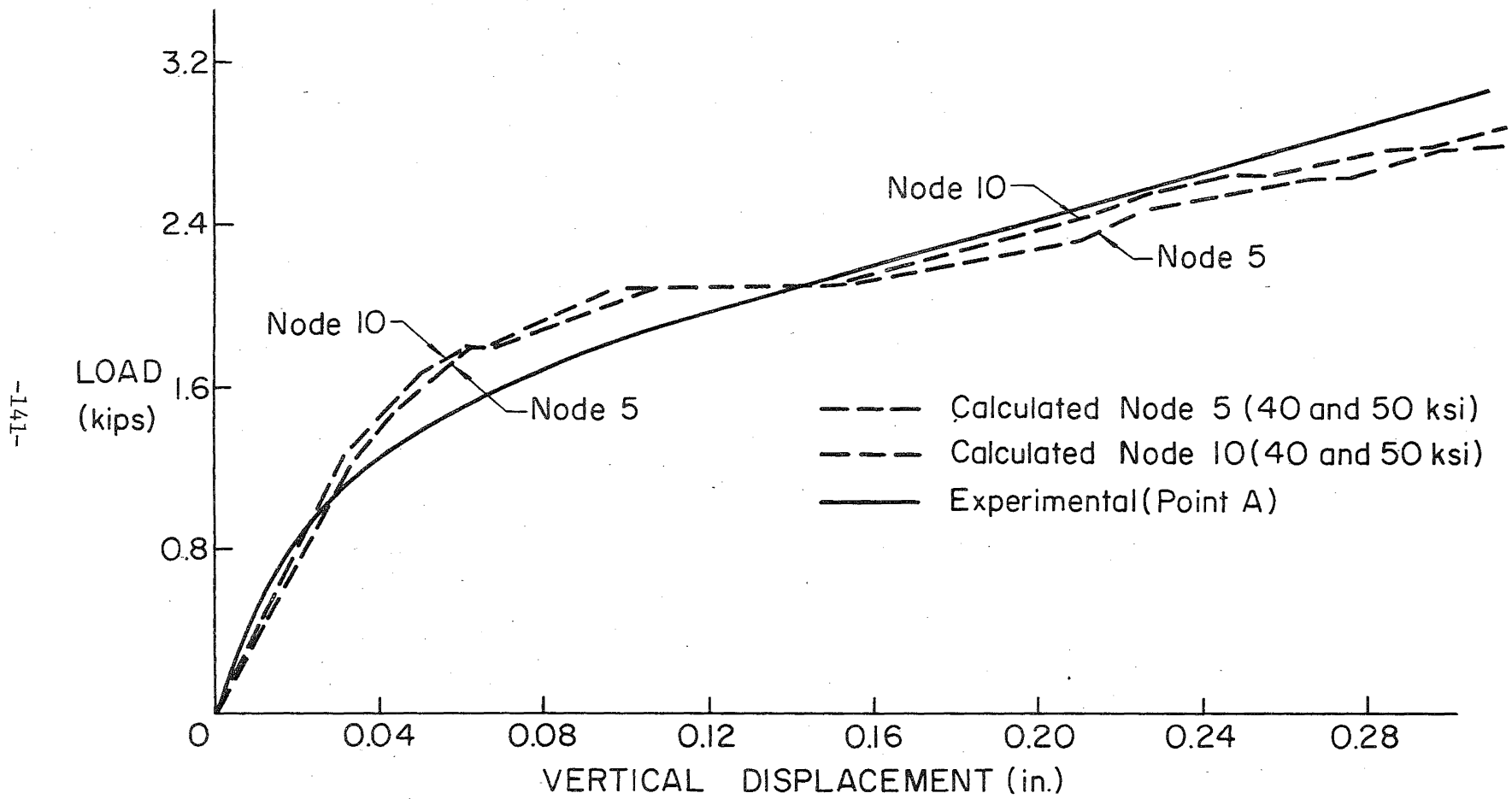


Fig. 36 Load-Deflection Histories for the Corner-Supported Slab

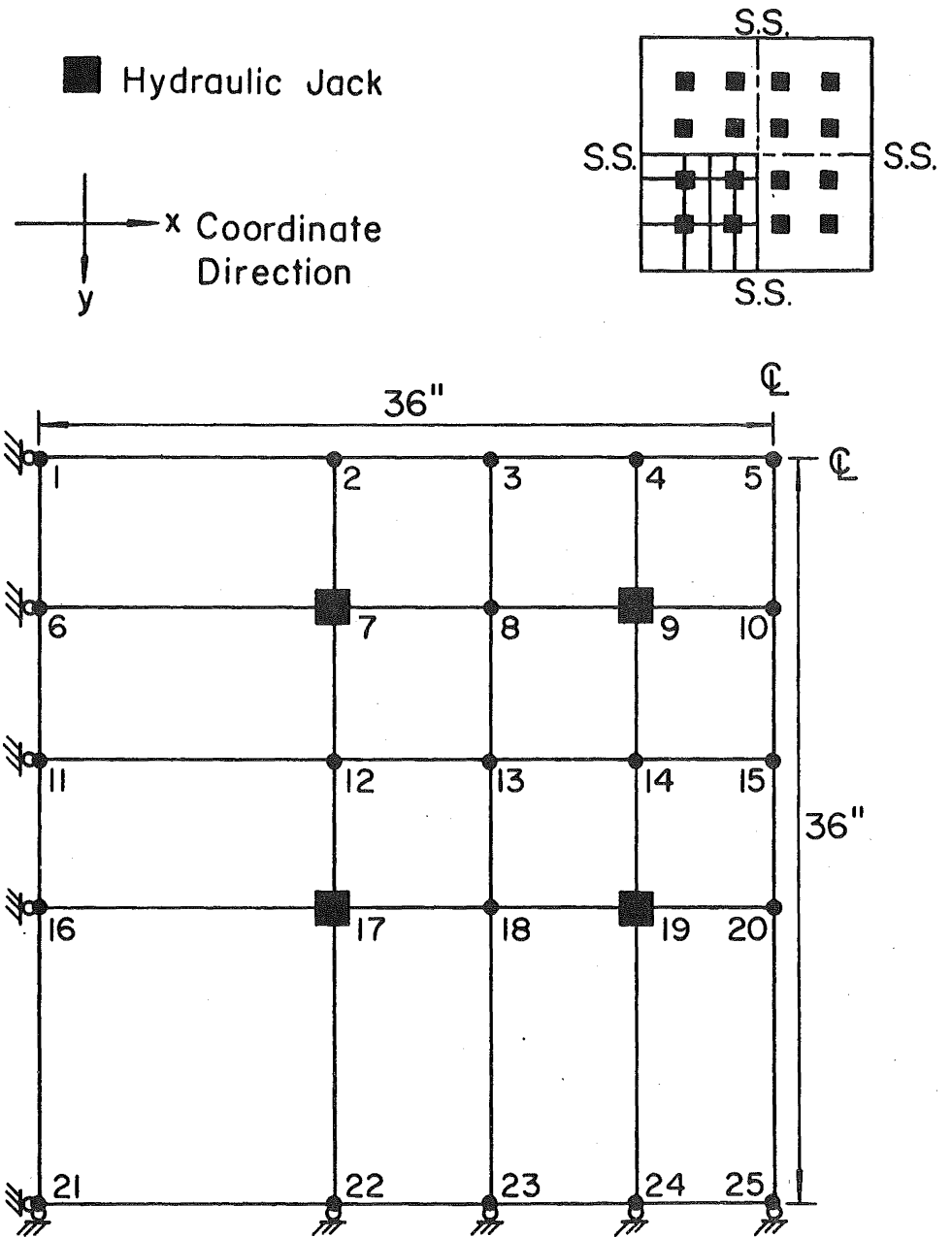


Fig. 37 Discretization and Loading for the Simply Supported Slabs
 (Ex. No. 4 and 5)

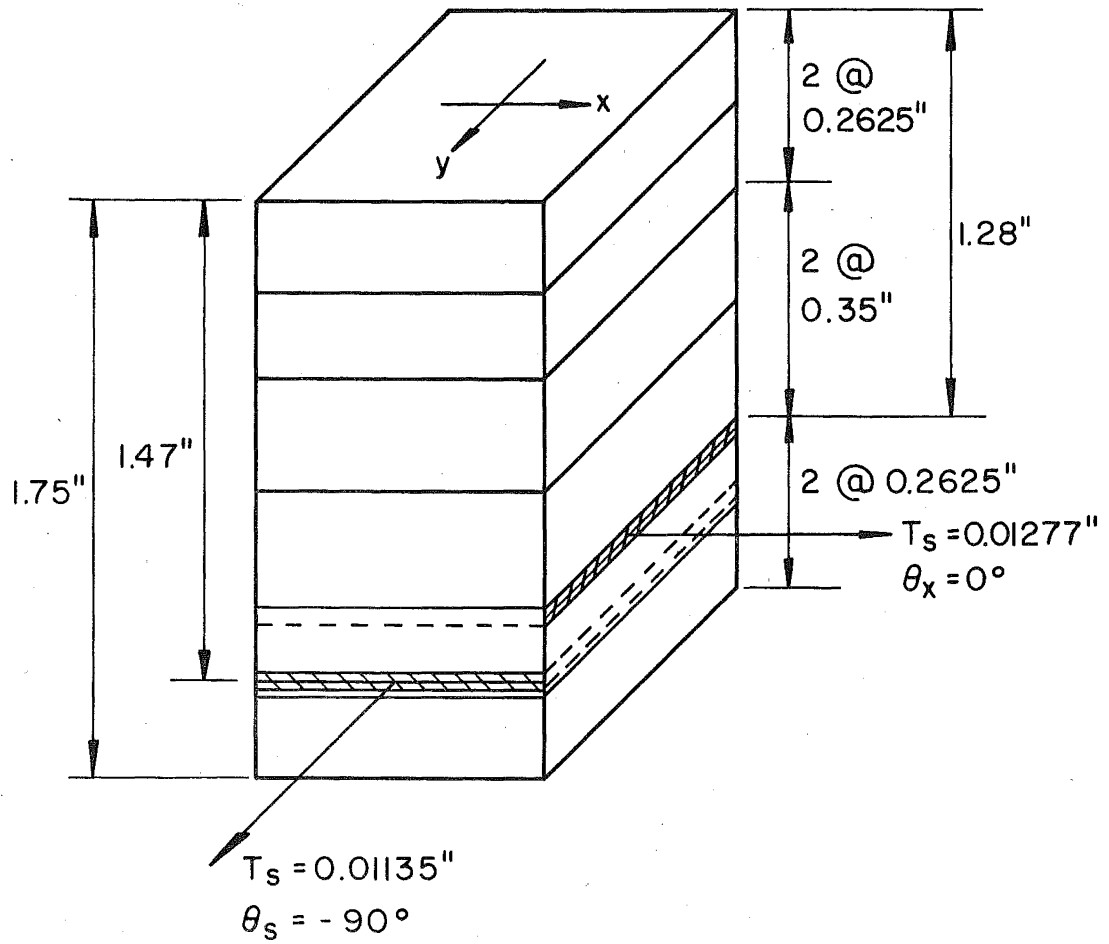


Fig. 38 Layering for the Simply Supported Slab (Example No. 4)

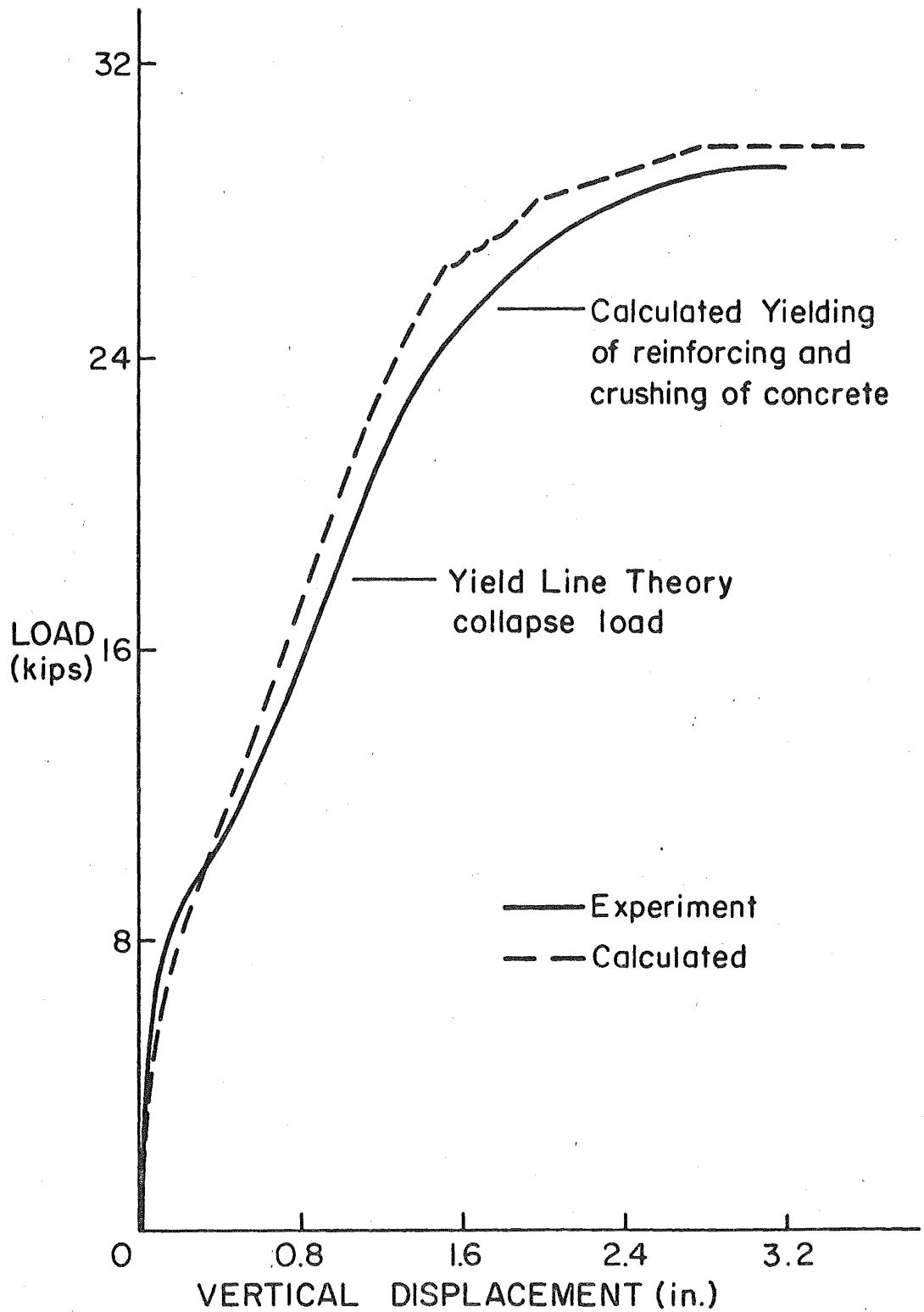


Fig. 39 Load-Deflection History for the Simply Supported Slab (Example No. 4)

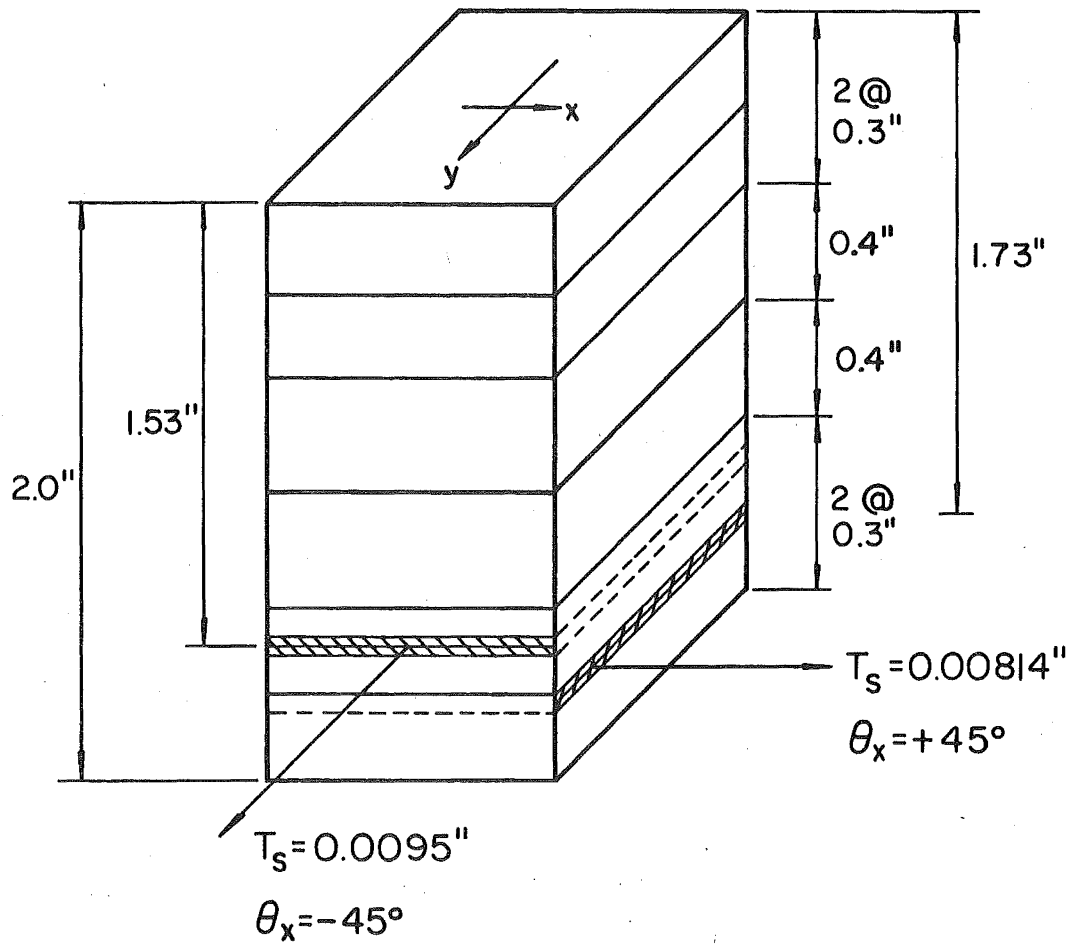


Fig. 40 Layering for the Simply Supported Slab
(Example No. 5)

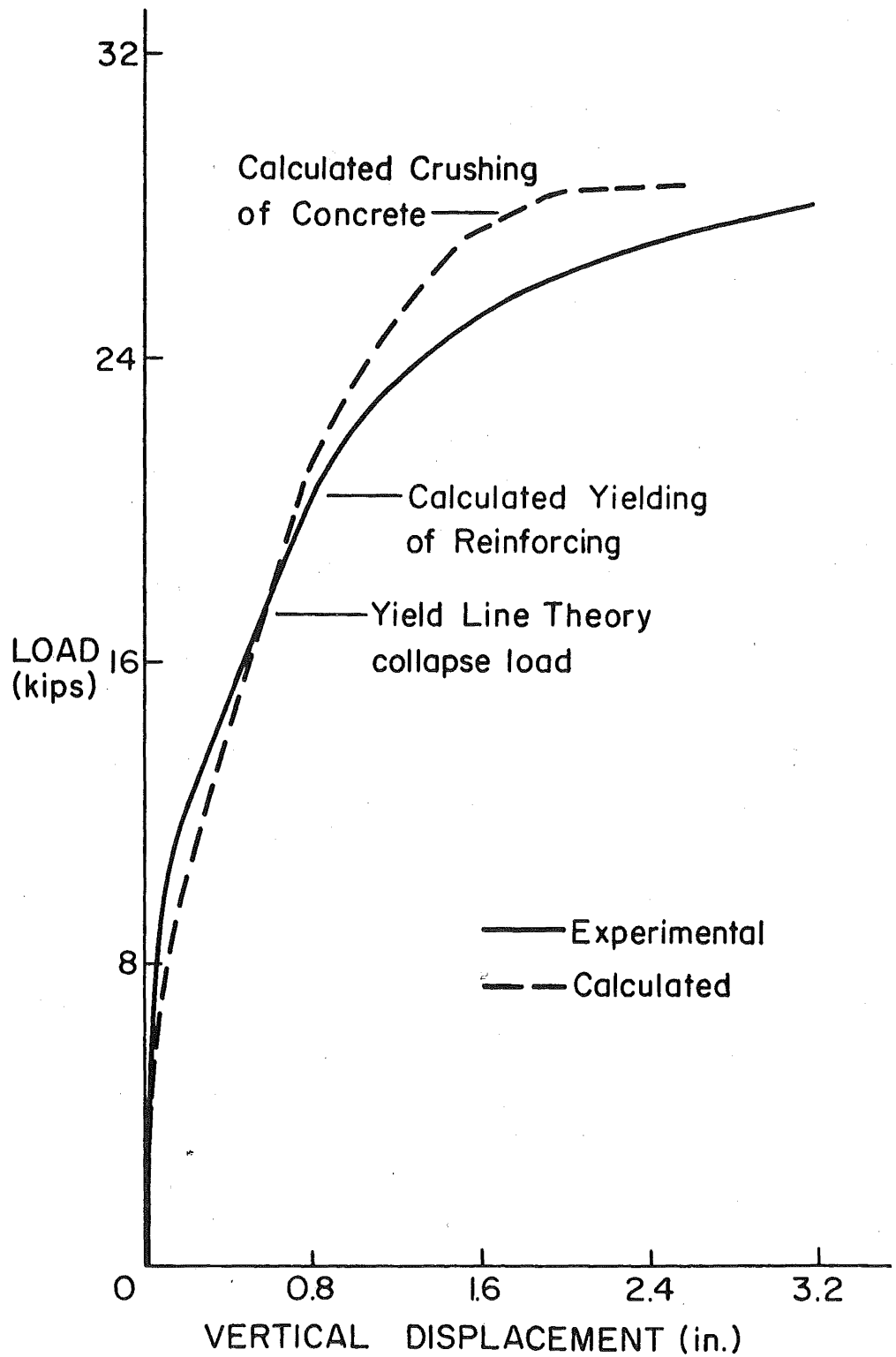


Fig. 41 Load-Deflection History for the Simply Supported Slab (Example No. 5)

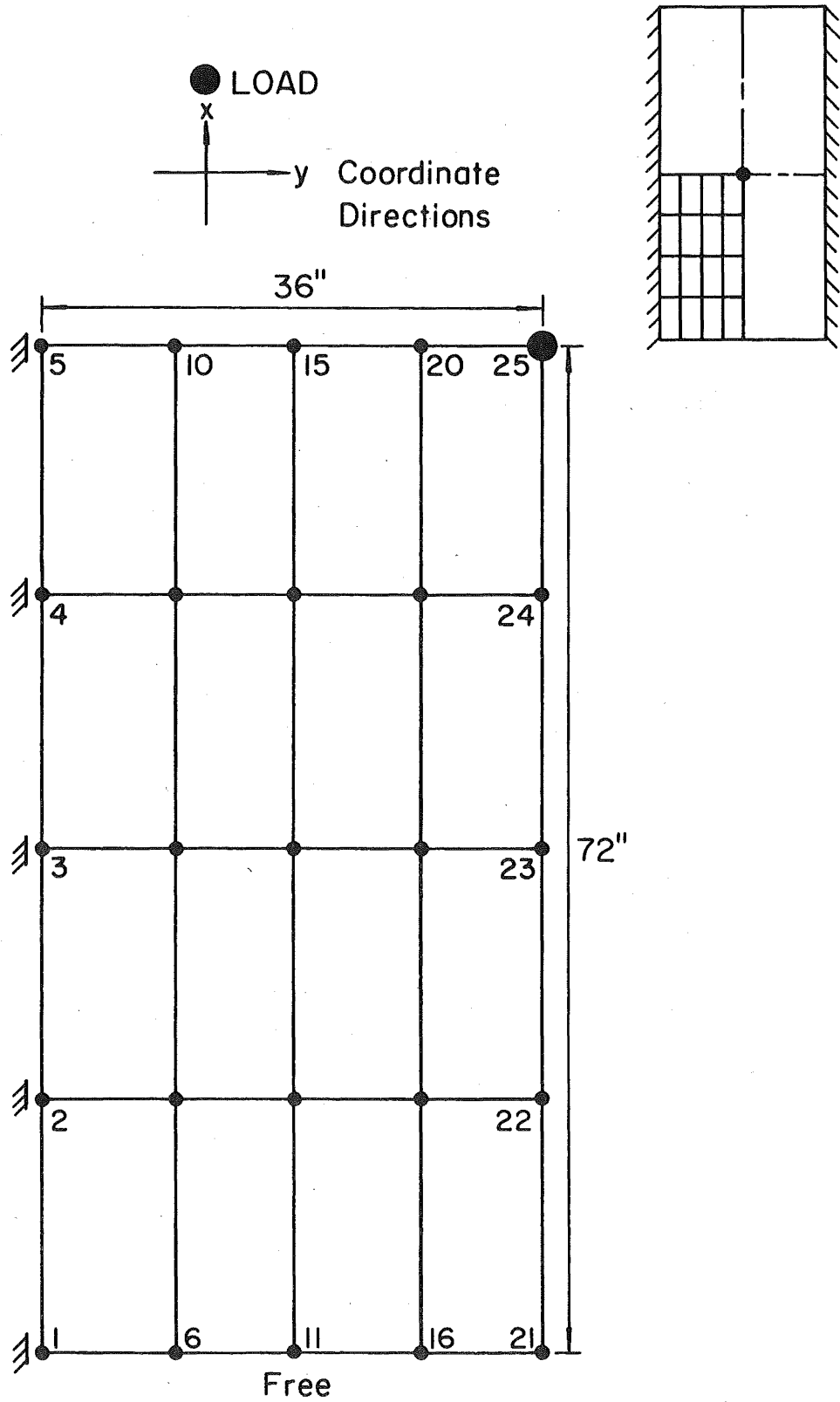
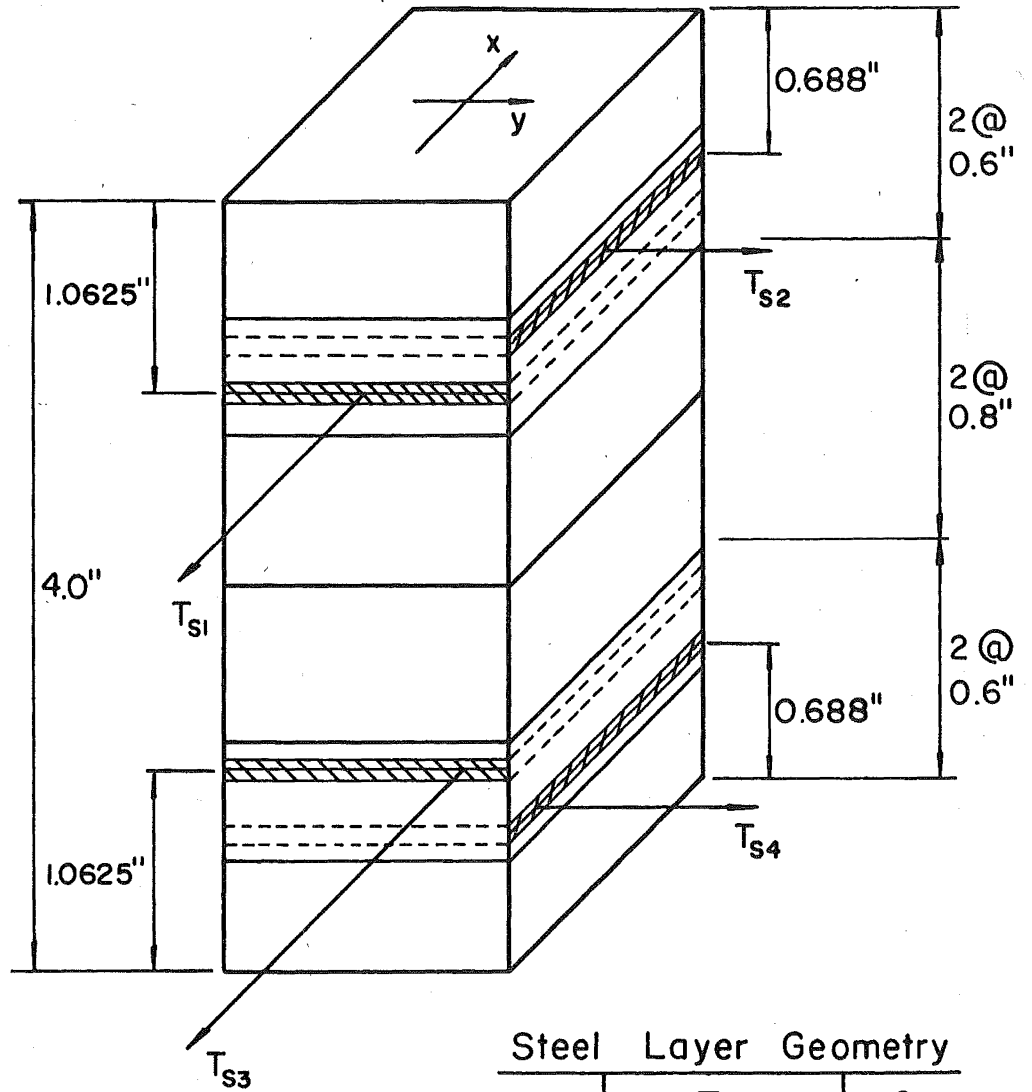


Fig. 42 . Discretization and Loading for the Fixed-Free Slab



Steel Layer Geometry		
	T_s	θ_x
T_{s1}	0.01160"	0°
T_{s2}	0.01310"	-90°
T_{s3}	0.01790"	0°
T_{s4}	0.01458"	-90°

Fig. 43 Layering for the Fixed-Free Slab

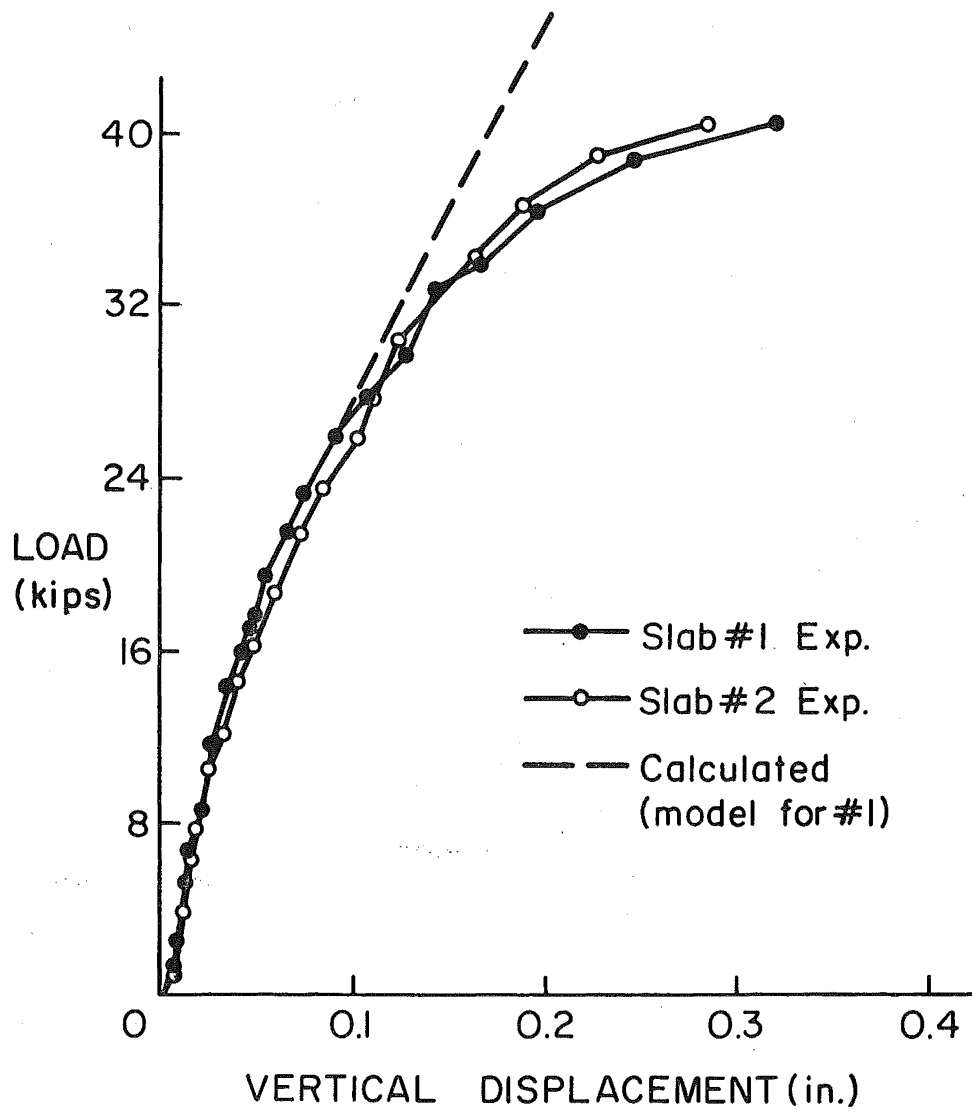


Fig. 44 Load-Deflection History for the Fixed-Free Slab

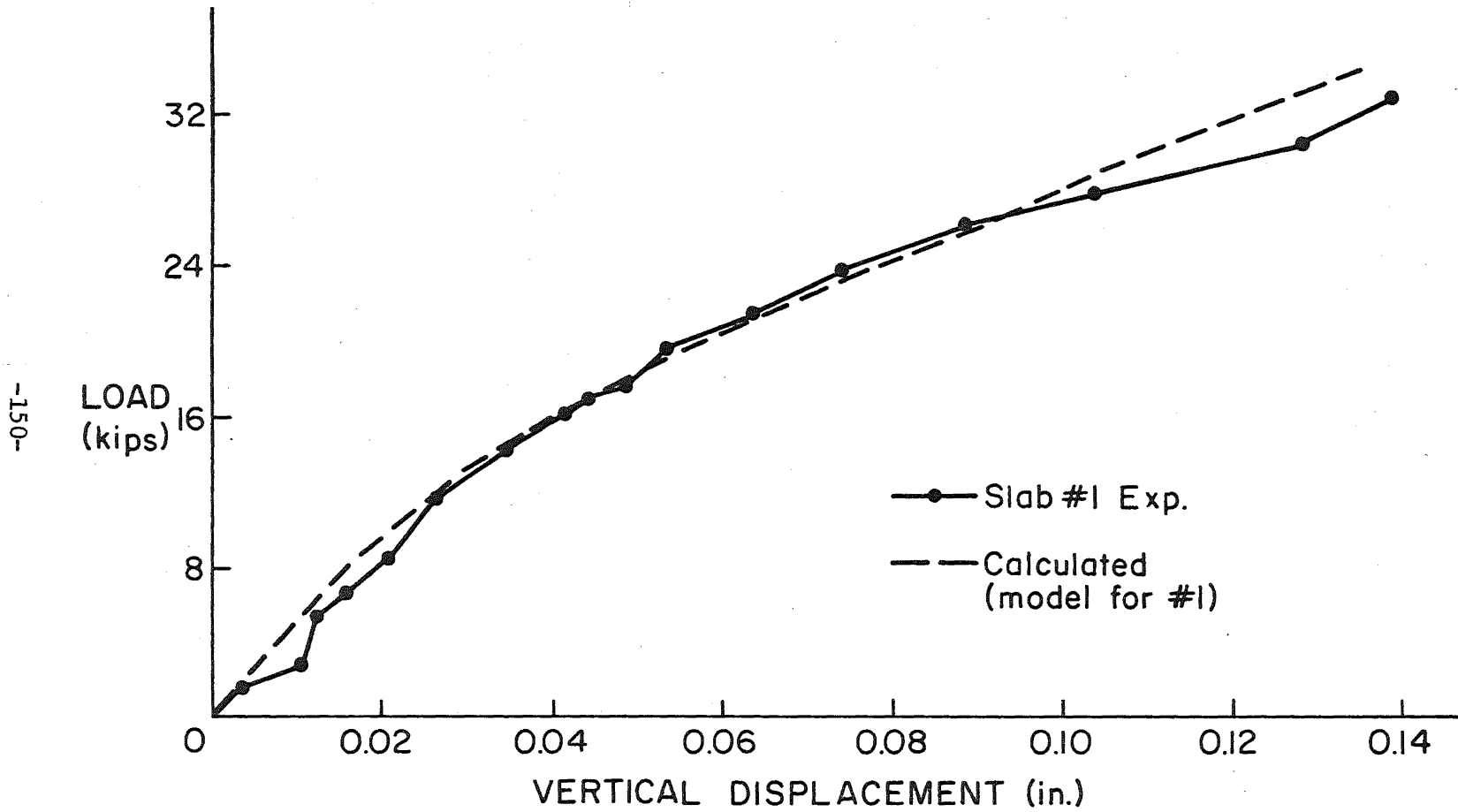


Fig. 45 Load-Deflection History for the Fixed-Free Slab

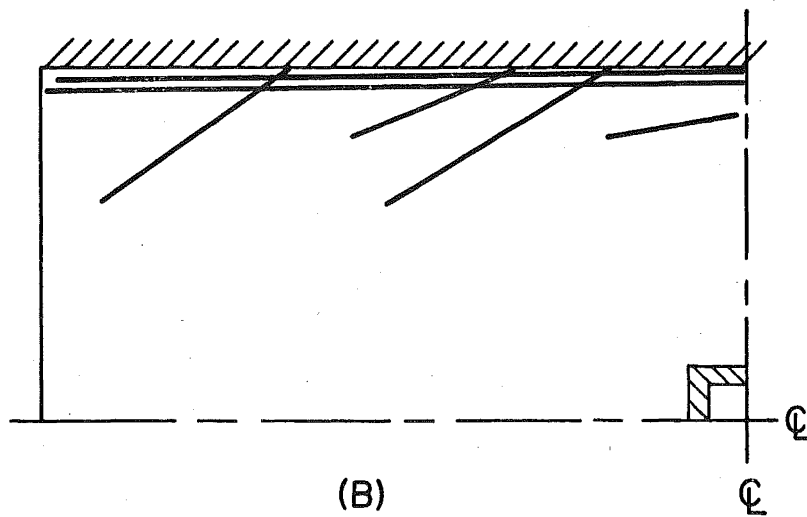
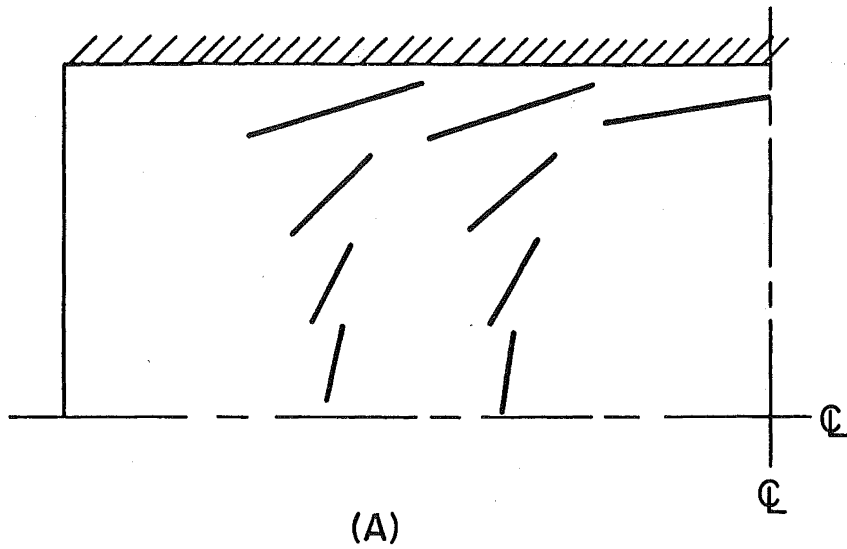


Fig. 46 Analytic (A) and Experimental (B) Top Surface Crack Patterns for the Fixed-Free Slab

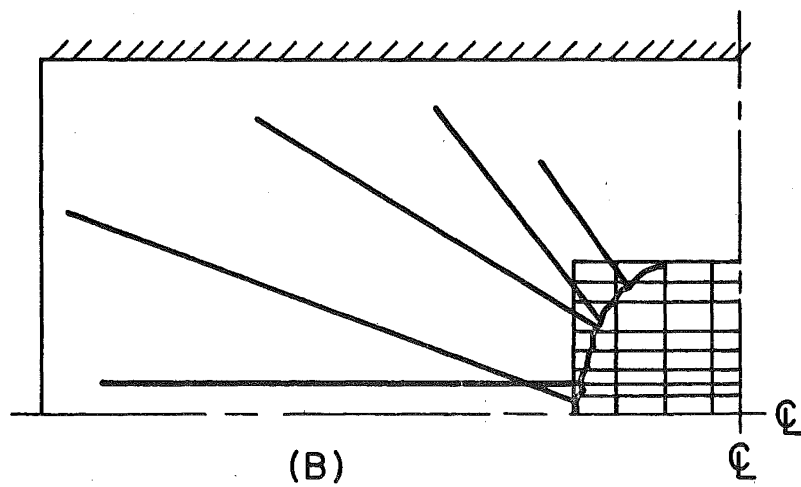
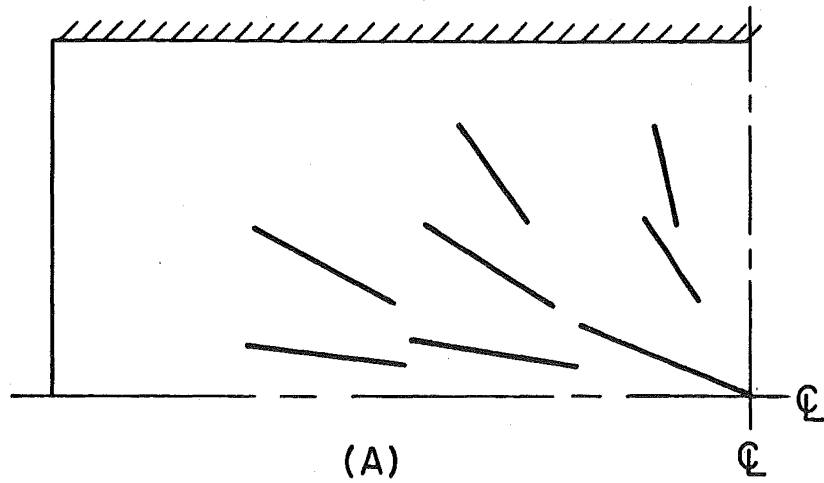


Fig. 47 Analytic (A) and Experimental (B) Bottom Surface Crack Patterns for the Fixed-Free Slab

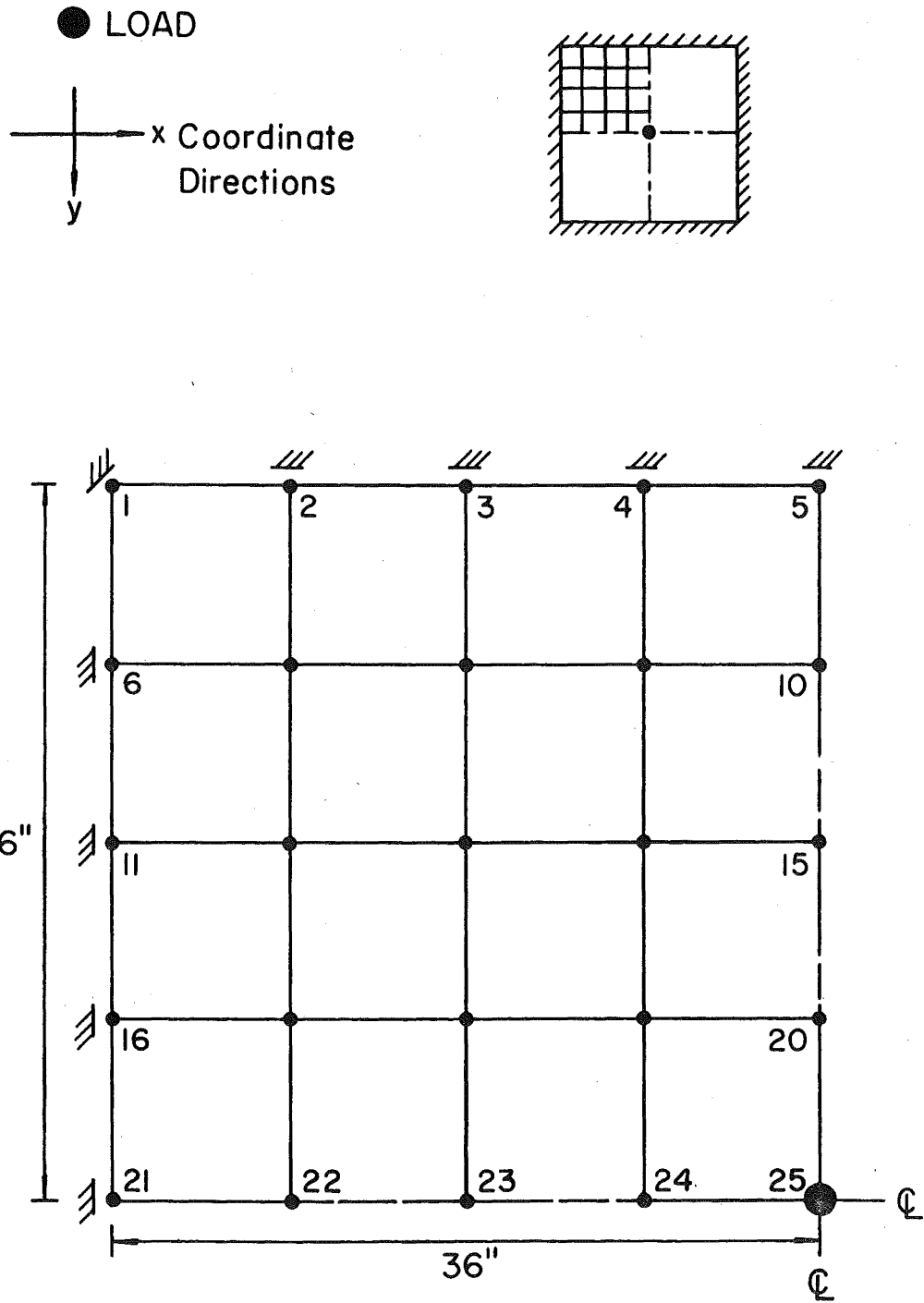
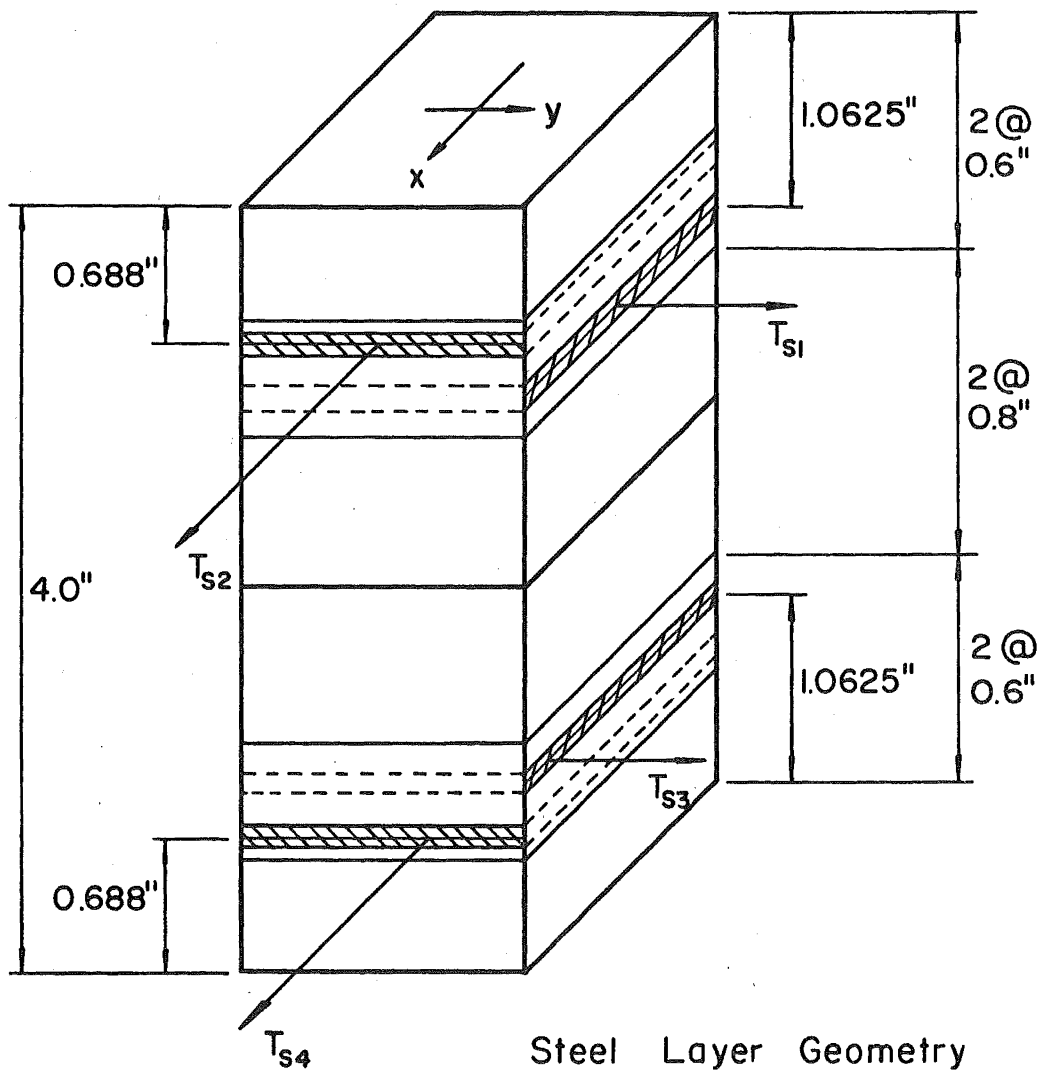


Fig. 48 Discretization and Loading for the Fixed-Fixed Slab



Steel Layer Geometry		
	T_s	θ_x
T_{s1}	0.01790"	0°
T_{s2}	0.01646"	-90°
T_{s3}	0.01790"	0°
T_{s4}	0.01646"	-90°

Fig. 49 Layering for the Fixed-Fixed Slab

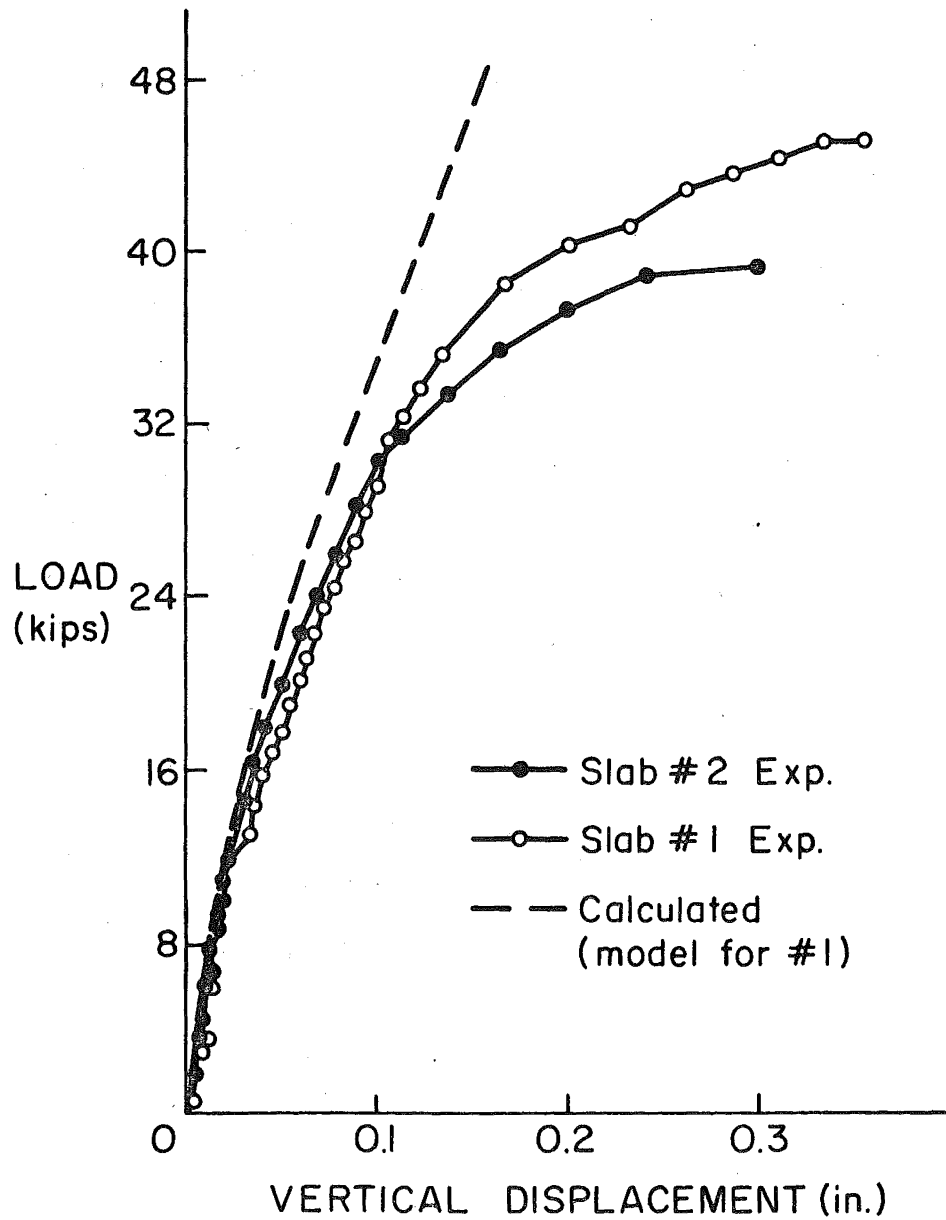


Fig. 50 Load-Deflection History for the Fixed-Fixed Slab

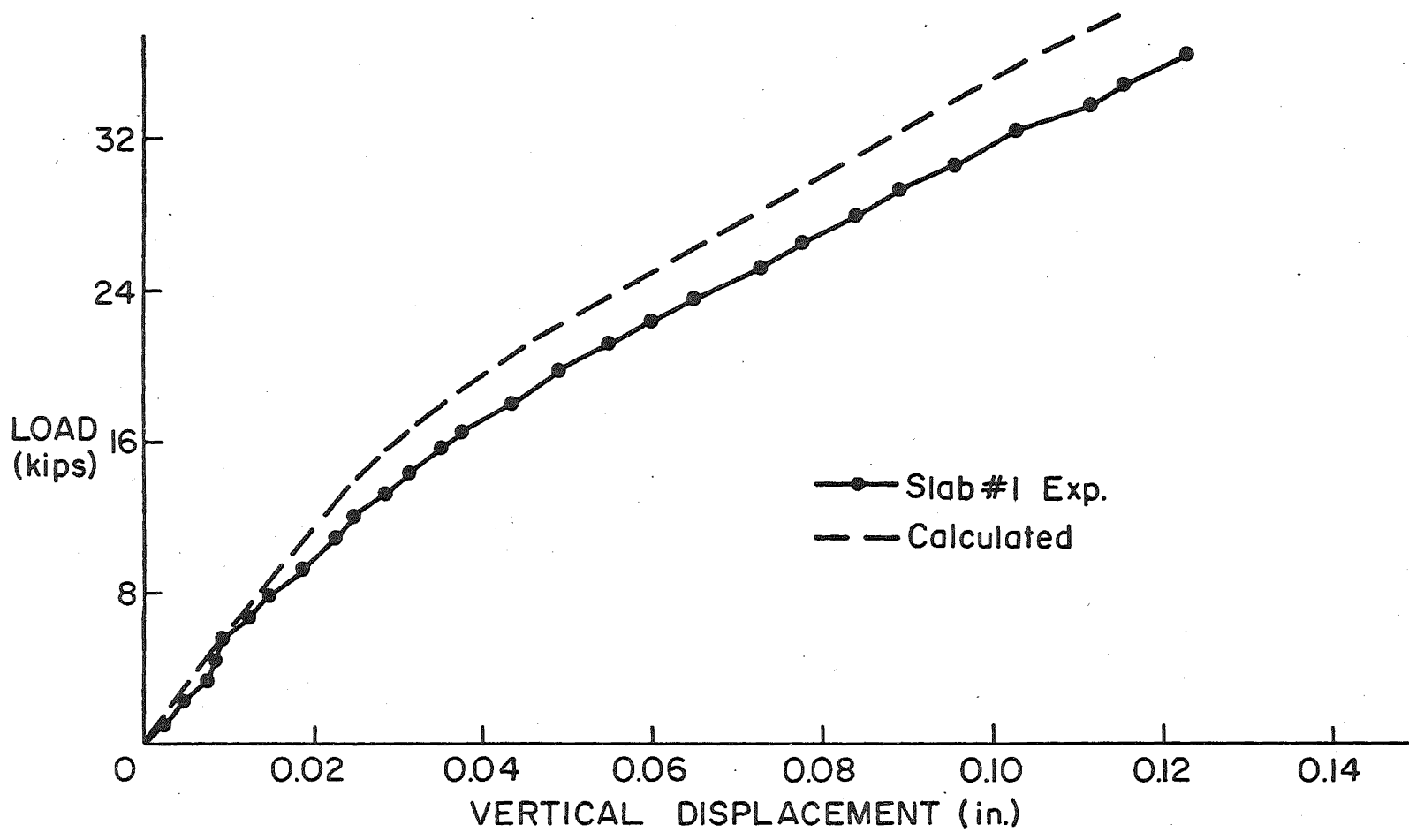


Fig. 51 Load-Deflection History for the Fixed-Fixed Slab

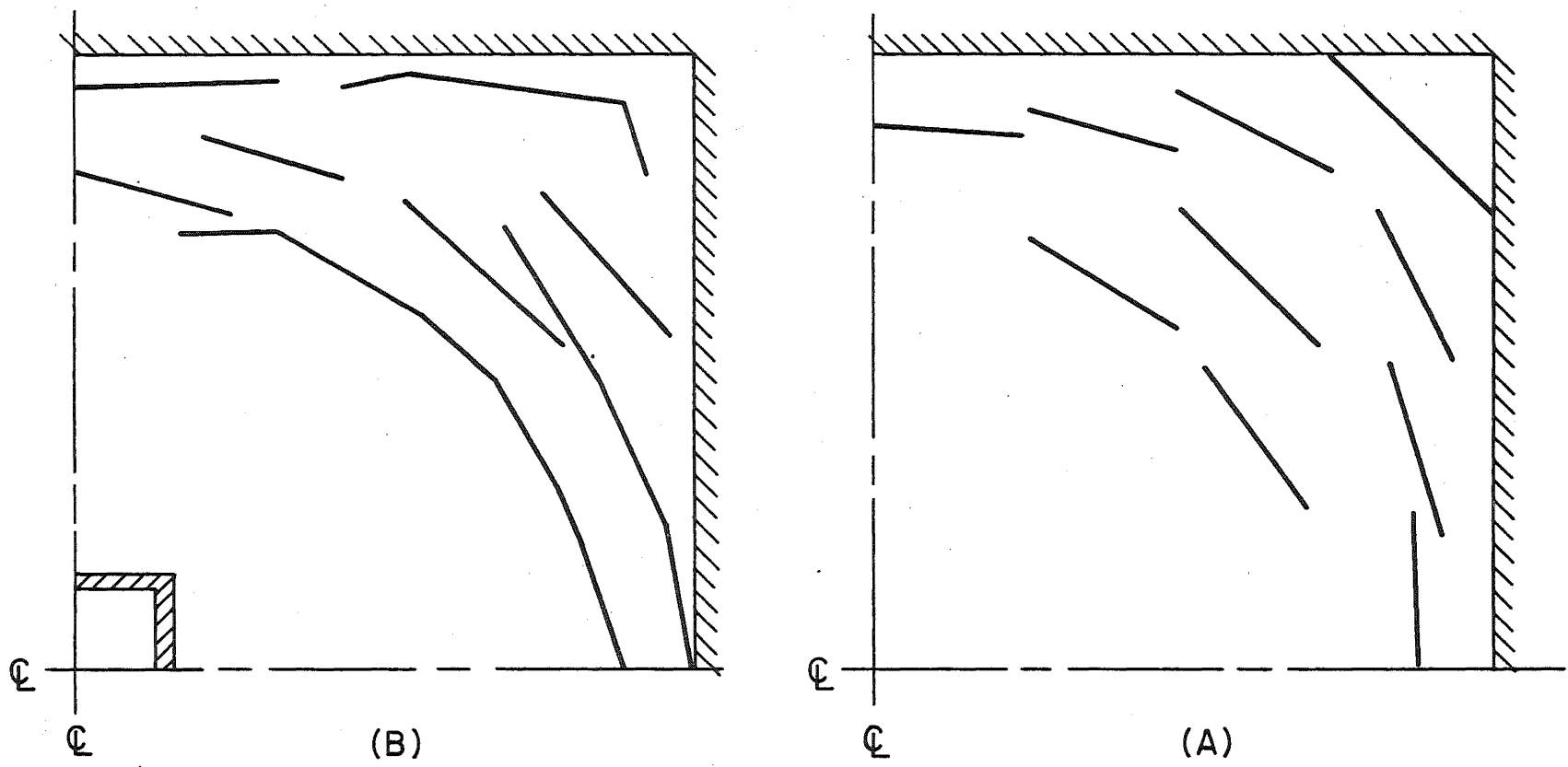


Fig. 52 Analytic (A) and Experimental (B) Top Surface Crack Patterns for the Fixed-Fixed Slab

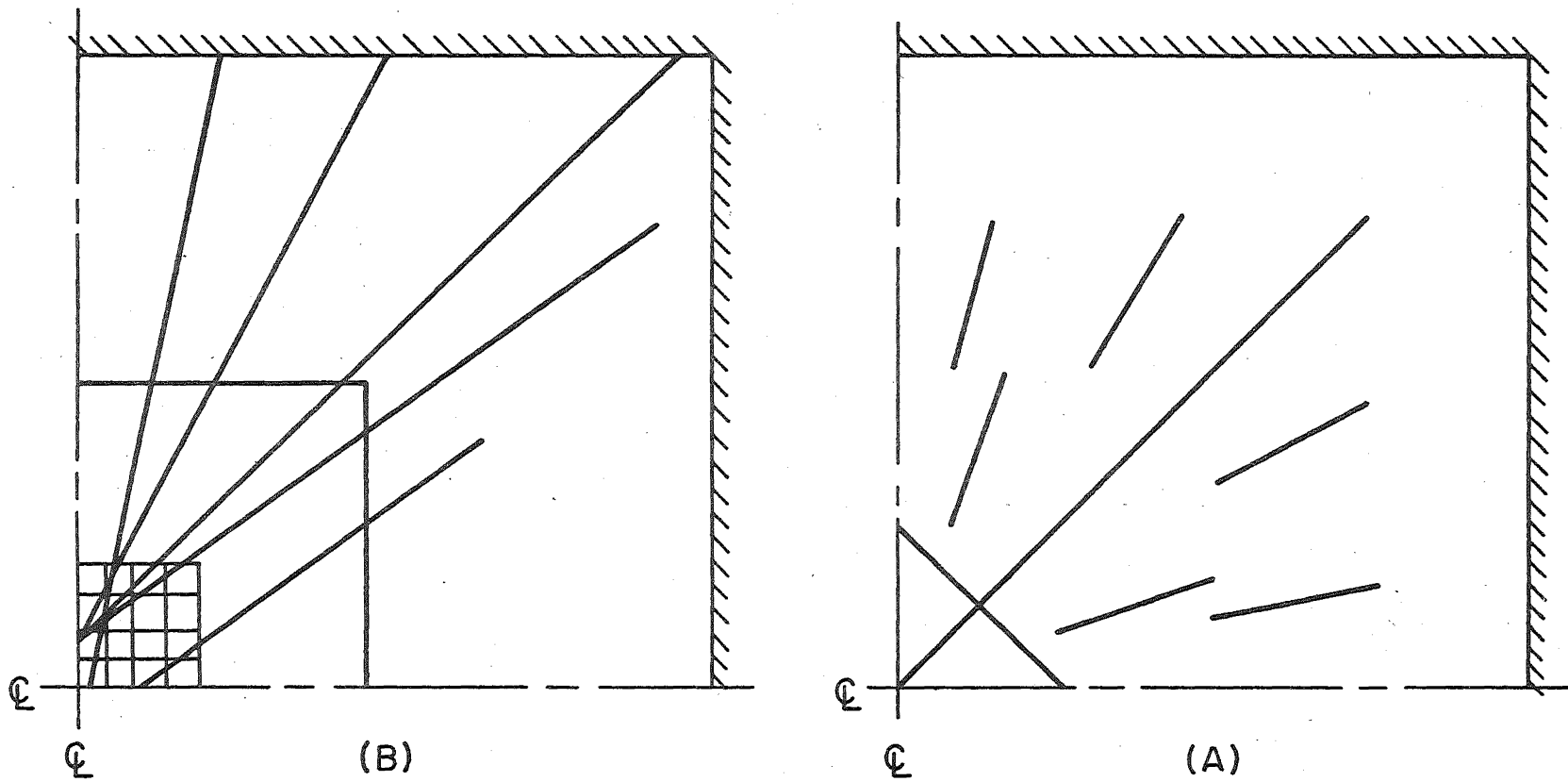


Fig. 53 Analytic (A) and Experimental (B) Bottom Surface Crack Patterns for the Fixed-Fixed Slab

9. REFERENCES

1. Adini, A. and Clough, R. W.
ANALYSIS OF PLATE BENDING BY THE FINITE ELEMENT METHOD, Report submitted to the National Science Foundation, Grant G7337, University of California, Berkeley, California, 1960.
2. Armen, H., Pifko, A. and Levine, H. S.
FINITE ELEMENT ANALYSIS OF STRUCTURES IN THE PLASTIC RANGE, NASA Contractor Report NASA CR-1649, National Aeronautics and Space Administration, Washington, D.C., 1971.
3. Barnard, P. R.
RESEARCHES INTO THE COMPLETE STRESS-STRAIN CURVE FOR CONCRETE, Magazine of Concrete Research, Vol. 16, No. 49, December 1964.
4. Bell, J. C. and Elms, D. G.
NON-LINEAR ANALYSIS OF REINFORCED CONCRETE SLABS, Magazine of Concrete Research, Vol. 24, No. 79, June 1972.
5. Bhaumik, A. K. and Hanley, J. T.
ELASTO-PLASTIC PLATE ANALYSIS BY FINITE DIFFERENCES, Journal of the Structural Division, ASCE, Vol. 93, ST5, October 1967.
6. Cardenas, A. and Sozen, M. A.
STRENGTH AND BEHAVIOR OF ISOTROPICALLY AND NONISOTROPICALLY REINFORCED CONCRETE SLABS SUBJECTED TO COMBINATION OF FLEXURAL AND TORSIONAL MOMENTS, Civil Engineering Studies, Structural Research Series No. 336, University of Illinois, Urbana, Illinois, 1968.
7. Cervenka, V.
INELASTIC FINITE ELEMENT ANALYSIS OF REINFORCED CONCRETE PANELS UNDER IN-PLANE LOADS, Ph.D. Dissertation, University of Colorado, Boulder, Colorado, 1970.
8. Clough, R. W.
THE FINITE ELEMENT METHOD IN STRUCTURAL MECHANICS, Chapter 7, of Stress Analysis, edited by O. C. Zienkiewicz and G. S. Hollister, John Wiley and Sons, New York, New York, 1965.

9. Clough, R. W. and Tocher, J. L.
FINITE ELEMENT STIFFNESS MATRICES FOR ANALYSIS OF PLATE BENDING, Proceedings of the Conference on Matrix Methods in Structural Mechanics, Wright-Patterson Air Force Base, Ohio, 1965.
10. Clough, R. and Felippa, C.
A REFINED QUADRILATERAL ELEMENT FOR ANALYSIS OF PLATE BENDING, Proceedings of the Second Conference on Matrix Methods in Structural Mechanics, Wright-Patterson Air Force Base, Ohio, 1968.
11. Hand, F. R., Pecknold, D. A. and Schnobrich, W. C.
A LAYERED FINITE ELEMENT NONLINEAR ANALYSIS OF REINFORCED CONCRETE PLATES AND SHELLS, Civil Engineering Studies, Structural Research Series No. 389, University of Illinois, Urbana, Illinois, August 1972.
12. Hand, F. R., Pecknold, D. A. and Schnobrich, W. C.
NONLINEAR LAYERED ANALYSIS OF RC PLATES AND SHELLS, Journal of the Structural Division, ASCE, Vol. 99, No. ST7, July 1973.
13. Holland, I. and Bell, K. (Eds.)
FINITE ELEMENT METHODS IN STRESS ANALYSIS, Tapir, Trondheim, Norway, 1969.
14. Hsu, T. T. C., Slate, F. O., Sturman, G. M. and Winter, G.
MICROCRACKING OF PLAIN CONCRETE AND THE SHAPE OF THE STRESS-STRAIN CURVE, Journal of the American Concrete Institute, Vol. 60, No. 2, February 1963.
15. Hughes, B. P. and Chapman, G. P.
THE COMPLETE STRESS-STRAIN CURVE FOR CONCRETE IN DIRECT TENSION, BULLETIN RILEM, No. 30, March 1966.
16. Jensen, V. P.
THE PLASTICITY RATIO OF CONCRETE AND ITS EFFECTS ON THE ULTIMATE STRENGTH OF BEAMS, Journal of the American Concrete Institute, Vol. 14, No. 6, June 1943.
17. Jofreit, J. C. and McNeill, G. M.
FINITE ELEMENT ANALYSIS OF REINFORCED CONCRETE SLABS, Journal of the Structural Division, ASCE, Vol. 97, No. ST3, March 1971.

18. Kostem, C. N.
SHEAR PUNCHING OF BRIDGE DECKS, Fritz Engineering Laboratory
Report No. 378B.4, Lehigh University, Bethlehem, Pennsylvania
(under preparation).
19. Kulicki, J. M. and Kostem, C. N.
THE INELASTIC ANALYSIS OF REINFORCED AND PRESTRESSED CONCRETE
BEAMS, Fritz Engineering Laboratory Report No. 378B.1, Lehigh
University, Bethlehem, Pennsylvania, November 1972. X
20. Kulicki, J. M. and Kostem, C. N.
A USER'S MANUAL FOR PROGRAM BEAM, Fritz Engineering Laboratory
Report No. 378B.2, Lehigh University, Bethlehem, Pennsylvania,
February 1973.
21. Kulicki, J. M. and Kostem, C. N.
FURTHER STUDIES ON THE NONLINEAR FINITE ELEMENT ANALYSIS OF
BEAMS, Fritz Engineering Laboratory Report No. 378A.5, Lehigh
University, April 1973. X
22. Kulicki, J. M. and Kostem, C. N.
NONLINEAR ANALYSIS OF CONCRETE FLEXURAL MEMBERS, Proceedings of
the International Conference on Planning and Design of Tall
Buildings, Vol. DS, Bethlehem, Pennsylvania, April 1973.
23. Kulicki, J. M. and Kostem, C. N.
THE INELASTIC ANALYSIS OF PRESTRESSED AND REINFORCED CONCRETE
BRIDGE BEAMS BY THE FINITE ELEMENT METHOD, Fritz Engineering
Laboratory Report No. 378A.6, Lehigh University, Bethlehem,
Pennsylvania, September 1973. X JMK DISS.
24. Kupfer, H., Hilsdorf, H. K. and Rusch, H.
BEHAVIOR OF CONCRETE UNDER BIAXIAL STRESSES, Journal of the
American Concrete Institute, Vol. 66, No. 8, August 1969.
25. Lamb, R. S. and Davis, G.
DISCUSSION OF NONLINEAR STRESS ANALYSIS OF REINFORCED CONCRETE
by Valliappan, S. and Doolan, T. F., (Proceedings Paper 8845),
Journal of the Structural Division, ASCE, Vol. 99, No. ST3,
March 1973.

26. Lin, C. S.
NONLINEAR ANALYSIS OF REINFORCED CONCRETE SLABS AND SHELLS,
Ph.D. Dissertation, University of California, Berkeley,
California, September 1972.
27. Liu, T. C.
STRESS-STRAIN RESPONSE AND FRACTURE OF CONCRETE IN BIAxIAL
COMPRESSION, Ph.D. Dissertation, Structural Engineering
Department, Cornell University, Ithaca, New York, 1971.
28. Liu, T. C., Nilson, A. H. and Slate, F. O.
BIAxIAL STRESS-STRAIN RELATIONS FOR CONCRETE, Journal of the
Structural Division, ASCE, Vol. 98, No. ST5, May 1972.
29. Lopez, L. A. and Ang, A. H. S.
FLEXURAL ANALYSIS OF ELASTIC-PLASTIC RECTANGULAR PLATES, Civil
Engineering Studies, Structural Research Series No. 305,
University of Illinois, Urbana, Illinois, May 1966.
30. Morley, C. T.
EXPERIMENTS ON THE DISTORTION OF STEEL BARS ACROSS CRACKS IN
REINFORCED CONCRETE SLABS, Magazine of Concrete Research,
Vol. 18, No. 54, March 1966.
31. Mufti, A. A., Mirza, M. S., McCutcheon, J. O. and Spottowski, R.
A STUDY OF NON-LINEAR BEHAVIOR OF STRUCTURAL CONCRETE ELEMENTS,
from Finite Element Method in Civil Engineering, ed. McCutcheon,
J. O. et al., McGill University, Montreal, Canada, June 1972.
32. Nelissen, L. J. M.
BIAxIAL TESTING OF NORMAL CONCRETE, HERON, Vol. 18, No. 1, 1972,
Stevin-Laboratory of the Department of Civil Engineering of the
Technological University and Institute TNO for Building
Materials and Building Structures, Delft, The Netherlands.
33. Neville, A. M.
HARDENED CONCRETE: PHYSICAL AND MECHANICAL ASPECTS, American
Concrete Institute Monograph No. 6, 1971.
34. Ngo, D. and Scordelis, A. C.
FINITE ELEMENT ANALYSIS OF REINFORCED CONCRETE BEAMS, Journal
of the American Concrete Institute, Proceedings, Vol. 64, No. 3,
March 1967.

35. Ramberg, W. and Osgood, W. R.
DESCRIPTION OF STRESS STRAIN CURVES BY THREE PARAMETERS, NACA,
TN 902, July 1943.
36. Saenz, L. P.
Discussion of EQUATIONS FOR THE STRESS STRAIN CURVE OF CONCRETE,
by P. Desayi and S. Krishnan, Journal of the American Concrete
Institute, Vol. 61, No. 9, September 1964.
37. Schnobrich, W. C., Salem, M. H., Pecknold, D. A. and Mohroz, B.
DISCUSSION OF NONLINEAR STRESS ANALYSIS OF REINFORCED CONCRETE
by Valliapan, S. and Doolan, T. F. (Proceedings Paper 8845),
Journal of the Structural Division, ASCE, Vol. 98, No. ST10,
October 1972.
38. Smith, G. M. and Young, L. E.
ULTIMATE FLEXURAL ANALYSIS BASED ON STRESS STRAIN CURVES OF
CYLINDERS, Journal of the American Concrete Institute, Vol. 53,
No. 6, December 1956.
39. Taylor, R., Maher, D. R. H. and Hayes, B.
EFFECT OF THE ARRANGEMENT OF REINFORCEMENT ON THE BEHAVIOR OF
REINFORCED CONCRETE SLABS, Magazine of Concrete Research,
Vol. 19, No. 58, March 1967.
40. Thomas, F. G.
THE STRENGTH AND DEFORMATION OF SOME REINFORCED CONCRETE SLABS
SUBJECTED TO CONCENTRATED LOADING, From Part VIII of Studies in
Reinforced Concrete, Technical Papers, Building Research,
Great Britain, 1939.
41. Tottenham, H. and Brebbia, C.
FINITE ELEMENT TECHNIQUES IN STRUCTURAL MECHANICS, Southampton
University Press, Southampton, England, 1970.
42. Valliapan, S. and Doolan, T. F.
NONLINEAR STRESS ANALYSIS OF REINFORCED CONCRETE, Journal of the
Structural Division, ASCE, ST4, April 1972.

43. Wegmuller, A. W. and Kostem, C. N.
ELASTIC-PLASTIC ANALYSIS OF PLATES, Proceedings of the IASS Symposium on Shell Structures and Climatic Influences, pp. 379-386, Calgary, Canada, July 1972.
44. Wegmuller, A. W. and Kostem, C. N.
FINITE ELEMENT ANALYSIS OF PLATES AND ECCENTRICALLY STIFFENED PLATES, Fritz Engineering Laboratory Report No. 378A.3, Lehigh University, Bethlehem, Pennsylvania, February 1973.
45. Wegmuller, A. W. and Kostem, C. N.
FINITE ELEMENT ANALYSIS OF ELASTIC-PLASTIC PLATES AND ECCENTRICALLY STIFFENED PLATES, Fritz Engineering Laboratory Report No. 378A.4, Lehigh University, Bethlehem, Pennsylvania, February 1973.
46. Whang, B.
ELASTO-PLASTIC ORTHOTROPIC PLATES AND SHELLS, Proceedings of the Symposium on Application of Finite Element Methods in Civil Engineering, Vanderbilt University, Nashville, Tennessee, November 1969.
47. Zellin, M. A., Kostem, C. N. and VanHorn, D. A.
STRUCTURAL BEHAVIOR OF BEAM-SLAB HIGHWAY BRIDGES, A SUMMARY OF COMPLETED RESEARCH AND BIBLIOGRAPHY, Fritz Engineering Laboratory Report No. 387.1, Lehigh University, Bethlehem, Pennsylvania, May 1973.
48. Zienkiewicz, O. C.
THE FINITE ELEMENT METHOD IN ENGINEERING SCIENCE, McGraw-Hill, New York, New York, 1971.
49. American Concrete Institute
BUILDING CODE REQUIREMENTS FOR REINFORCED CONCRETE (ACI 318-63), Detroit, Michigan, 1963.
50. Unpublished Student Report, CE 157, Lehigh University, Group "0", 1970.